FINAL REPORT

(08/10/98 - 12/30/03)

EVALUATION OF LABORATORY TESTING SYSTEMS FOR ASPHALT MIXTURE DESIGN AND EVALUATION

VOLUME I

Contract No.: BB-888
UF Project No.: 4504-659-12

Dr. Reynaldo Roque
Dr. Bjorn Birgisson
Mr. Daniel Darku
Mr. Christos A. Drakos

Department of Civil & Coastal Engineering
University of Florida
Gainesville, FL 32611

Submitted to:

Florida Department of Transportation

September 2004

ACKNOWLEDGMENTS

The authors would like to acknowledge and thank the Florida Department of Transportation (FDOT) for providing technical and financial support and materials for this project. Special thanks go to engineers and technicians of the Bituminous Section of the State Materials Office for their contributions in items of their expert knowledge, experience, and constructive advice throughout the course of this work. Their efforts are sincerely appreciated and clearly made a decisive impact on the quality of the research.

EXECUTIVE SUMMARY

Instability rutting is a major distress mode in hot mix asphalt (HMA) pavements that occurs when the structural properties of the compacted mix cannot resist near surface critical stress conditions caused by traffic loads. This mode of failure reduces serviceability and creates the hazard of hydroplaning because of accumulated water in the wheel-path ruts. Rehabilitation of this type of rutting usually involves asphalt concrete (AC) overlay or mill and replace. It was determined that there is no reliable existing approach for instability-rutting assessment of HMA. This study was undertaken to identify or develop laboratory test methods suitable for assessing instability rutting potential of asphalt mixture.

It was determined that critical stress states associated with instability rutting involve shear in the presence of minimal confinement or tension, which is a stress state that cannot be induced by existing laboratory tests in their present form. A modified version of the asphalt pavement analyzer (APA) was developed with a loading device that induces stress states similar to those found under radial truck tires. In addition, a modified measurement and interpretation method that is far more sensitive to the presence of instability rutting was developed for the APA. For purposes of quality control, a test method involving measurements obtained during instability induced using the gyratory compactor was developed.

The primary accomplishments of this work may be summarized as follows:

- Identified potential stress states that might be conducive to impending instability based on measured surface contact stresses under radial truck tires. Current mixture design and evaluation procedures do not properly account for these critical stress states – high near-surface shear stress with reduced confinement or tension.

- Determined that existing equipment, testing, and interpretation procedures may not capture these stress states and their effects.

- Identified test methods that would provide measurements of instability rutting resistance based on stress states identified above.

- Three approaches were identified to evaluate mixtures under conditions of impending instability:
  - Evaluation during the compaction process using the Servopac gyratory compactor, suitable for mix design and QC/QA
  - Mixture evaluation using a laboratory physical model with modified APA
  - Hollow Cylinder as a research tool for evaluation of the impending instability concept

- Specific procedures were developed and evaluated on a range of mixtures of known relative performance and verified the ability of the devices to distinguish between mixtures with varying performance. Specific parameters and criteria suitable for mixture design and specification purposes were determined.

The following conclusions were drawn from this study:

- Existing systems – even the dynamic modulus approach proposed as part of the new AASHTO pavement design guide – are unable to screen mixtures susceptible to instability rutting.

- Keys to developing a relevant test are a) to capture the critical stress states associated with instability (APA), and b) to measure the mixture's strength at impending instability (Servopac).

- Evaluation using the existing APA device could immediately improved by obtaining a detailed profile of the rutted surface, but greater 'reliability' can be achieved by introducing a modified loading system that more closely represents tire stresses.

The following recommendations are based on the findings and conclusions from this study:

- The implementation of the system on a large scale would require the capability to easily apply two angles of gyration and to measure the gyratory shear strength during the compaction process (Servopac or with modification to existing gyratory compactors widely available at this time)

- The new data-measurement method should be implemented immediately with the existing APA equipment.

- Whenever possible, specimens should be tested at both 7%AV and 4%AV when evaluating the mixture's ability to resist instability with the APA.

- At this point there is not enough evidence to support a move to higher temperature testing for a single-condition test (specimen tested at one temperature).

TABLE OF CONTENTS

Page

LIST OF TABLES

LIST OF FIGURES

Figures Page

CHAPTER 1

INTRODUCTION

1.1 BACKGROUND

A major distress mode of flexible pavements is permanent deformation, also known as *rutting*. Rutting is characterized by a depression that forms in the wheel paths and can be the result of permanent reduction in volume (consolidation/traffic densification), permanent movement of the material at constant volume (plastic deformation/shear), or a combination of the two. This mode of failure reduces serviceability and creates the hazard of hydroplaning because of accumulated water in the wheel-path ruts. Rehabilitation of rutted pavements usually involves asphalt concrete (AC) overlay, recycling, or replacement of all structural layers.

The Superpave™ mix design and analysis method was developed more than a decade ago under the Strategic Highway Research Program (SHRP) [Leahy et al. 1994]. Many agencies in North America – including the Florida Department of Transportation – have adopted the Superpave method of performance-grade (PG) binder specification and the volumetric mixture design method. Although the Superpave volumetric design procedure has resulted in some improvements over the Marshall method of mixture design, it is still devoid of a general strength test that would determine the mixture's suitability for resistance to rutting and cracking. The industry has expressed the need for a simple 'pass–fail' type of test to complement the Superpave volumetric mix design method, especially for use on design–build or warranty projects.

Numerous performance prediction models – numerical and physical – have been implemented to classify an asphalt mixture's ability to resist rutting. In an effort to control this type of distress, many institutions and agencies are searching for a simple performance test that would indicate the rutting potential of hot-mix asphalt (HMA). For this purpose the suitability of various loaded-wheel testers (LWT), as a physical model, is being examined throughout the country. The LWTs provide an accelerated performance evaluation by subjecting the designed mix to repeated loading under various environmental conditions (moisture and temperature). Some of the most popular devices used are the Georgia Loaded Wheel Tester (GLWT), Asphalt Pavement Analyzer (APA), Hamburg Wheel Tracking Device (HWTD), and the French Pavement Rutting Tester (FPRT) [Cooley et al. 2000, Federal Highway Administration (FHWA) 1998].

A series of studies on the suitability of wheel testers to predict the rutting performance of asphalt mixtures gave mixed results [Epps et al. 1997, Bonaquist et al. 1998]. These types of physical models are classified as empirical or performance-related tests because they do not measure a fundamental property that can be used to explain and identify the mechanisms resulting in surface distress. The models' accuracy relies on how well (realistically) conditions have been simulated in the lab.

Pavement performance has been negatively influenced by the change in traffic type and volume in recent years. More than 98% of trucks are now using radial tires that can withstand higher inflation pressures and higher loads. Studies have shown that radial tires induce high lateral stresses that cause tensile stresses at the surface of the pavement [Myers 1997]. Furthermore, it was shown that tire structure has a significant influence on contact stresses; in fact, stress states induced by radial and wide-base radial tires were determined to be potentially more detrimental to the pavement's surface than stress states induced by bias ply tires [Myers et al. 1999]. Thus, it is important that the load characterization in the physical model captures the complexity of the load experienced in the field.

In most LWTs, the loading device – in the form of a wheel or a pressurized hose – is tracked back and forth over a testing sample to induce rutting. The load follows the same path in both directions (no wander). In recent tests with the Heavy Vehicle Simulator (HVS), researchers have found that there is a difference in the rate of accumulated permanent deformation between loading in unidirectional and bi-directional mode [Harvey and Popescu 2000, Tia et al. 2001]. The unidirectional loading had a higher rate of rutting (reached failure in fewer cycles) over the same pavement sections than the bi-directional loading.

1.2 PROBLEM STATEMENT

Factors that influence the amount of rutting or contribute to the pavement's resistance to failure have not been clearly identified. Therefore, the lack of confidence in existing physical models has inhibited their application for prediction of pavement rutting. This study will evaluate the importance of capturing the specific loading, environmental, structural, and construction characteristics on the development of a reliable physical model. There is a need to identify this set of conditions – realistic contact stresses (loading), thermal gradients in asphalt layer (environment/structural), and test specimen conditioning (construction) – that may dictate performance. Traditionally, mixture evaluation includes average conditions that do not typify the critical condition or capture the key factors that lead to this kind of failure.

1.3 HYPOTHESIS

Rutting performance of mixtures may be governed by a set of critical field conditions – compaction, load, temperature, and sequence of loading. Therefore, it is essential to identify the critical design condition (mechanism) that must be replicated in a laboratory physical model. A physical model that will employ this set of critical conditions might produce more reliable results for mixture rutting performance.

1.4 OBJECTIVES

The main objective of this study is to identify the loading, environmental, and construction (density) factors that are critical/essential in defining the mechanism of rutting. The identification of these conditions will logically lead to the development of a reliable physical model. The current version of the APA was selected for the experimental program; necessary modifications will be made to incorporate new testing procedures, which more realistically simulate traffic and environmental conditions existing on pavements.

The primary objectives of this research study are listed below:

- Identify the characteristics of a loading device necessary to represent a tire load more realistically.
- Design and construct a new loading device to induce more realistic contact stresses.
- Verify the effects of loading characteristics on rutting performance.
- Examine the importance of unidirectional versus bi-directional loading in the physical model.
- Evaluate the importance of density/loading history on rutting performance.
- Investigate the sensitivity of the physical model to mixtures with different densities as produced by compaction and/or aggregate gradation of the mixtures.
- Recommend test configuration and procedure/system for mixture evaluation. As envisioned, the procedure will define the magnitude and sequence of loading as well as test-temperature requirements.

1.5 SCOPE

The research focuses on identifying the critical conditions that contribute to the mechanism(s) of rutting. Defining the conditions that might initiate and propagate rutting will lead to the development of better performance prediction models – physical and numerical.

However, it will not be feasible to examine all possible parameters that affect rutting within the limited time. Thus, this research will focus on the effects of the following:

- Load configuration. A new loading device (rib) will be evaluated against the existing pressurized hose. The contact stresses will be measured for both devices and then used in finite element modeling (FEM) to calculate the induced stress states in the specimen.
- Temperature. Two temperatures – 64 and 70^{o}C – have tentatively been selected for evaluation of mixture's sensitivity to temperature changes.
- Mixture density. Mixtures will be tested at two levels – 93-94, and 95-96% – of maximum theoretical density (MTD).
- Three mixtures of known field performance will be used for the initial development and the evaluation/validation of the physical model. The following mixtures were chosen from the Superpave™ monitoring project:

  Poor field performing mixture – I-10 Madison County.

  Good field performing mixture – Turnpike Palm Beach.

  Good performing mixture – HVS coarse-graded mix.

The Pine gyratory compactor will be used to prepare 150-mm-diameter by 75-mm-thick mixture specimens. In this research, beams will not be considered because of compaction issues and the potential for variability that may influence the analysis.

1.6 RESEARCH APPROACH

The research is divided into two parts – the analytical and the experimental. The analytical part includes the conceptual design, the finite-element analysis (FEA) of contact stresses, and the analysis of the stress states within the physical model. Subsequently the experimental part includes the laboratory testing with the physical model and data analysis. A research-approach outline is detailed below:

- Literature Review: examine existing ideas, theories, and results published on tire contact stresses, critical stress states, and rutting in asphalt concrete pavements. Also, review work done on other accelerated physical models – LWT, Accelerated Loading Facilities (ALF), and HVS – and the effects of certain parameters – load, temperature, and density – on the reported results.

- Tire Contact Stresses: design a loading device to induce stresses that would be representative of the actual stresses induced by truck tires, based on the tire contact stresses studies.
- New Loading Device: construct and test the new loading device for compatibility and durability issues. Measure the contact stresses under both loading devices – rib and pressurized hose – and compare the stress distribution. Analyze the measured contact stresses with FEM to calculate the stress states in the test specimen, and compare the results for the two loading devices.
- Validate New Loading Device: test two mixtures with known field performance – good and poor – in the modified APA and evaluate the new loading device's ability to produce reliable results.
- Compare Loading Devices: test mixtures with known field performance that the existing APA failed to correctly predict. Compare the results from the modified APA to the field performance of the mixtures.
- Evaluate Factors Affecting Performance Prediction: 1) examine the effects of unidirectional versus bi-directional loading, 2) test at different temperatures and densities to obtain temperature-density trends for rut depth development, 3) examine the effects of sequence of loading. Analyze the test data and establish the test conditions that are critical in predicting rutting performance.
- Validate Proposed Test Conditions: test mixtures with known performance and evaluate the reliability of the results.

CHAPTER 2

LITERATURE REVIEW

2.1 OVERVIEW

In recent years permanent deformation in HMA pavements has generated much concern as many states have experienced an increase in the severity and extent of this type of failure. Research suggests that the steady increase in truck-tire pressure and axle load, which has been noted for the past 20 years, altered the tire-pavement contact stress characteristics. As a result, the pavement surface is exposed to higher stresses than the levels assumed when designing in accordance with the 1993 AASHTO Guide for Design of Pavement Structures.

Concern about high truck-tire pressures and rutting led to a national symposium and sparked interest on tire-pavement interface stresses. Subsequent research concluded that increased truck weights and tire pressures had led to an increase in pavement distress. Measurements of the tire-pavement contact stresses helped identify possible reasons behind surface-initiated cracking and near-surface rutting.

Focus also shifted to material selection, mix design, and construction practices improvements that could minimize rutting. One of the attempts to improve HMA mixture performance was the development and subsequent adoption of the Superpave Volumetric Mixture Design Method. Although the Superpave design procedure resulted in some improvements over previous mixture design methods, it has yet to incorporate a general strength test that would determine the mixture's ability to resist rutting and cracking. The need for a simple 'pass–fail' type of test to complement the Superpave volumetric mix design method forced various agencies to search for a suitable performance test.

This chapter reviews some of the literature available on the subjects of permanent deformation, tire-pavement interface stresses, accelerated pavement testers, and laboratory methods for predicting mixture performance. The literature review focuses more on the three most popular torture tests – HWTD, FPRT, and APA – with more weight on the leading candidate, the Asphalt Pavement Analyzer.

2.2 PERMANENT DEFORMATION

Permanent deformation, also known as *rutting*, is an unrecoverable deformation in the form of a depressed channel in the wheel path of the pavement. Rutting can be attributed to excessive consolidation, formed by an accumulation of permanent deformations caused by repeated heavy loads, or lateral movement of the material, caused by shear failure of the asphalt concrete layer, or a combination of the two.

2.2.1 Consolidation Rutting

Consolidation rutting occurs when one or more layers of the pavement structure (usually the subgrade) undergo further densification by reduction of air voids, or loss of moisture in the case of clay soils. The structure is especially susceptible to this type of distress when there is insufficient compaction during pavement construction. A layer with insufficient density is prone to further densification under traffic, especially in hot weather (for asphalt concrete layers) and at intersections where the loads are slow-moving or static. Figure 2-1 shows a schematic of consolidation rutting which is distinguished by a depression that occurs in the wheel path with no humps on either side of that depression [Huber 1999].

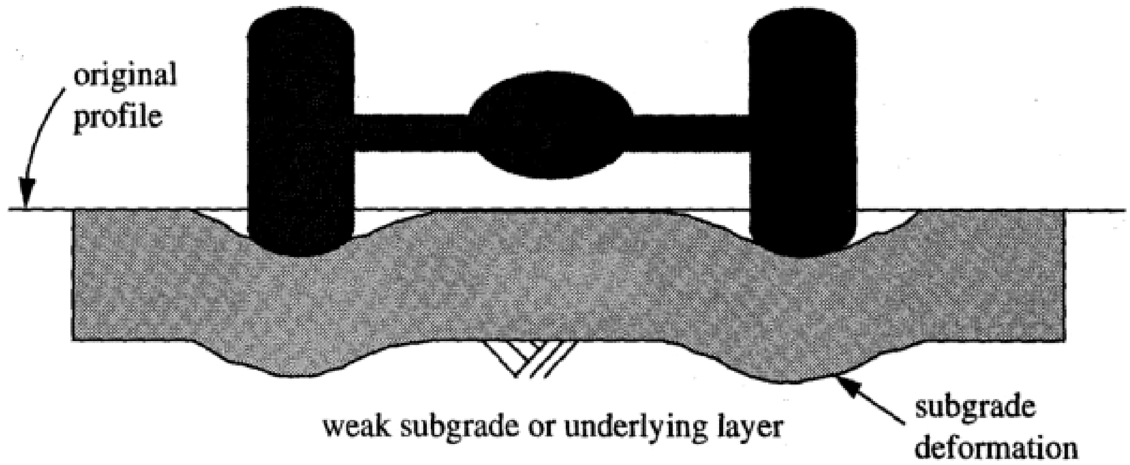

Figure 2-1. Schematic of consolidation rutting.

The subgrade (native soil) is the most vulnerable layer for consolidation rutting because it is the weakest material of the pavement structure. If the pavement structure fails to reduce the vertical stress/strain to allowable limits on the subgrade level, either by improper thickness design or by unexpected increase of load magnitude, under repeated loading the layer will experience excessive consolidation [Huang 1993]. Once the foundation (subgrade) has collapsed, the remaining yielding layers in the pavement structure will conform to the new contour shape of the supporting layer, resulting in subsidence ruts. These ruts tend to be fairly wide (30 - 40 in) with a shallow sloping saucer-shaped cross section [Huber 1999].

2.2.2 Instability Rutting

Instability rutting is strictly an AC layer type of failure, usually within two inches from the surface, and it is attributed to the mixture characteristics of the HMA. The surface material is laterally displaced along shear planes within the AC layer, which shows signs of mixture instability (low shear resistance). Figure 2-2 shows a schematic of instability rutting which is characterized by longitudinal ruts in the pavement with humps of material on either side of the rut [Huber 1999].

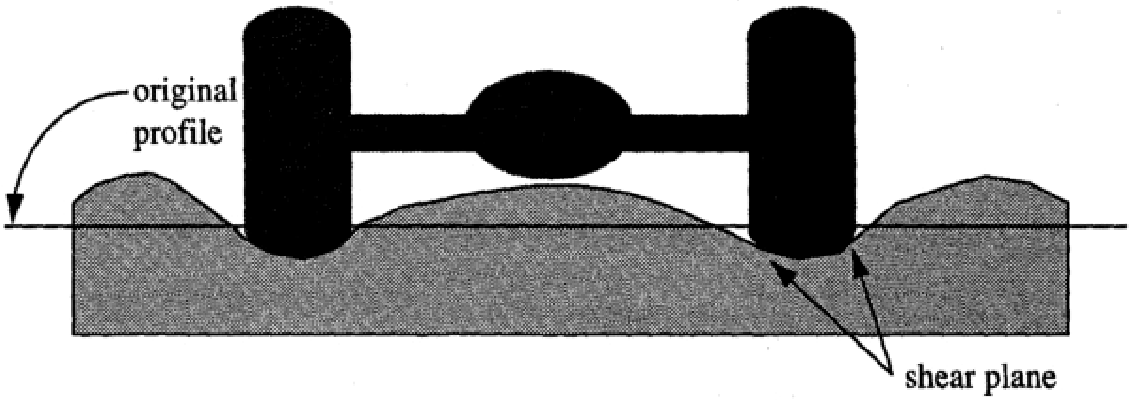

Figure 2-2. Schematic of instability rutting.

Asphalt concrete is a bonded granular material mix of aggregates and asphalt cement. Under repeated traffic loads, the aggregates do not deform but rather rigidly translate and rotate within the asphalt binder [Wang et al. 1999]. This effect (aggregate movement) is amplified at low initial compaction or at high asphalt content. Instability rutting is the surface manifestation of the aggregate skeleton evolution under repeated traffic loading of mixtures with low shear resistance. Temperature, rate of loading, and magnitude of loading directly affect the performance of the mix and influence the severity of this type of distress.

2.3 TIRE-PAVEMENT INTERFACE STRESSES

Engineers have tried for many years to measure the three-dimensional contact stresses between a tire and the pavement. The results of such measurements would help tire engineers to design better, more resilient tires, and would also enable pavement engineers to analyze the stress states under a tire and evaluate their influence on the structure.

Woodside et al. (1992) developed a device to measure the contact stress patch between the tire and underlying material in the laboratory. A steel-bed transducer array measured normal and tangential contact stresses, in static or dynamic mode, under radial tires. The steel plate system was fitted with 12 transducers and repeatedly measured a strip transversely every 5 mm over the entire contact patch. The device recorded 90 contact stress measurements for each test. The contact stresses were then used in the evaluation of durability of surface chippings on asphalt overlays. Results concluded that implementation of surface chippings of 1 mm macro-texture may improve skid resistance on pavements.

Researchers in South Africa measured three-dimensional stresses under bias-ply, radial, and wide-based radial truck tires at different loads and inflation pressures with the Vehicle-Road Pressure Transducer Array (VRSPTA) System [De Beer et al. 1997]. The experimental setup consisted of 13 triaxial strain gauge steel pins (spaced 17mm transversely) mounted on a steel plate and fixed flush with the road surface. Figure 2-3 shows some of the VRSPTA results that reveal a non-uniform vertical and lateral stress distribution.

Dr. Marion Pottinger of Smithers Scientific Services, Inc. (Ravenna, Ohio) developed a device to measure the tire-pavement contact stresses under truck tires. The device measures vertical, transverse, and longitudinal forces and displacements under a moving tire using a series of 16 transducers, as shown in Figure 2-4. The tire is held at one location while the steel bed is moved in the longitudinal direction, forcing the tire to roll over the transducers that measure displacements and stresses. The procedure is repeated by placing the tire at different transverse positions to acquire a detailed pattern of the three-dimensional stresses under the tire. Measurements taken at every 0.14 inches in the transverse and 0.10 inches in the longitudinal direction resulted in about 4000 stress measurements in each of the three axes under the tire-contact area [Myers et al. 1999].

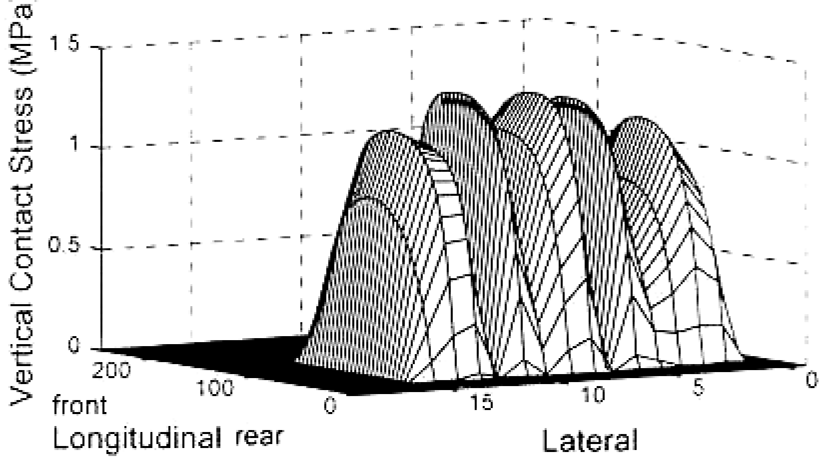

Vertical contact stress distribution.

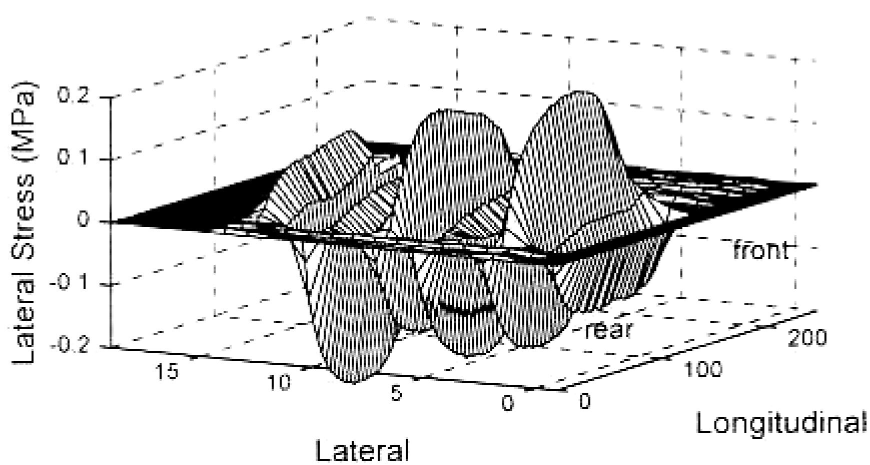

Lateral contact stress distribution.

Figure 2-3. Three-dimensional vertical and lateral contact stress distributions under radial (R22.5) truck tire at rated load [after De Beer et al. 1997].

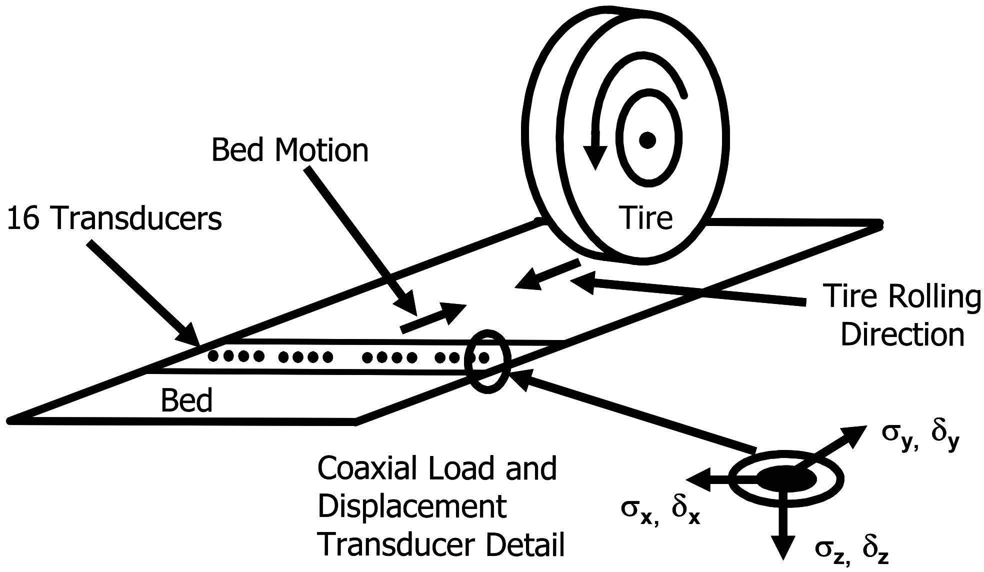

Figure 2-4. Schematic of the Smithers system used to measure tire contact stresses.

Analysis of Pottinger's results gave new information about the way tires load the pavement and the factors that influence the contact stress distribution. It appears that the most important factor is the tire structure. Bias-ply tires have a more flexible tread that allows the tire to bulge out upon inflation. When the tire is loaded the contact area becomes flat and the bulging is reversed, causing transverse stresses to pull the pavement towards the center of the tire. This is commonly referred to as the *pneumatic effect* and it is more prevalent in bias-ply tires.

A phenomenon referred to as the *Poisson effect* has a significant bearing on transverse shear stresses. This effect is based upon the principle that, unless restrained, most materials expand laterally when loaded vertically. When individual ribs under a tire are loaded they attempt to expand laterally, and transverse stresses are generated when the surface of the pavement tries to restrain the expansion. This effect induces transverse shear stresses that pull the pavement apart under each rib.

The Poisson effect, which induces tension under each tire rib, is present in both radial and bias-ply tires. However, because of the large pneumatic effect, tensile stresses are eliminated in all but the center rib of the bias-ply tire. The tensile stresses from the Poisson effect dominate the transverse contact stress distribution in radial tires because the pneumatic effect is negligible. The composite of the pneumatic and Poisson effects for each tire type is shown schematically in Figure 2-5 [Roque et al. 1998].

Recent work at the University of Florida focused on the effects of tire type, loading, and inflation pressure on measured contact stresses under various types of truck tires – radial, bias-ply, and wide-base radial. Stress states induced by radial and wide-base radial tires were determined to be potentially more detrimental to the pavement's surface than stress states induced by bias-ply tires. The tire structure caused a significant difference in the distribution of lateral contact stresses under radial and bias-ply tires, whereas no significant difference was found in the vertical stress distribution.

Distributions of lateral and vertical contact stresses under the three tire types are shown in Figures 2-6 and 2-7, respectively. The studies concluded that the contact stress distributions measured under radial truck tires appear to contribute to the prevalence in recent years of surface-initiated wheel path cracking and near-surface rutting [Drakos et al. 2001, Myers et al. 1999].

2.4 PREDICTING MIXTURE PERFORMANCE

There are three general types of laboratory mixture design and evaluation tests – performance related, performance based, and torture tests. Performance-related tests measure properties or responses related to mixture performance (density, air voids, etc.) but individually are insufficient to drive a performance prediction model. Performance-based tests measure

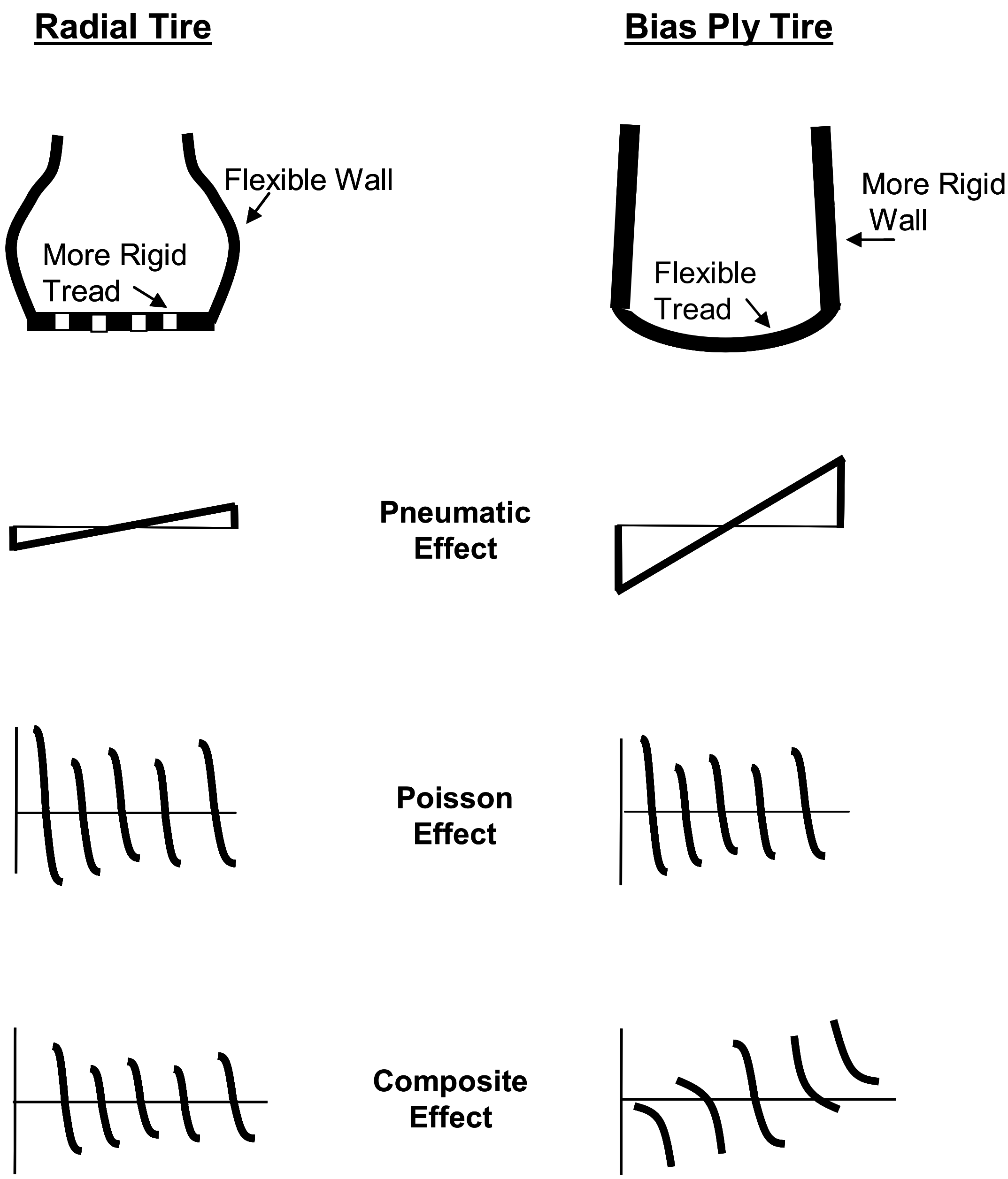

Figure 2-5. Structural characteristics of bias-ply and radial truck tires and their effects on the pavement surface [after Roque et al. 1998].

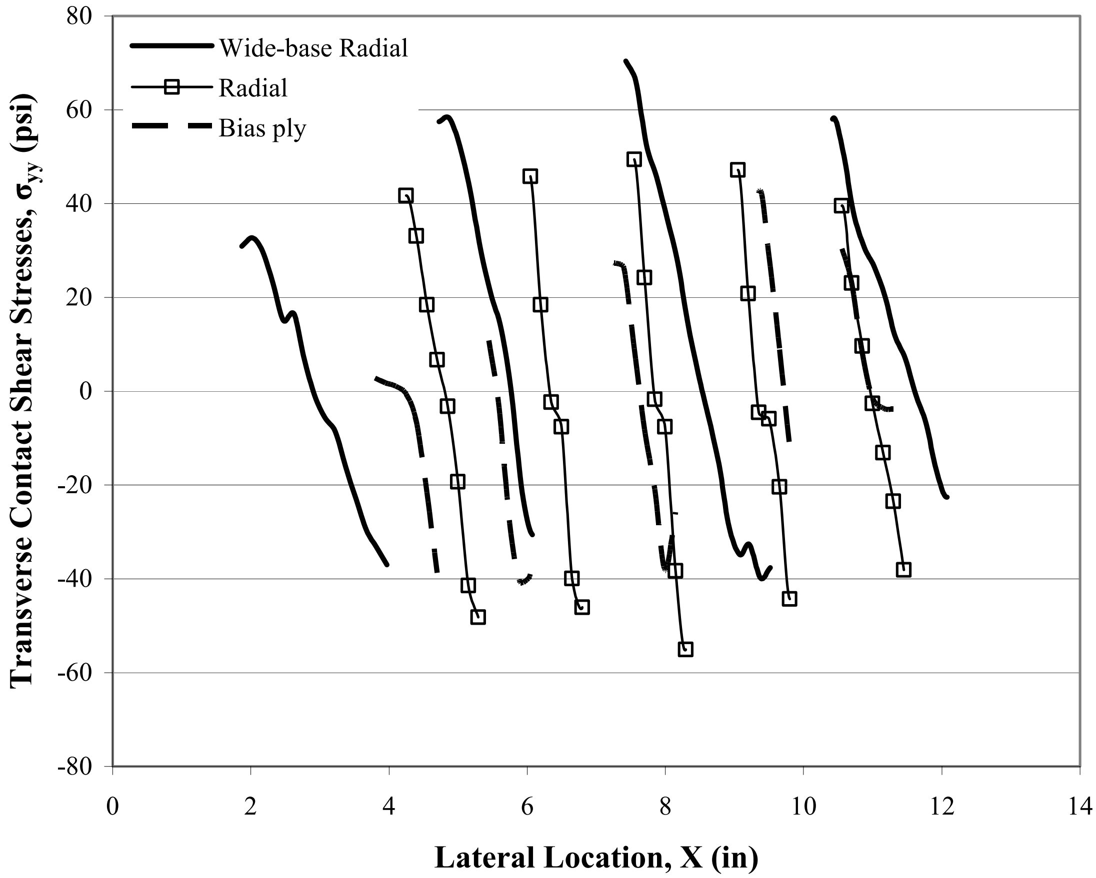

Figure 2-6. Transverse contact shear stresses measured for a bias-ply, radial, and wide-base radial tire at the appropriate rated load and inflation pressure [after Myers et al. 1999].

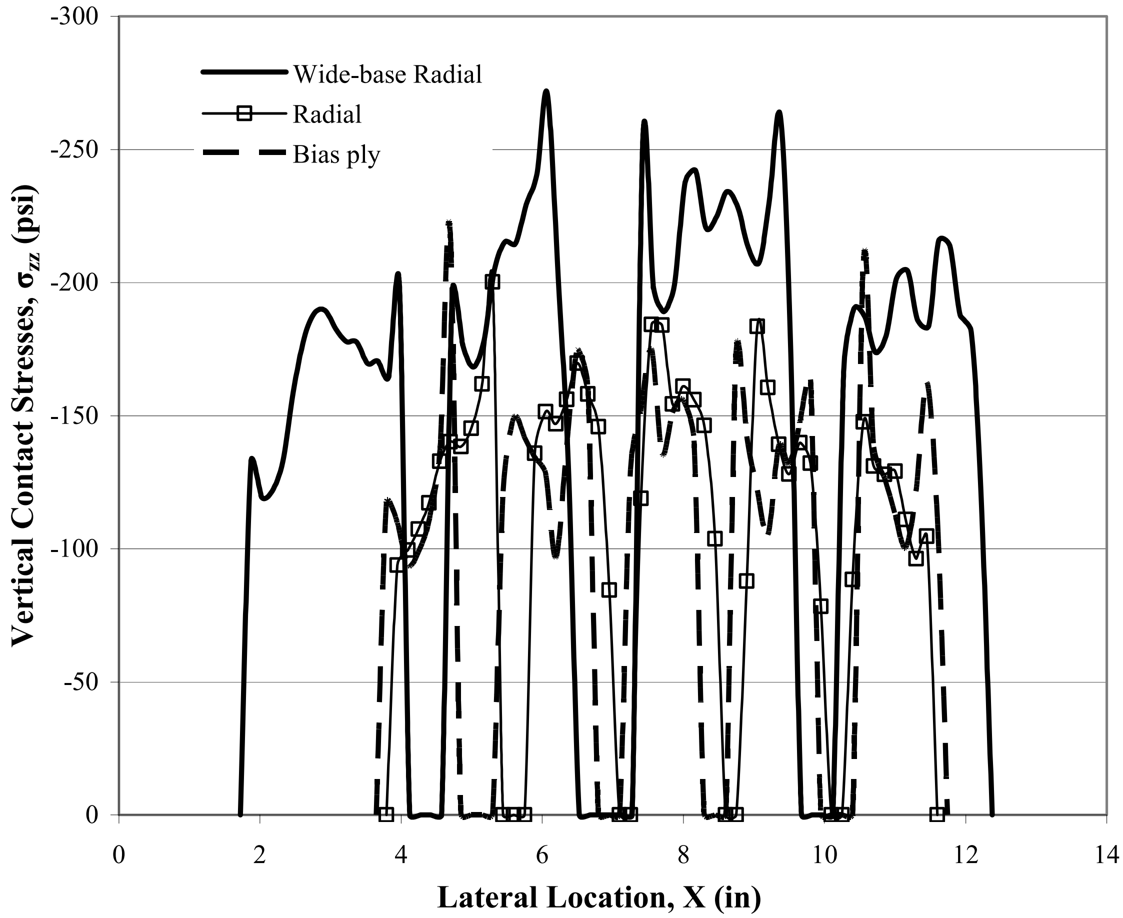

Figure 2-7. Vertical contact stresses measured for a bias-ply, radial, and wide-base radial tire at the appropriate rated load and inflation pressure [after Myers et al. 1999].

material properties (resilient modulus, complex modulus, etc.) that can be used in fundamental response models to predict mixture response to imposed truck and environmental loads. Torture tests, also known as *index tests*, are empirical and apply very severe or extreme loading conditions on the test specimen to evaluate a type of failure condition in the mix [FHWA 1998].

As stated above, there is a growing need for a simple performance test (SPT) that can accurately predict the mixture's ability to resist rutting and cracking. M.W. Witczak defined the SPT as follows:

A test method(s) that accurately and reliably measures a mixture response characteristic or parameter that is highly correlated to the occurrence of pavement distress (e.g., cracking and rutting) over a diverse range of traffic and climatic conditions. [Witczak et al. 2002, p.1]

Based on the definition above, it is not necessary for the SPT to predict the entire distress or performance history of the HMA mixture, but the test results must indicate the mixture's ability to resist fracture and permanent deformation under defined conditions. Various agencies are conducting evaluation studies to identify the most suitable test that would accompany the volumetric design. The following sections discuss some of the most popular candidates: three torture tests and the performance-based Superpave Shear Tester.

2.5 ACCELERATED PAVEMENT TESTERS

The use of accelerated pavement testing (APT) for determining mixture performance has increased in the past 20 years because of APT's ability to apply traffic loads in a short time. APT facilities enable us to evaluate potential materials, designs, and features, in a 'real' (actual size) environment. In a review of existing APT facilities, J.B. Metcalf defined the APT as:

Full scale accelerated pavement testing is defined as the controlled application of a prototype wheel loading, at or above the appropriate legal load limit to a prototype or actual, layered, structural pavement system to determine pavement response and performance under a controlled, accelerated, accumulation of damage in a compressed time period. [Metcalf 1998, p. 556]

The appeal of the APT facilities is that they give the closest simulation to real condition of an actual in-service pavement, in terms of materials and construction procedures, though the effects of aging and the environment are in most cases limited. Most APT facilities use load systems that approximate actual traffic by incorporating wheel wander and unidirectional loading capabilities (the wheel does not load in both directions). These facilities are able to work around the clock and produce early results with a high level of credibility.

In the search for a simple performance test, accelerated pavement testing facilities provide reliable mixture-performance information to evaluate results from various LWTs [Bonaquist et al. 1998, Epps et al. 1997, Romero and Stuart 1998]. These results can be used to evaluate the LWT's ability to capture the true performance characteristics of the HMA.

2.6 SUPERPAVE™ SHEAR TESTER

The Superpave™ Shear Tester (SST), previously known as the *Simple Shear Tester*, was produced by the Strategic Highway Research Project (SHRP) that measures mixture properties to determine pavement performance. The SST is a servo-hydraulic system that can apply axial loads, shear loads, and confinement pressures to asphalt concrete specimens at controlled temperatures while monitoring sample deformation [Shenoy et al. 2001]. The machine has six main components: testing chamber, test control system, environmental system, hydraulic system, air pressurization system, and measurement transducers. Figure 2-8 is a close-up of the testing chamber.

The specimens have a diameter of 150 mm (5.90 in) and a height of 50 mm (1.97 in); however, the system can test specimens with diameters and heights up to 200 mm (7.87 in) with only minor modifications. The environmental system is able to precisely maintain the temperature inside the testing chamber anywhere between 0 and 70^{o}C.

Figure 2-8. The SST test chamber.

Three tests are usually performed with the SST: a) Simple Shear at Constant Height test (SSCH), b) Frequency Sweep at Constant Height test (FSCH), and c) Repeated Shear at Constant Height test (RSCH). The American Association of State and Highway Transportation Officials (AASHTO) Provisional Standard TP7-94 contains a detailed description of the SST test in the different modes of operation.

There is an ongoing evaluation of this test procedure to establish the accuracy and repeatability of results. A study by the Federal Highway Administration (FHWA) showed that the SST tests can accurately discriminate between different asphalt binders, but are insensitive to aggregate changes [FHWA 1998]. Other researchers have reported high variability (15-30%) and that their results depended on the data analysis method [Romero et al. 1998].

An evaluation study performed in North Carolina on three pavement sections with known performance showed that the SST was able to rank the mixtures according to their field performance [Tayebali et al. 1999]. A recent study used the SST and the HWTD to test two mixtures – Superpave and Marshall – for rutting and stripping susceptibility. Both tests – SST and HWDT – gave consistent results and showed that the Superpave mix was more resistant to permanent deformation [Wang et al. 2001].

2.7 TORTURE TESTS

Torture testing devices subject a test specimen of the mixture to repeated loading applied by a traveling wheel. The tests do not require any preparation other than the molding of the specimen, and the results usually report the rut depth on the mixture specimen as a function of the load applications. Some of the most popular torture testing devices include the APA, the HLWT and the FPRT, all of which use the same basic principle that the rut depth measured from the specimen can be correlated to field performance.

Although the idea is simple and seems to pinpoint a direct measurement that can be an indication of the mixture's performance, recent studies have shown that the tests failed to distinguish between good and poor performing mixtures [Collins et al. 1996, Stuart et al. 1997]. The load-transfer mechanism, boundary conditions (confinement), and the ratio of the size of the loading wheel to the aggregate size are some of the reasons that limit the success of LWTs [FHWA 1998].

Overall, the idea of the loaded wheel tester has a very intuitive appeal because it is simple, relatively low cost, and easy to use. However, the tests correlate the rut-depth measurement directly to field performance without identifying any fundamental properties that will help us improve our mixture design.

2.7.1 Hamburg Wheel-Tracking Device

The Hamburg wheel-tracking device measures the combined effects of rutting and moisture damage by rolling a steel wheel across the surface of an asphalt concrete sample immersed in hot water. Esso A.G. of Hamburg, Germany developed the device in the 1970, and originally called it the “Esso Wheel-Tracking Device.” Initially, the City of Hamburg used the testing machine to measure rutting susceptibility of HMA. The sample was subjected to 9,540 wheel passes at 40 or 50^{o}C, and the resulting rut depth was used as a pass/fail criterion to ensure mixture performance [City of Hamburg 1991].

Today, the Hamburg testing machine is manufactured by Helmut-Wind, Inc. of Hamburg, Germany. It can test two asphalt slab samples simultaneously with dimensions of 320 mm in length by 260 mm in width, and thickness of 40, 80, or 120 mm. The samples are prepared to 7 ± 1 % air voids, and are submerged into 50^{o}C water for the test. A steel wheel, measuring 203.5 mm (8 in) in diameter and 47 mm (1.85 in) in width, loads each sample with a fixed load of 705 ± 22 N (158 ± 5 lbs) at a rate of 50 passes per minute [Aschenbrener, Texas Department of Transportation]. A linear variable differential transformer, with an accuracy of 0.01 mm, continuously measures the rut depth in each slab and prints out the data every 20, 50,100, or 200 wheel passes. Figure 2-9 is a picture of the Hamburg wheel-tracking device without the data-acquisition machine.

Various institutions use different criteria and testing procedures to evaluate mixes in the Hamburg device. The City of Hamburg uses a maximum allowable rut depth of 4 mm at 19,200 wheel passes, whereas the Colorado Department of Transportation (CDOT) recommends maximum allowable rut depths of 4 mm at 10,000 and 10 mm at 20,000 cycles [Aschenbrener].

Figure 2-9. The Hamburg wheel-tracking machine.

In an evaluation study at the FHWA, researchers tested the rutting susceptibility of certain mixtures with the full-scale ALF and compared the ALF results to the predicted performance from the HWTD. The study noted that the tracking device could discriminate mixtures with widely different binder grades, but failed to give consistent results for mixtures with closer grade binders. Furthermore, the research showed that the HWTD was unable to predict a decrease in rutting susceptibility for mixtures with altered gradation (maximum nominal aggregate size), even though test results from the ALF clearly showed less rutting [Stuart and Mogawer 1997, Stuart and Izzo 1995].

2.7.2 French Pavement Rutting Tester

The French Pavement Rutting Tester tests slabs of HMA to evaluate their resistance to permanent deformation. The machine, shown in Figure 2-10, uses an environmental chamber to keep the test temperature at 60°C and loads the sample with a smooth, reciprocating, pneumatic rubber tire inflated to 0.60 ±0.03 MPa (87 ±4 psi). Similar to the Hamburg tester, the FPRT can

Figure 2-10. The French pavement rutting tester.

test two slabs simultaneously measuring 500 mm (19.7 in) long, 180 mm (7 in) wide, and 50-100 mm (1.97-3.93 in) thick. Hydraulic jacks push the slabs upward to apply the 5,000 ±50 N (1,124 ±11 lb) load [Corté and Serfass 2000].

The test sequence includes 1,000 cycles at 150-25^{o}C to simulate traffic densification and to take initial slab thickness measurements. The slabs are then conditioned for 12 hours at 60 ±2^{o}C before the start of the test. The average rut depth in each slab is measured manually at 30, 100, 300, 1,000, and 3,000 cycles when testing 50-mm slabs, and at 300, 1,000, 3,000, 10,000, and 30,000 cycles when testing 100-mm slabs. Finally, the average percent rut depth is calculated based on the initial thickness of the slab [Corté and Serfass 2000].

The FHWA evaluation study mentioned in the section above [Stuart and Mogawer 1997] reported results for the FPRT. Similar to the HWTD, the French pavement rutting tester accurately discriminated mixtures with widely different binder grades, but lacked precision in identifying mixtures with distinctly different gradations.

2.8 ASPHALT PAVEMENT ANALYZER

In 1985 the Georgia Department of Transportation (GDOT), in association with the Georgia Institute of Technology (GT), initiated Research Project No. 8503 for the development of a pass/fail laboratory test for the rutting resistance of HMA. The prototype GLWT was a modification of the Benedict Slurry Seal tester, originally designed to test slurry seals [Collins et al. 1995].

The initial version of the GLWT consisted of an aluminum wheel attached to a reciprocating arm moved along a pressurized hose, creating the desirable contact pressure. Constant temperature was maintained during testing by placing the LWT in an airtight room, where an electric heater with a thermostat was used to heat the room to 95^{o}F. The test was performed with 75- or 100-psi hose pressure, and 50-, 75- or 100-lb load. Rut measurements were taken at 40, 100, 400, 1000 and 4000 cycles [Lai 1986].

To promote the concept of using GLWT as a supplemental strength test to the Superpave design procedure, the device was modified in 1992 to be able to evaluate rutting potential of samples prepared by the Superpave gyratory compactor. The new device had the ability to test six gyratory samples simultaneously in an environmentally controlled chamber. Other modifications included operation control, adjustable hose pressure (up to 120 psi), and load (up to 250 lbs) [Collins et al. 1996].

The APA is a further modification of the GLWT, first manufactured in 1996 by Pavement Technology, Inc (PTI). Since it is a new generation of the GLWT, it follows the same testing philosophy. Load is applied onto a pressurized linear hose by a pneumatic loaded wheel and tracked back and forth over a testing sample to induce rutting. The APA has the additional capability of testing for moisture susceptibility and fatigue cracking while the specimens are submerged in water.

Extensive studies have been conducted to evaluate the ability of the APA to distinguish between mixtures of known performance. Most of these studies tried to establish a relation between rut depths obtained in the laboratory tests and the field performance of the mixture.

The Florida DOT has performed a series of tests with the APA. Although the device successfully ranked mixtures according to their rutting potential, some variability from test to test and from location to location was found. It was also reported that gyratory samples and beams rut at statistically different levels [Choubane 1998]. To reduce variability, PTI installed new pressure regulators and reconfigured the air supply tubing, but a subsequent study indicated that although variability was decreased the middle position consistently yielded in higher rut depths than the left or right positions [Sholar 1999].

A similar study compared test results from WesTrack [Epps et al. 1997] to rutting predictions from three LWT devices. The APA ranked the mixtures according to their WesTrack performance with 89% accuracy [Williams et al. 1999]. The National Center for Asphalt Technology (NCAT) indicated that the APA was sensitive to mixtures with different asphalt binder and varying gradation (ARZ, BRZ, and TRZ) [Kandhal et al. 1999].

The FHWA also conducted a study at Turner-Fairbank Highway Center. Comparison of LWTs test results to the ALF showed that the LWTs were able to distinguish between mixtures that had good and poor performances when those were prepared with the same aggregate gradation and different binder. When the aggregate gradations were varied, none of the LWTs were able to separate the mixtures, even though the ALF testing showed that there were significant differences in pavement performance [Romero and Stuart 1998].

2.9 SUMMARY

The discussion presented in this chapter indicates that no one SPT can reliably predict HMA performance. The SST, although it is a mechanistic-developed test, is a very expensive and complex machine to operate, making it unsuitable for a simple performance test. From the three torture tests reviewed – HWTD, FPRT, and APA – the Asphalt Pavement Analyzer seems to be the leading candidate.

Recent evaluation studies showed that the APA has the potential to accurately rank mixtures according to their field performance. However, the APA proved to be unable to capture the difference in performance for mixtures with altered gradation.

Based on this literature review, it is essential to identify the critical design condition(s) (mechanisms) that might lead to near-surface rutting. We must attempt to replicate these conditions in a laboratory physical model (torture test). A physical model that will employ this set of critical conditions might produce more reliable results for mixture rutting performance.

CHAPTER 3

APA LOADING MECHANISM

3.1 OVERVIEW

Tire-pavement interface contact-stress studies indicated the importance of lateral stresses in the development of critical stress-states near the surface of the pavement [Drakos et al. 2000, Myers et al. 1999]. These studies have shown that radial tires induce stresses that are more detrimental to pavements than bias-ply tires and that the difference has been attributed mainly to tire structure.

The theory behind torture tests such as the APA is that a specimen is subjected to an accelerated loading sequence in the laboratory and the end-result (rut depth) can be correlated to the rutting performance of the mixture in the field. However, the ability of the test to replicate field conditions in the laboratory determines the reliability of the results. The hypothesis was that the APA loading mechanism was not capturing the lateral stresses found under radial tires.

The idea that the APA hose could not generate these lateral stresses was based on initial observations of the contact area between the sample and the hose which was measured at approximately 8 mm. This limited contact area cannot reproduce the Poison's effect found under each individual rib on the tire tread. This chapter deals with the effort to develop an alternate loading device geared to capture some of the complex stress distributions found in the field.

3.2 LIMITATIONS OF LOADED WHEEL TESTERS

Loaded wheel testers operate on the same basic principle: a test specimen of mixture is subjected to repetitive loading by a traversing wheel, and the surface depression in the sample is then measured and reported as a function of load cycles. These types of torture tests are classified as empirical or performance-related tests because they do not measure a fundamental property that can be used to explain and identify the mechanisms resulting in surface distress.

The APA, like most of the LWTs, attempts to replicate field conditions in a controlled laboratory environment. In this sense, good correlation between results from the APA with field performance relies on how well (realistically) conditions have been simulated in the lab. The following issues raise some considerations on the ability of the APA to approximate field conditions:

- Loading scale effects. The loaded area under the pressurized hose is very small (narrow) in proportion to the nominal maximum aggregate size [FHWA 1998, Lai et al. 1990].
- Boundary conditions. In the APA the test specimens are resting on a metal plate that limits deflections and increases confinement.
- Load application. Earlier work [De Beer et al. 1997, Myers et al. 1999] showed that radial truck tires induce high lateral stresses that can cause tension on the surface of the pavement [Drakos 2000]. It is believed that the pressurized hose of the APA does not simulate the effects of the stiff treat of the radial tire, thus not inducing any lateral stresses.

Lai and Lee (1990) evaluated the stiffness effects of the pressurized hose by testing asphalt samples with a relatively stiff and a relatively soft hose. Figure 3-1 shows the imprints of the contact area used for comparison purposes. As expected, under the same load, the stiffer hose generated a more elongated and narrow contact area whereas the softer hose produced a shorter and wider contact area.

Although the researchers believed that the stiffer hose would generate greater rutting, a series of tests proved that the softer hose consistently gave slightly higher rut depths. Unfortunately, there are no direct measurements of the contact stresses between the hoses and the asphalt specimen surface. Nonetheless, this finding is of great importance to the development of the new loading configuration because it demonstrates the significance of stress distribution to the rutting behavior of samples in the APA.

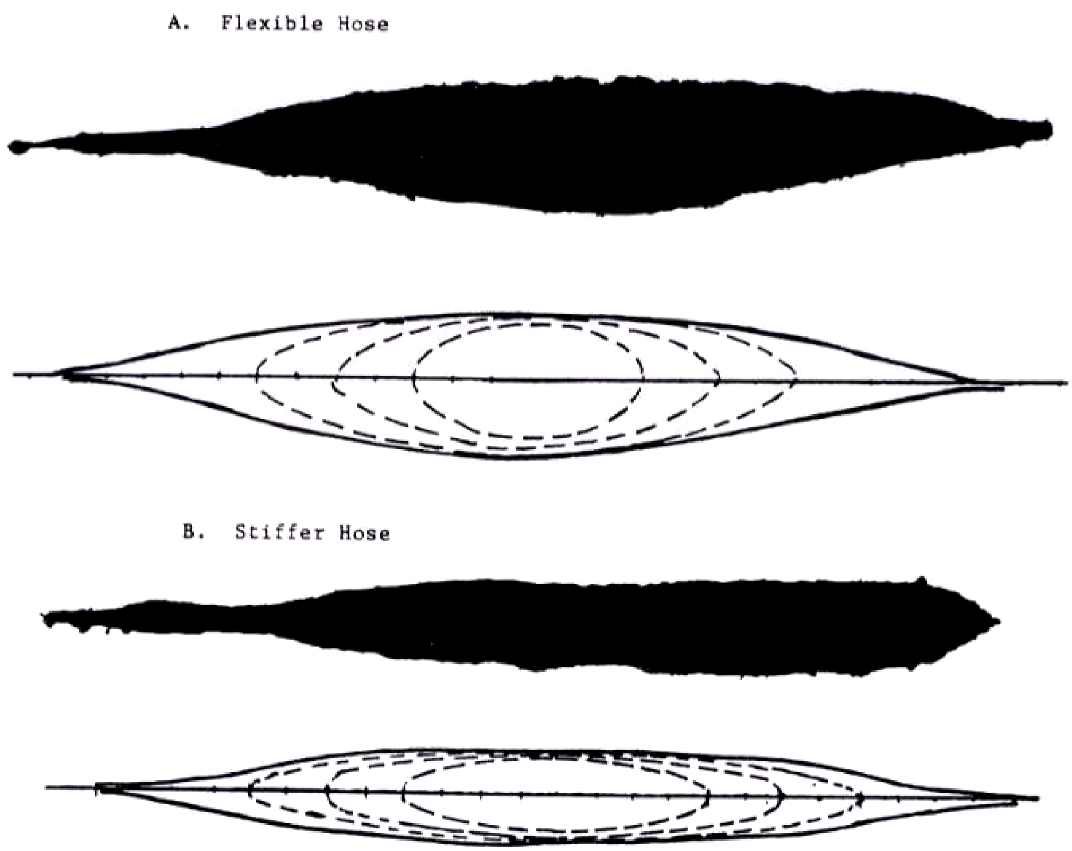

Figure 3-1. Contact imprints of the rubber hoses with asphalt beam sample [after Lai and Lee 1990].

3.3 NEW APA LOADING MECHANISM

The concept for a new APA loading mechanism is based on the observations and conclusions from the tire-pavement interface stresses studies. Analyses performed with the elastic layer analysis program BISAR and the finite element program ADINA provided information on the pavement's response under modeled tires from measured contact stresses. Myers et al. (1999), Drakos et al. (2001), and Birgisson et al. (2002) have identified the lateral stresses induced by radial tires as the fundamental cause of stress reversals (tension) and high magnitude shear stresses near the surface of the pavement. These stress states cause a reduction in confinement near the pavement's surface near the edge of the loaded area, which reduces the resistance to shear stress within the mixture.

The hypothesis was that the stiff pressurized hose used by the APA to load the specimen does not reproduce the lateral stresses found under radial truck tires. The objective was to develop a new loading mechanism, modeled after a radial truck tire, to replicate these stress conditions in the APA specimen.

3.3.1 Development of a Tire Model

The initial task was to develop a reasonable tire model that represents the structural behavior and response of a typical radial truck tire tread. Earlier work by Roque et al. (2000) showed that the radial tire loading behavior can be simulated with a combination of steel and rubber. This step would enable us to estimate the right amount of steel and rubber needed to built a device that captures the loading behavior of the radial tire. Figure 3-2 shows the structural characteristics of a radial truck tire with the radial plies and the steel strands that run through the rubber, around the tire.

Radial and bias-ply tires are totally different from a structural point of view and the actual structural make-up of these tires is proprietary information not available to the general public. However, Smithers Scientific Services, Inc. provided some basic response data regarding the behavior of typical radial truck tires and their structural characteristics that were used along with a basic knowledge of the structural behavior of radial truck tires to develop a two-dimensional model of a radial truck tire tread [Myers 2000].

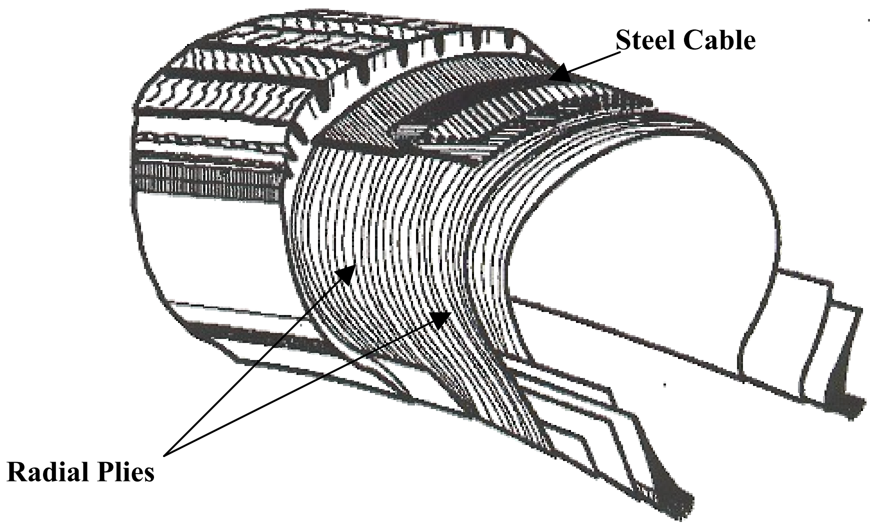

Figure 3-2. Structural characteristics of a radial tire.

As previously discussed, the structural behavior of radial truck tires is governed by a wall structure of very low stiffness and a very stiff tread structure resulting from the steel strands used to reinforce the tread. The cross section of a typical radial tire is illustrated in Figure 3-3 and shows a tread area that is 8.0 inches wide and 1.44 inches high. The steel reinforcement was concentrated in an area that is 0.33 inches high, approximately 0.93 inches above the outer surface of the tire.

Following the guidelines from Roque et al. (2000), the model was constructed with the MSC/Patran pre-processor software and it is illustrated in Figure 3-4. The steel strands were modeled as a solid strip of steel, and the connection between the steel strands and the rim was modeled as a pin connection at either end of the steel strip used to represent the strands. Table 3-1 presents the modulus and Poisson's ratio values used for the tire rubber and the steel strip. Finally, the ABAQUS finite element program was used to run the elastic analysis and retrieve the deformation and stress distributions under the tire model.

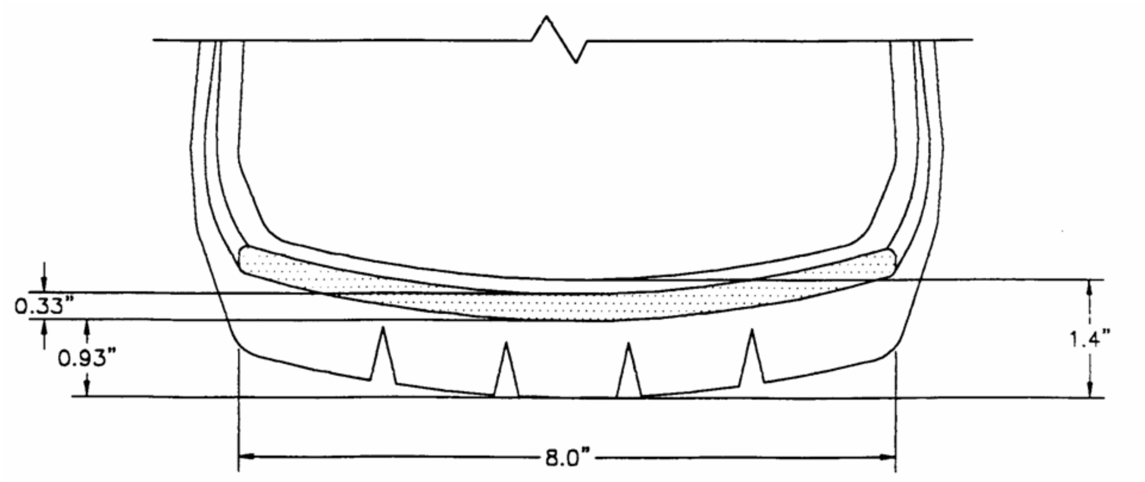

Figure 3-3. Schematic cross-section of a typical radial tire.

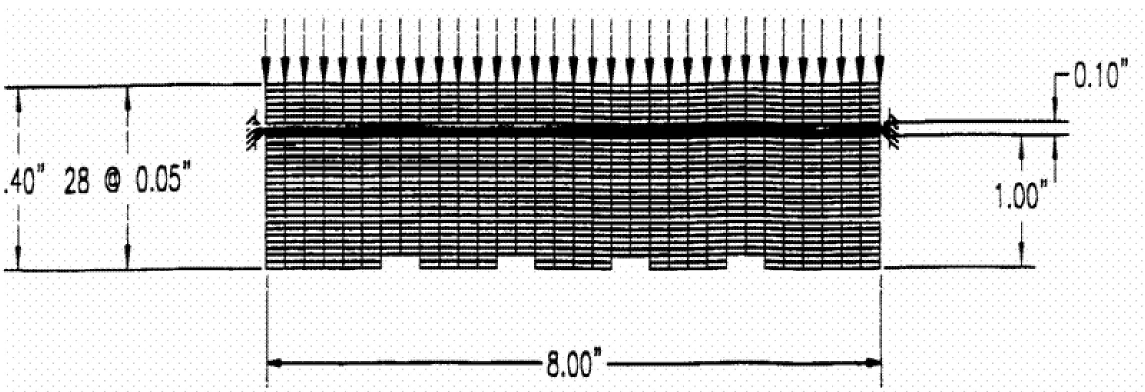

Figure 3-4. Finite element representation of the tread structure of a radial tire.

Table 3-1. Material properties used in the tire FEM.

Tire Part	Material	Elastic Modulus, E (psi)	Poisson's Ratio, ν
Reinforcing Beads	Steel	2.90E+07	0.15
Tire Tread	Rubber	1.16E+03	0.48
Tire Grooves	Air	9.80E-06	0.49

3.3.2 Verification of the Tire Model

As mentioned in Section 2.3, Dr. Marion Pottinger of the Smithers Scientific Services, Inc. successfully measured the tire-pavement contact stresses under truck tires. Pottinger's device measured vertical, transverse, and longitudinal forces and displacements under a moving tire using a series of 16 transducers on a steel plate. To verify the accuracy of the model, Pottinger's contact stress measurements were compared to stresses predicted under the FEM tire on a steel foundation.

The final thickness of the steel strip was determined by varying the thickness until the predicted stress response of the modeled tire matched the measured response of the real tire. Thus, the FEM tire matched the overall stiffness and stress-distribution behavior of the tire tread. It was determined that a 0.1-inch-thick steel strip embedded in the modeled tire tread resulted in the same structural response as the steel-strand reinforcement in the actual tire.

Figures 3-5 and 3-6 – vertical and transverse stress distribution respectively – indicate that the tire model predicted both vertical and transverse contact stresses similar to those measured under the real tire. Although there is some variation in magnitude, the tire model accurately captured the patterns of both the vertical and transverse contact stress distributions.

Figure 3-6 is particularly important because it demonstrates the model's ability to capture the transverse contact stress reversals under the individual tire ribs. As stated earlier, these transverse stresses were found to be detrimental to the top-down cracking and near-surface rutting performance of HMA. The next step was to build an individual rib replica that would serve as the load transfer mechanism in the APA.

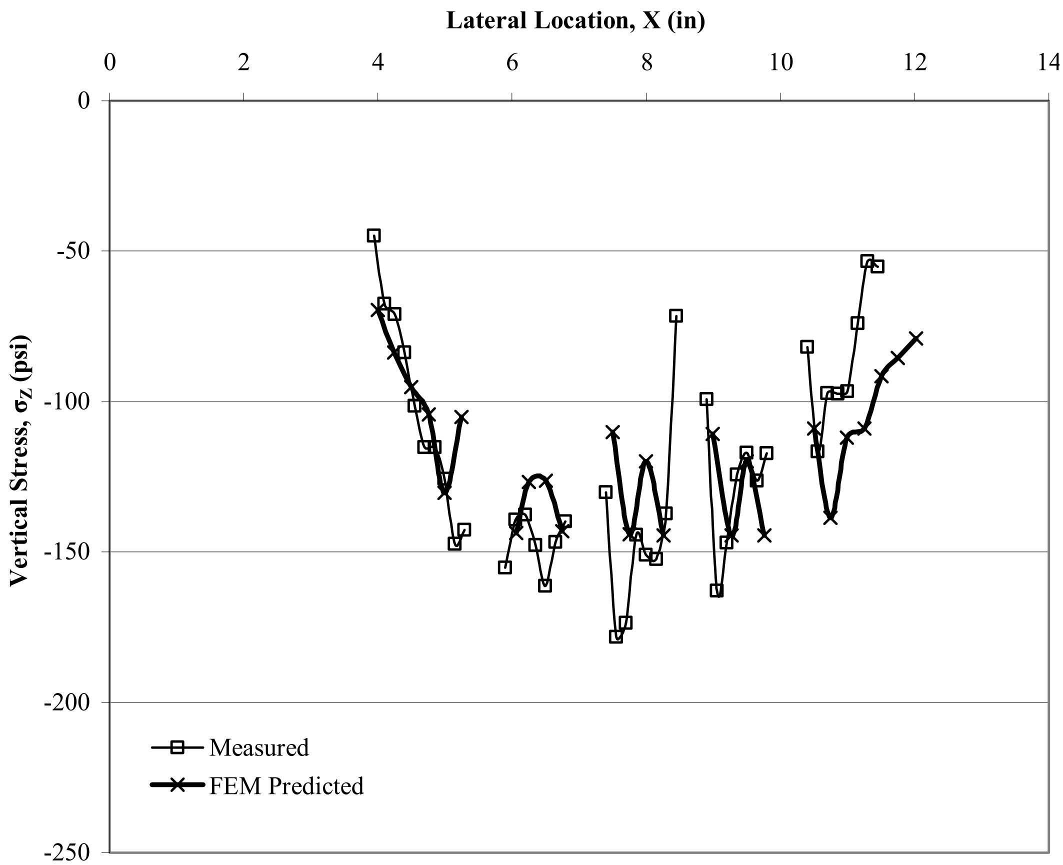

Figure 3-5. Measured and predicted vertical stress distribution at surface of steel bed.

3.3.3 Concept Loading Strip

In the previous section, analyses showed that the FEM tire was able to capture the complex stress distribution measured under a radial tire. The idea for the APA loading mechanism was to substitute the pressurized hose with a steel-rubber configuration based on the tire finite element model. Figure 3-7 shows a schematic of the concept device, called the *loading strip*, where a thin rectangular steel plate (14 gauge) is attached on top of a medium-durometer (45-55) rubber. The solid steel wheel applies the load on the thin steel plate that distributes the stresses on the sample through the rubber part of the device.

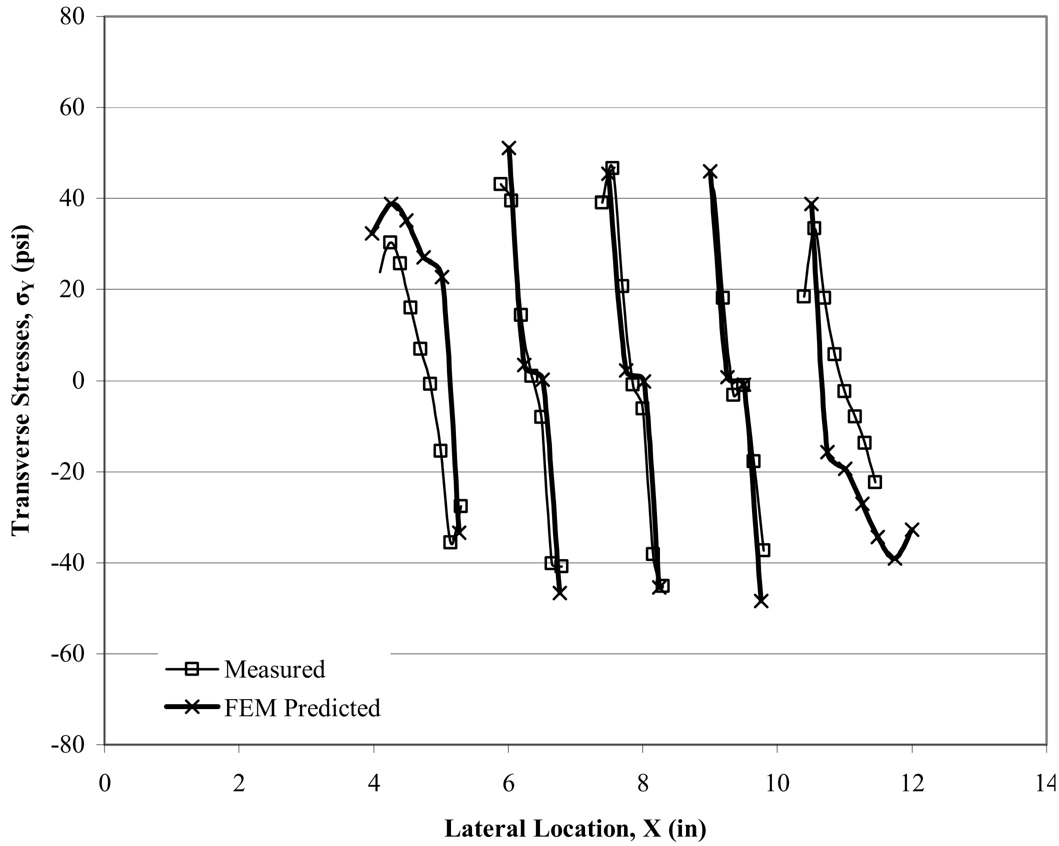

Figure 3-6. Measured and predicted transverse stress distribution at surface of steel bed.

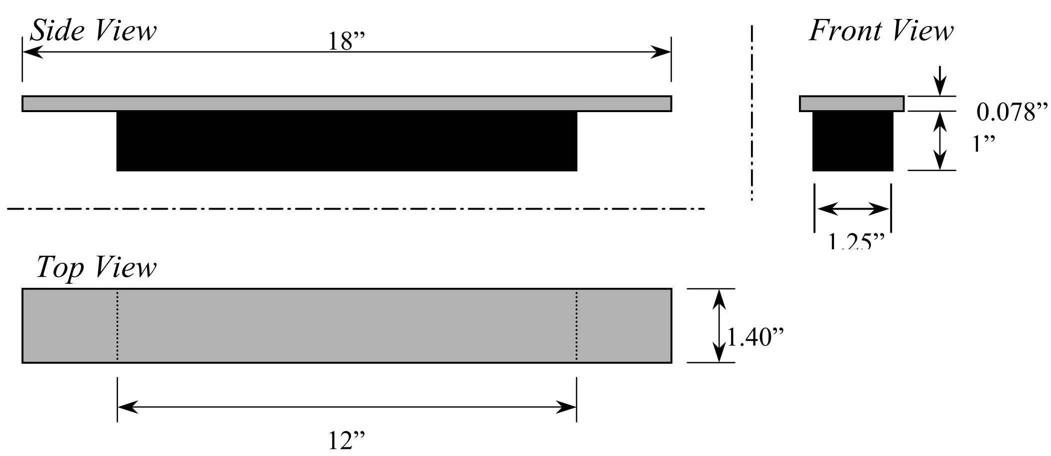

Figure 3-7. Schematic of the loading strip.

Ideally, the loading strip stress-distribution behavior would represent that of a single rib from the radial tire tread. The magnitude of the applied stresses was anticipated to be significantly lower; however, the stress-distribution pattern was expected to be similar. The steel plate would uniformly distribute the stresses to the rubber and also increase the stiffness of the device, whereas the rubber member would apply the vertical load and also create the Poisson's effect that induces lateral stresses as found under radial tires.

3.4 PRELIMINARY CONTACT STRESS CALCULATIONS

The preliminary contact stress calculation was the first confirmation that the loading characteristics of the two devices were different. It was important, however, that the average vertical stress (σ_{z_avg}) under the loading strip did not exceed that of the pressurized hose. This ensured that the main difference in the contact stress distribution was the presence of lateral stresses under the loading strip.

Initially, carbon paper was placed under the APA hose to measure the contact area, but at static mode the imprint was not clear. Then, at a hardware demonstration at the DOT, a technician measured the actual contact stresses using a pressure-sensitive mat. For the loading strip, a finite element model was used to predict the stress distribution at the rubber-specimen interface before it was physically constructed.

3.4.1 APA Pressurized Hose Stresses

Tekscan Inc. provided an initial estimate of the vertical stress distribution under the pressurized hose when a technician visited the FDOT for a presentation of the company's Pressure Measurement System (PMS). The Tekscan PMS is an extremely thin (~0.1 mm), flexible tactile force sensor that is capable of measuring pressures from 0-2 psi (0-15 kPa) to 0-

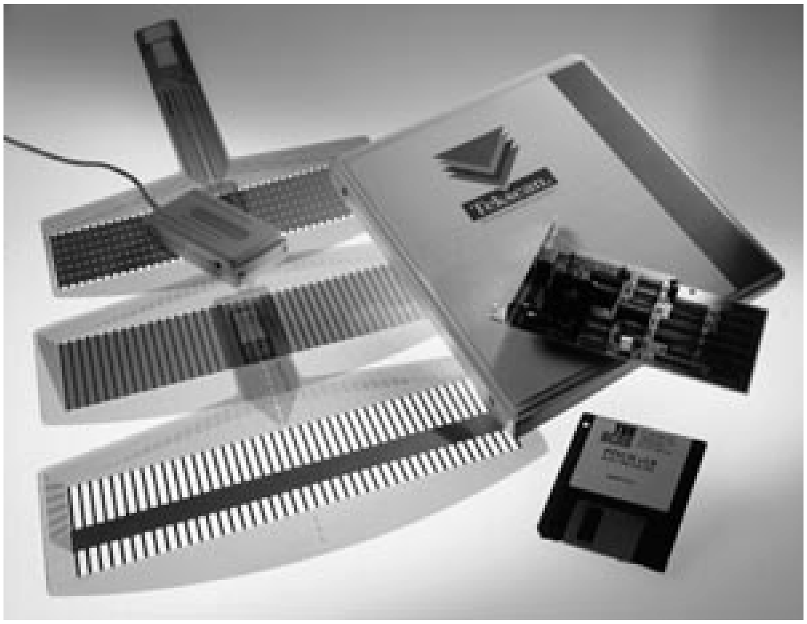

Figure 3-8. Tekscan pressure measurement system.

25 ksi (0-175 Mpa). Figure 3-8 shows the wide range of shapes, sizes, and spatial resolutions (sensor spacing) of available sensors. Sensing locations within a matrix can be as small as 0.0009 square inches (0.140 mm^2); therefore, a one-square-centimeter area can contain an array of 170 of these locations [Tekscan, Inc.]. The Virtual System Architecture (VSA) integrates the sensors into a uniform whole and displays the information on a computer screen.

Tekscan's products function in both static and dynamic measurement environments, allowing the development of load profiles and peak load attainment. During the demonstration, the technician placed the sensor mat under each of the three pressurized hoses in the APA, and recorded the vertical contact stresses while the machine was operating (dynamic mode). This data-acquisition method provided a vertical stress profile under the hose for the entire run (back and forth) throughout the specimen. Since neither UF nor the FDOT owns a Tekscan measurement system, the access to the data was limited.

The recorded vertical stresses revealed that their distribution is not even along the specimen. Figure 3-9 illustrates the measured vertical stress distribution under the pressurized hose (100 psi) with a wheel load of 100 lb. The color gradient indicates the stress intensity ranging from light gray (low pressure, <10 psi) to black (high pressure, >80 psi). The stress distribution in Figure 3-9 shows two dark-shaded peaks (high stress) at the edges of the contact area. Initially this anomaly was attributed to the uneven surface of the specimen and, more specifically, from large aggregate that might be bridging the hose over some small gaps. Later on, based on the hose contact stresses measured on a steel bed, it appeared that these peaks were a hose-structure phenomenon that will be discussed in greater extent in the following sections.

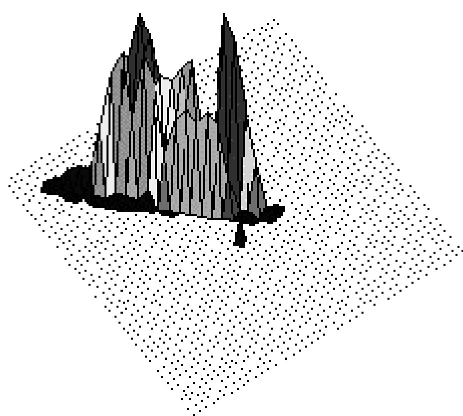

Figure 3-9. Graphical interpretation of vertical stresses under the pressurized hose.

The software approximates the contact area based on the number of cells that report pressure. In the case of the APA, there was some residual stress from the lowering arm (the frame that holds the hoses in place) that was touching the mat. Analysis of the spreadsheet provided by the Tekscan technician yielded to an estimated contact area of 1.54 in^2 (993.5 mm^2), which gives an average vertical stress of 64.9 psi (477.8 kPa).

3.4.2 Loading Strip FEM

Before fabrication, the concept device was modeled in finite elements to estimate the stress distribution at the loading strip-specimen interface. Figure 3-10 shows a side view and a top view of the three-dimensional model used for the stress analyses. An estimate of the stress distribution under the loading strip was important to ensure that the average vertical stress (σ_{z_avg}) under the loading strip would not exceed the σ_{z_avg} under the pressurized hose.

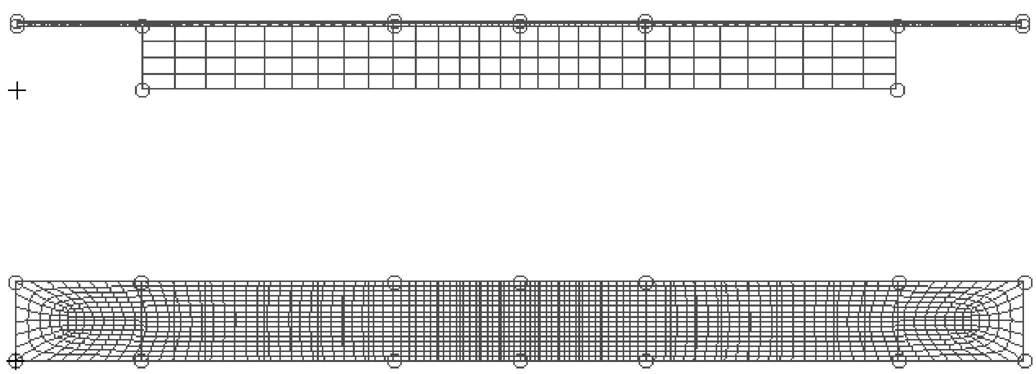

Figure 3-10. Finite element model of the loading strip.

The finite element model was constructed with the MSC/Patran pre-processor software and the elastic analyses run with the ABAQUS engine. The model consisted of 20-node 'brick' elements, and the material properties used for the steel and rubber parts of the loading strip are the same as in the tire model (Table 3-1).

Because of the rectangular shape of the rubber on the loading strip, it was easy to assume that the width of the contact area would be constant at 1.25 inches. Thus, the only requirement to approximate the contact area was to estimate the length of the pressure patch. It was clear that the contact area under the loading strip would greatly exceed the initial contact area of the APA hose. The initial contact area under the hose differs from the final because, as the material deforms, the hose 'sinks' into the material, increasing the contact area.

Based on the assumption that the contact area would be greater under the loading strip, the FEM model was analyzed at a higher load level (150 lb) to calculate the extent of the pressure patch and the average vertical stress. The FEM predicted the pressure-patch length to 4.5 inches; thus the resultant area was 5.6 in^2 and the average stress approximately 26 psi.

3.5 MEASURED CONTACT STRESSES IN THE APA

At the beginning of this chapter the hypothesis was that the pressurized hose of the APA does not capture the essential lateral stress distribution found under radial tires. A new concept loading device (loading strip) was designed and tested with the help of numerical modeling that would simulate real tire stress distribution. In order to verify the above hypothesis, both loading devices – pressurized hose and the loading strip – were sent to the Smithers Scientific Services plant in Ravenna, Ohio, to measure the actual contact stresses at the loading device-specimen interface.

3.5.1 Measurement System

As mentioned in Section 2.3, Smithers Scientific Services, Inc. developed the Flat Surface Tire Dynamics Machine (FSTDM) to measure contact stresses at the tire-pavement interface. The device measures vertical, transverse, and longitudinal forces and displacements under a moving tire by using a series of 16 transducers.

Dr. Pottinger fabricated custom end-restraints and a loading foot that allowed load control to within ±1 lb, to accommodate the pressurized hose and the loading strip on the

FSTDM. Figure 3-11 shows a picture of the FSTDM with the loading foot during calibration. The 500-lb cell was calibrated using a pedal force transducer, as seen in the lower right-hand corner of the picture.

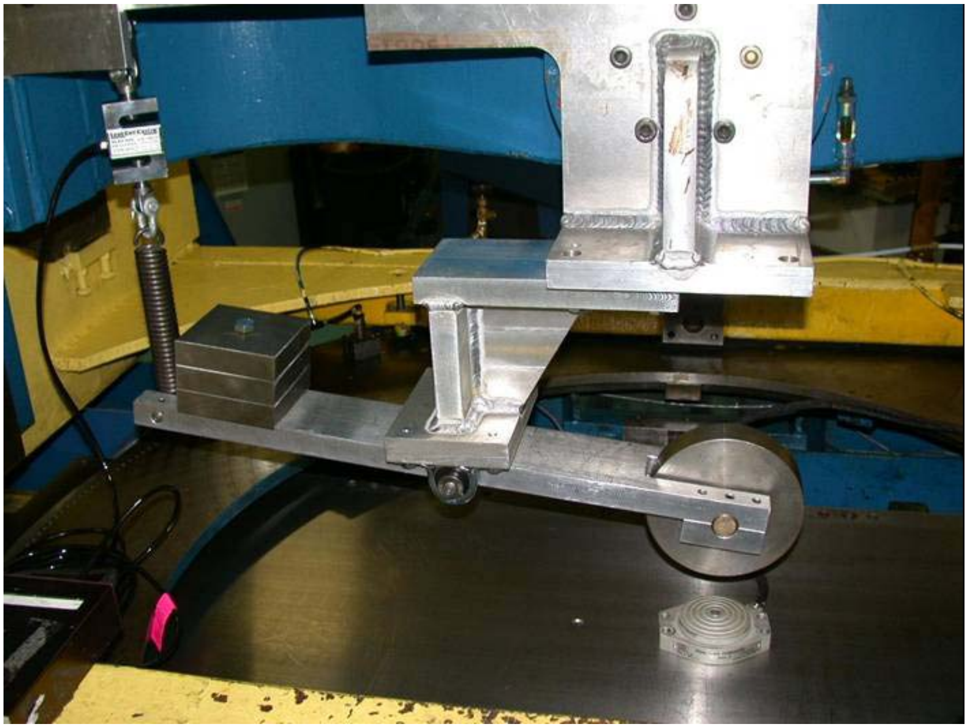

Figure 3-11. Contact stress measuring apparatus setup and calibration.

The loading strip was tested with three different loads – 110-, 130-, and 150-lb – whereas the pressurized hose was tested at two load levels – 100-, and 120-lb. The loading foot with the steel wheel remained stationary, while the bed with the loading device (hose/loading strip) moved in the longitudinal direction. The movement of the bed forced the steel wheel over the loading device and the transducers measured the displacements and stresses at the contact interface.

3.5.2 Hose-Specimen Interface Stresses

Results from the APA pressurized hose contact stresses verified the initial hypothesis that the contact area under the hose is too narrow to produce any significant lateral stresses. Figure 3-12 shows the pressurized hose, which is attached to the moving bed, and the concave steel wheel loading the hose directly above the transducers.

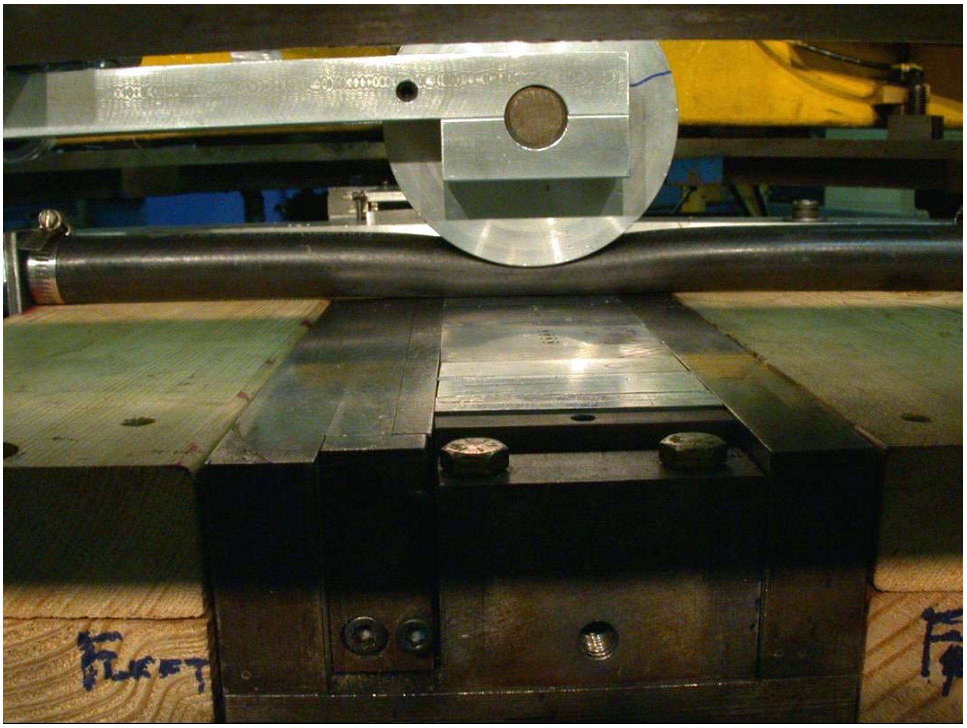

Figure 3-12. Close-up picture of the pressurized hose test.

In his report, Dr Pottinger stated that the narrow (8mm) contact area was not wide enough to record any lateral stress on the transducers. Figure 3-13 illustrates the vertical stress distribution under the hose. Similar to the Tekscan results (Figure 3-9), the measured vertical stresses show two humps at each side of where the steel wheel loads the hose, caused by the semi-rigid structure of the hose.

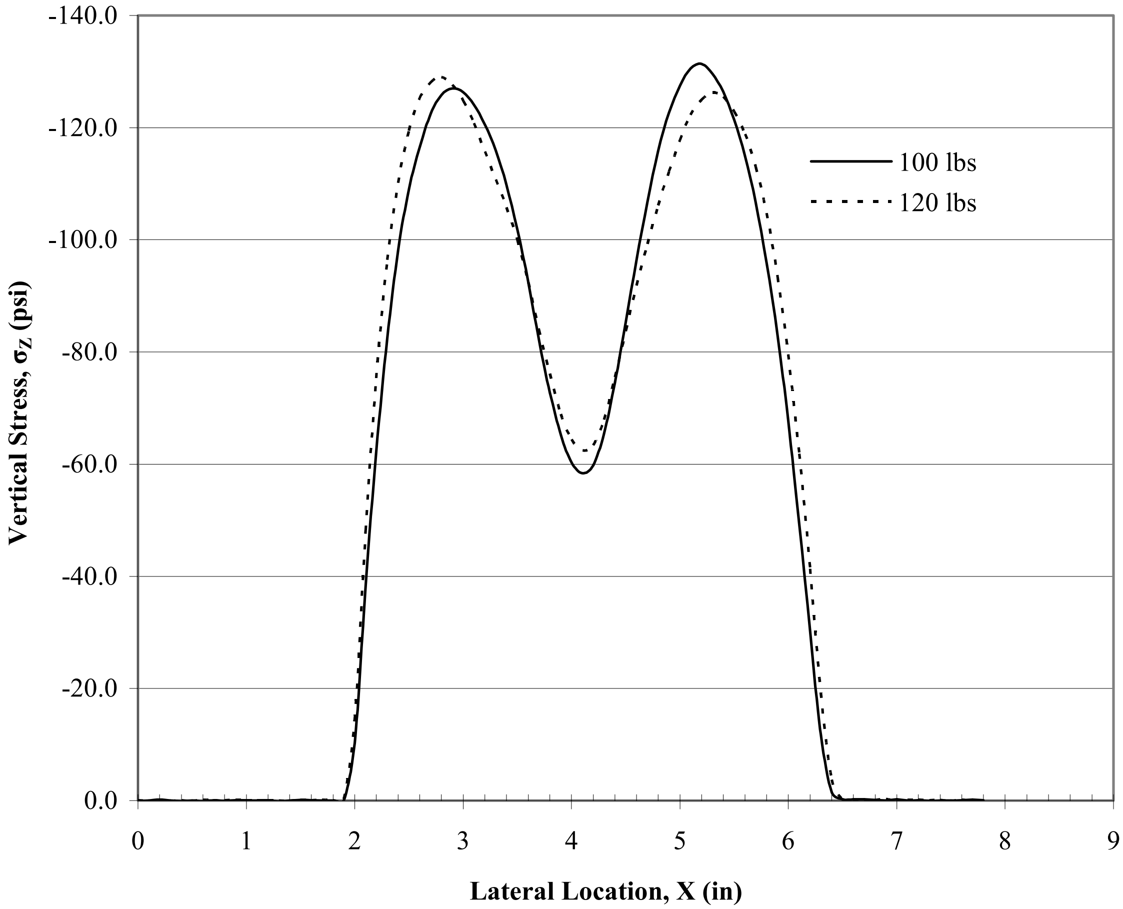

Figure 3-13. Vertical stress distribution under the pressurized hose.

3.5.3 Loading Strip-Specimen Interface Stresses

Smithers Scientific Services measured the contact stresses under the loading strip for three load levels – 110-, 130-, and 150-lb. Figure 3-14 is a picture of the steel wheel applying pressure on the loading strip which is fixed on the moving bed. Dr. Pottinger noticed that in the case of the loading strip, the solid wheel had to be centered over the loading strip to avoid asymmetric stress distribution. Contrary to the solid wheel, the concave wheel acts as a channel that continuously aligns the rubber hose with the traversing movement of the loading arm.

Figure 3-14. Close-up picture of the loading strip test.

Figure 3-15 illustrates the vertical stress distribution under the loading strip for the three load levels. Unlike the pressurized hose results, the vertical stress distribution under the loading strip resembles that of an elastic material with the stress peaking in the middle of the normal distribution. As expected, the magnitude of the vertical stresses is much lower under the loading strip due to the increase of the contact area. The highest measured vertical stress under the loading strip for the high load (150 lb) was 35 psi, whereas the pressurized hose recorded 130 psi vertical stress for the 100-lb load.

Figure 3-16 shows that the transverse stress distribution under the loading strip accurately captures the Poisson's effect found under individual tire ribs. The Poisson's effect states that, unless restrained, most materials expand laterally when loaded vertically. When individual ribs under a tire are loaded they attempt to expand laterally, and the surface of the pavement tries to

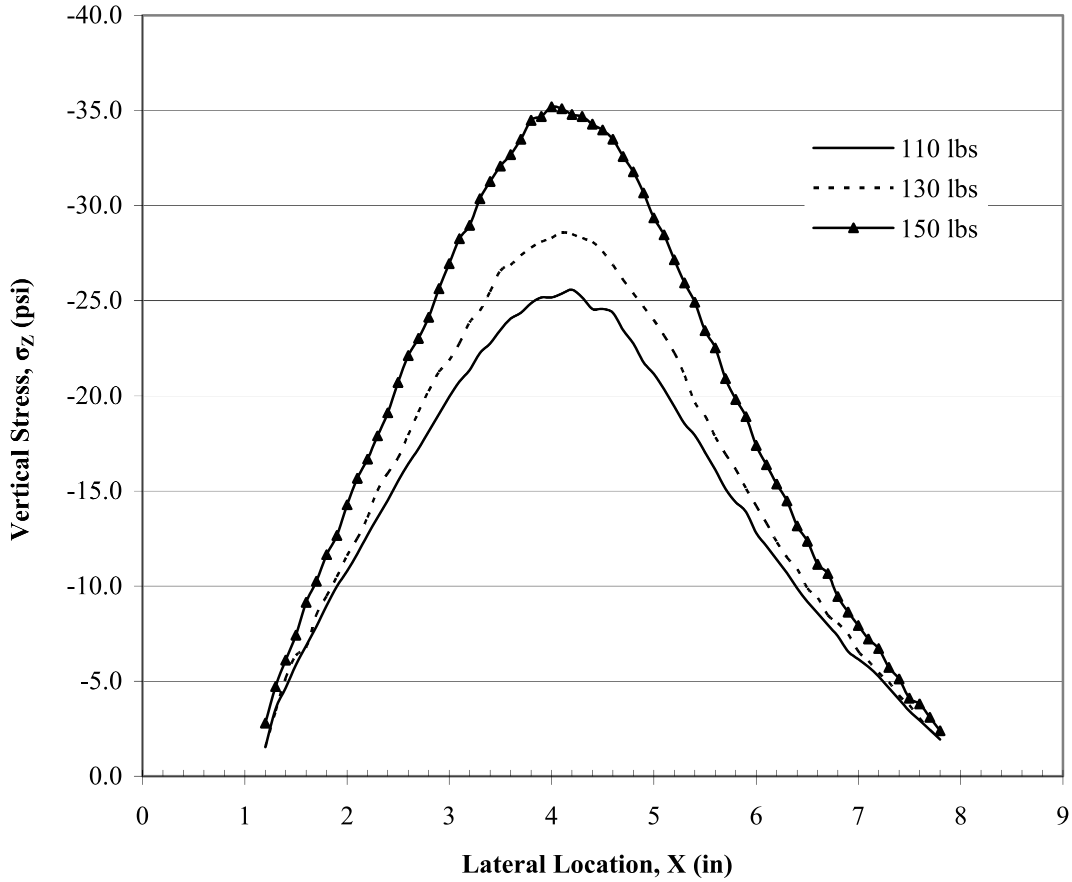

Figure 3-15. Vertical stress distribution under the loading strip.

restrain the expansion thus generating transverse stresses. Similar to the tire ribs but lower in magnitude, the loading strip induces lateral stresses that change sign (direction) at opposite sides of the loading strip.

3.6 SUMMARY

The discussion in this chapter focused on the contact-stress distribution between the specimen and the pressurized hose in the APA and the effort to develop an alternative loading mechanism to capture the complexity of the actual tire-pavement interface stresses. Actual contact-stress measurements verified that the limited initial contact area under the pressurized

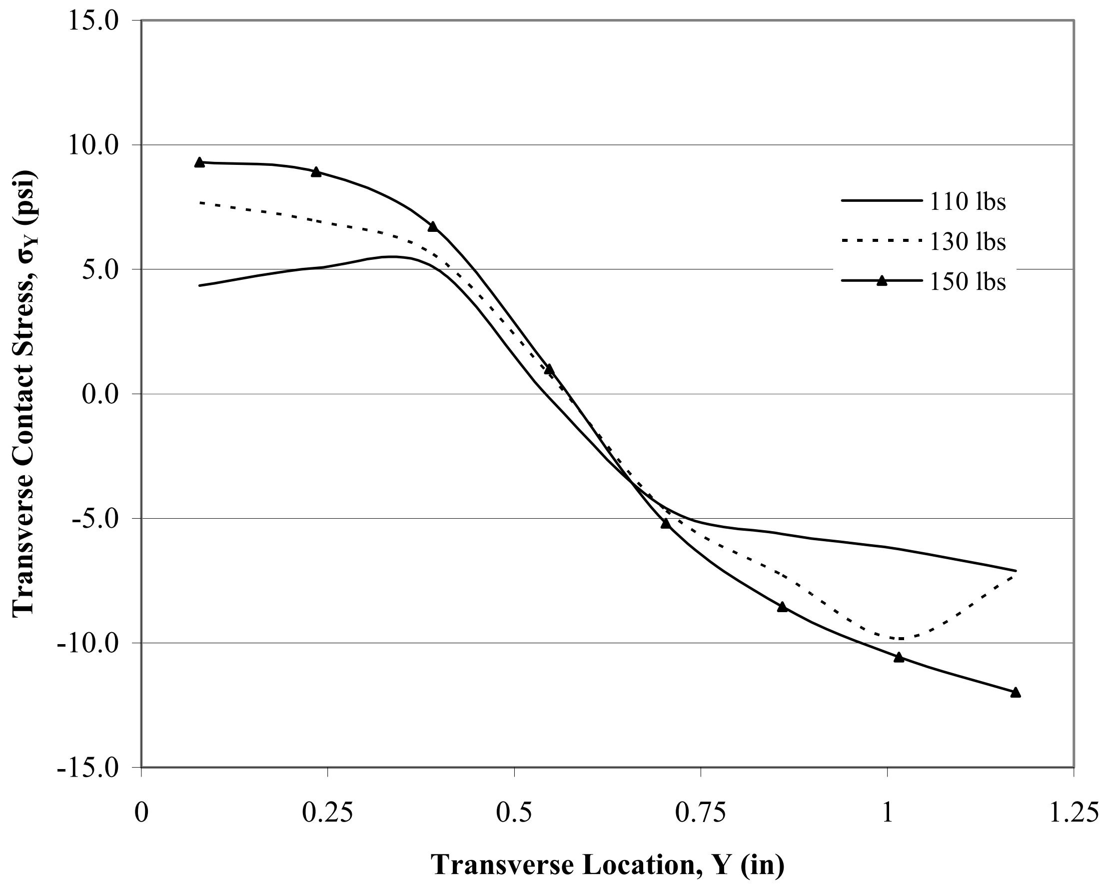

Figure 3-16. Lateral stress distribution under the loading strip.

hose could not induce lateral stresses on the surface of the HMA sample. However, results from the proposed loading device (loading strip) showed that the distribution of the lateral contact stresses closely resembles that found under individual tire ribs.

CHAPTER 4

STRESS ANALYSES

4.1 OVERVIEW

Recent experimental studies revealed that tire contact stresses are distributed in a highly non-uniform manner and differ significantly for various tire types [De Beer et al. 1997, Marshek et al. 1986, and Myers et al. 1999]. These stresses include not only vertical normal stresses, but also transverse and longitudinal surface shear stresses. One proposed hypothesis on the mechanism behind instability rutting is that radial tires, with their complex non-uniform loading, may be inflicting significant stress states in the HMA that are not predicted with traditional uniform vertical loading patterns [Drakos 2000]. Elastic layer and finite element analyses of asphalt pavements for three load cases – radial tire load, bias-ply tire load, and uniformly distributed vertical load – showed that radial-tire loads induce more severe stress states near the surface of the pavement.

The measured contact stresses under the two loading mechanisms – hose and loading strip – also revealed some expected differences in the contact-stress distribution. Lateral stresses under the loading strip resembled the distribution found under a single rib on the radial tire tread. Finite element modeling of the APA test showed that the loading strip, similar to the radial tires, induced some tension near the surface of the specimen. These stress states tend to induce shear stresses that shove the material away from the loaded area similar to instability rutting.

4.2 PAVEMENT STRESS ANALYSES

To evaluate the effect of the contact stresses found under various tires, the measured tire-pavement interface stresses were applied as a load on a pavement structure and the resulting stress states were analyzed. In the past, finite elements have not been used to model three-dimensional tire loads due to the complexity of modeling a radial-tire load in three dimensions. Instead, the elastic multi-layer analysis program BISAR [De Jong et al. 1973] was used to predict the pavement responses.

Typical pavement structures consist of a thin asphalt concrete layer over a base course, which rests on the semi-infinite subgrade. To produce an accurate model of the non-uniform load and provide adequate boundary conditions requires a large number of elements, and the associated amount of memory is not available on current PCs. The University of Florida recently purchased a Silicon Graphics Interface (SGI) multi-processor computer with extensive memory and faster computing time than the average PC that made the three-dimensional finite element analysis of HMA pavements possible.

4.2.1 Multi-Layer Elastic Stress Analyses

The initial approach to model three-dimensional tire contact stress was to approximate the complex loading conditions with uniform circular loads. BISAR can apply circular uniform loads with a single vertical stress and one stress in the lateral direction of a specific angle. A series of small uniform circular loads of varying vertical (σ_z) and lateral (σ_x & σ_y) stresses would represent the non-uniform tire stresses.

Figures 4-1 and 4-2 illustrate the load configuration for the bias-ply and radial tires, respectively. It took 209 load circles to simulate the lateral and non-uniform vertical stress distribution under the bias-ply tire, and 145 load circles to represent the radial tire. The magnitude, orientation, and location of the vertical and lateral stresses of the individual circular loads used to represent the bias-ply and radial tire contact stresses are listed elsewhere [Drakos 2000].

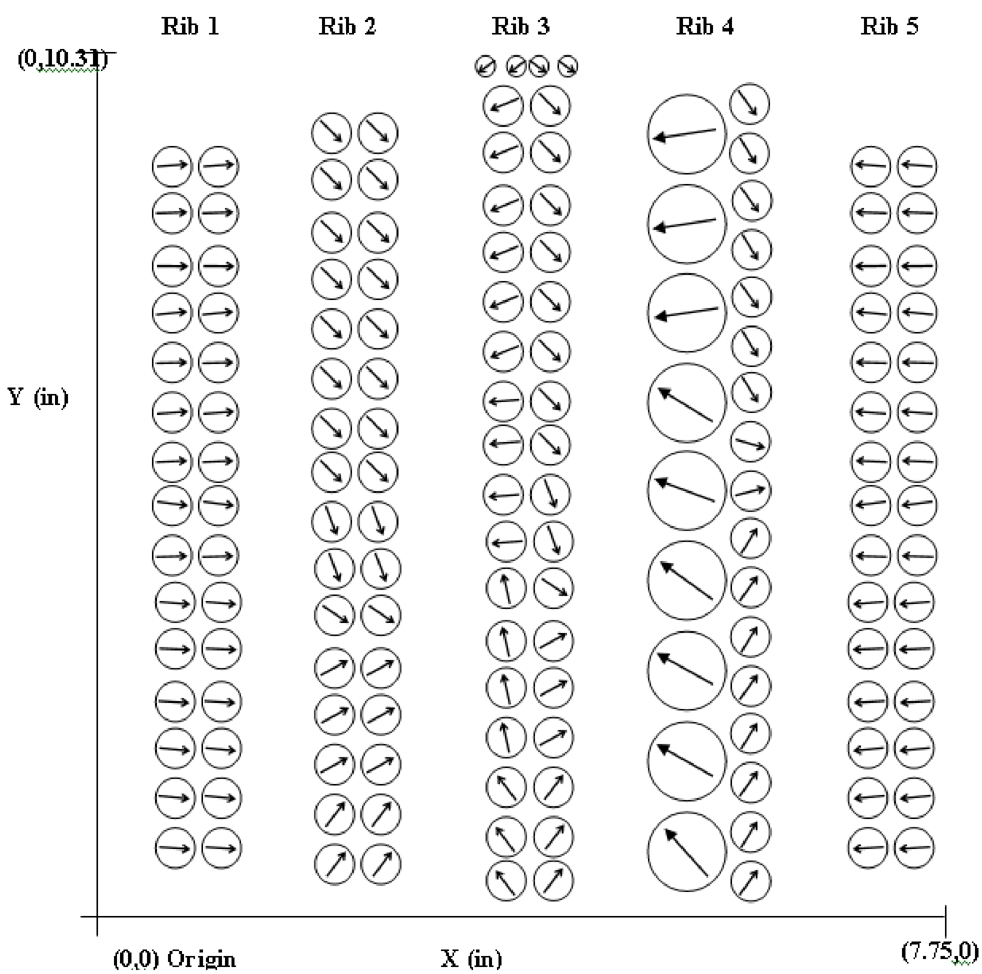

Figure 4-1. Load configuration used in BISAR to represent measured stresses under bias-ply truck tire [Drakos 2000].

For the bias-ply tire, Figure 4-1 illustrates the existence of a significant transverse stress component near the edge of the load, which tends to pull the pavement in towards the center of the tire. This development can be explained by the overwhelming pneumatic effect that is induced by bias-ply tires as explained in section 2.3. On the other hand, Figure 4-2 shows that the radial tire creates a 'pushing outward' effect under each individual rib. This trend is attributed to the dominance of the Poisson's effect in radial tires.

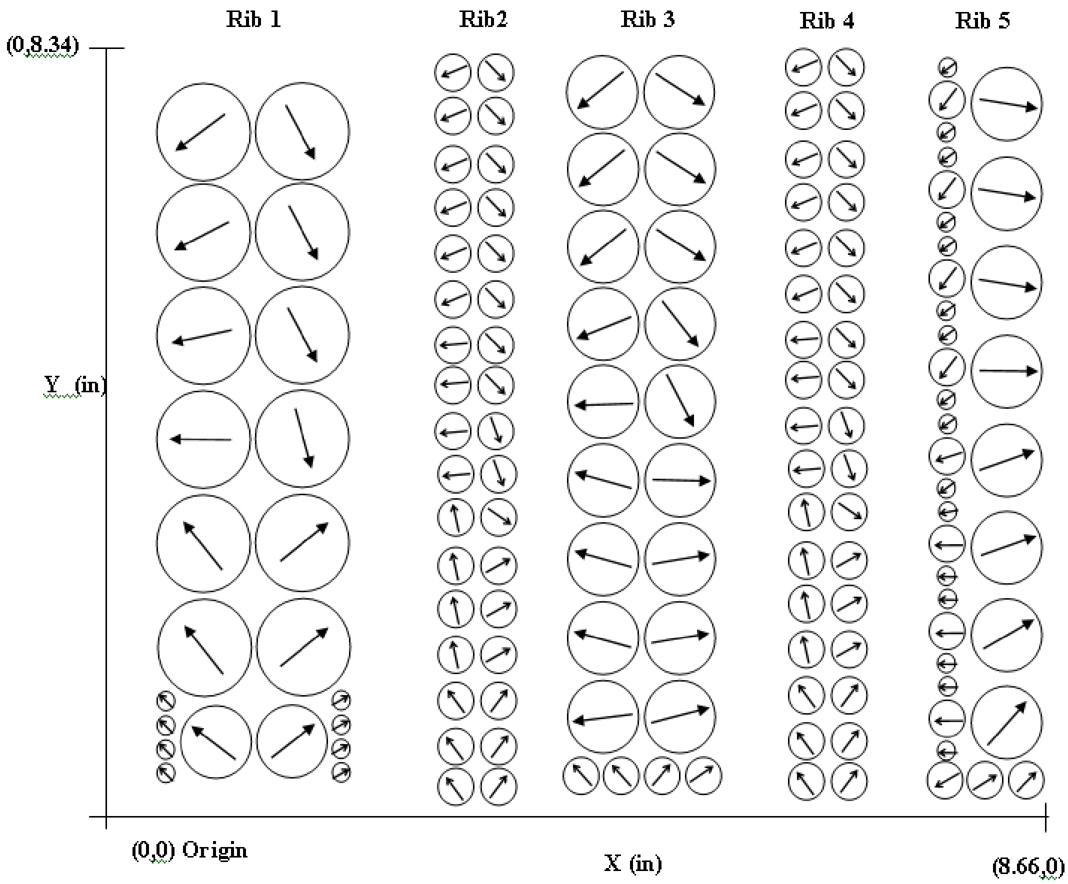

Figure 4-2. Load configuration used in BISAR to represent measured stresses under radial truck tire [Drakos 2000].

4.2.2 BISAR Results

Figure 4-3 illustrates the maximum shear stress distribution for the modeled radial and bias-ply truck tires. The responses were predicted along the surface of the pavement at 0.2-inch increments. High shear stress values were calculated under the left-most rib of the modeled radial load, whereas much lower values developed under the bias-ply tire load.

The high shear stresses predicted under the modeled radial tire hinted that shear planes might be developing under the load, similar to a bearing-capacity type of failure. To investigate this hypothesis the direction of the predicted maximum shear stress, at each output point under the tire load, was plotted as a vector.

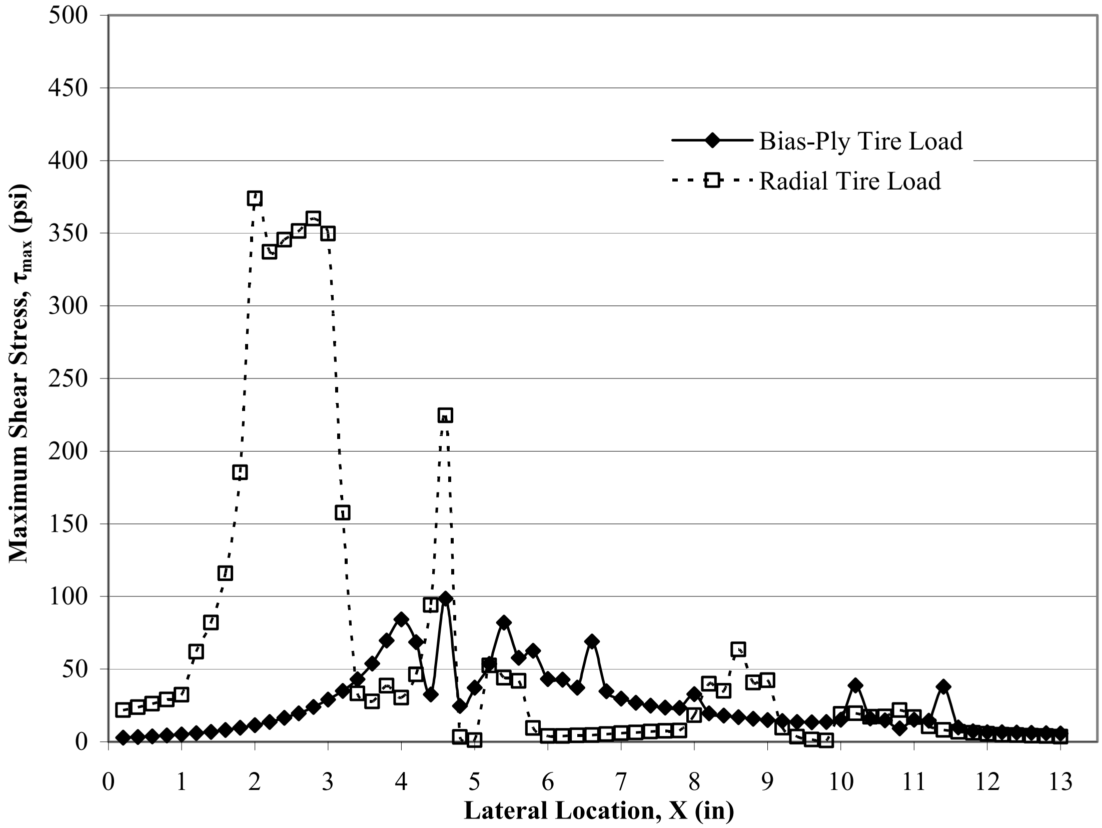

Figure 4-3. Maximum shear stress distribution.

Angle α was defined as the smallest angle formed between the maximum shear stress plane and the horizontal. Figure 4-4 demonstrates the sign convention used by the analysis program and the calculation of angle α, which was used to plot the direction of the shear stress plane.

Figure 4-5 shows the two equal and opposite maximum shear stresses that act on a particular element. In this case, the smallest angle is formed between the negative maximum shear stress and the horizontal plane. Thus, the plotted directional arrow (vector) would represent the direction of the negative maximum shear stress.

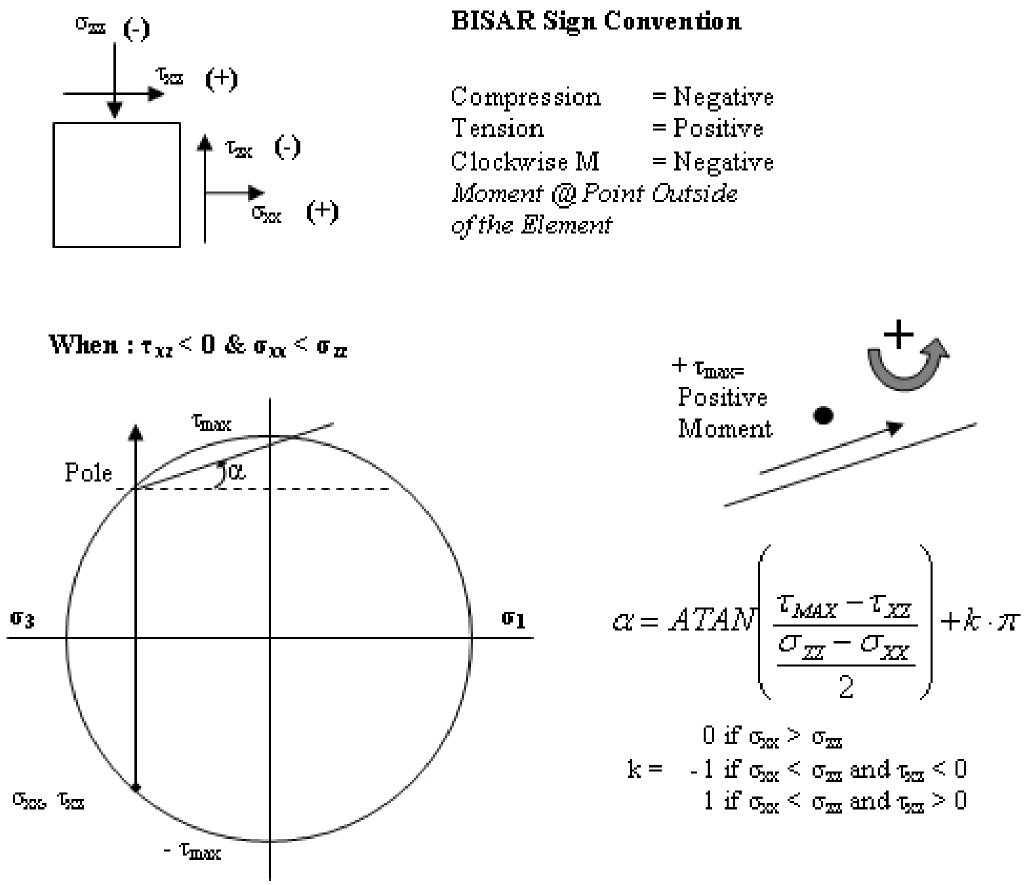

Figure 4-4. BISAR sign convention and maximum shear stress angle α.

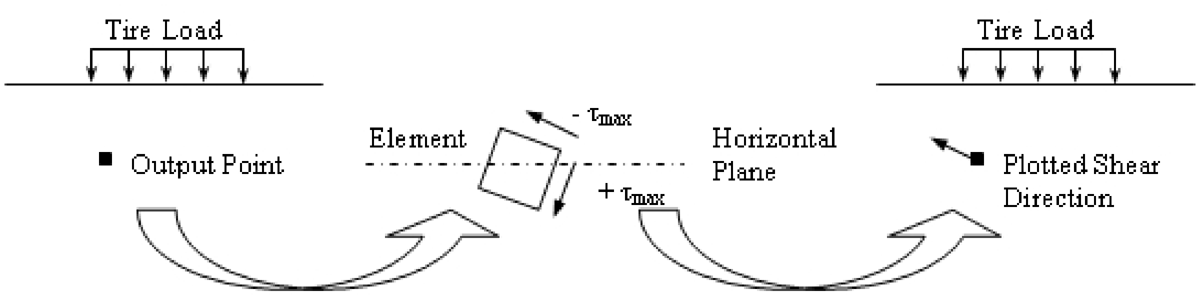

Figure 4-5. Schematic of the maximum shear stress direction representation.

Figure 4-6 shows the magnitude and direction of the maximum shear stress distribution along a vertical section for the modeled radial tire load. The arrows indicate the direction of the maximum shear stress closer to the horizontal, and the contour plot (shaded area) in the background specifies the magnitude of the shear stress. The direction of the shear stresses under

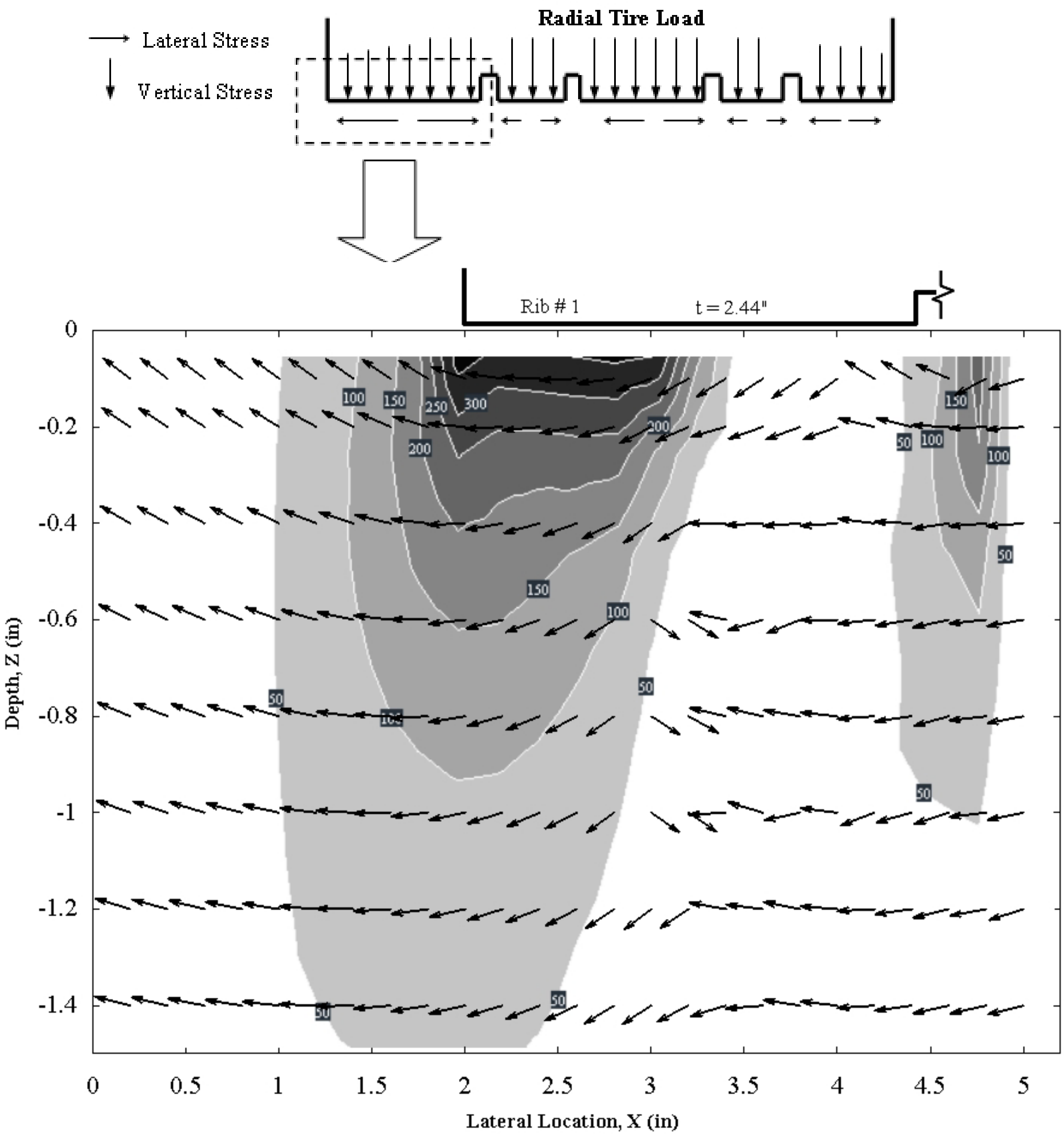

Figure 4-6. Magnitude and direction of maximum shear stresses under radial tire load.

the right-most rib of the radial tire indicates the formation of shear planes that tend to 'shove' the material away from the tire. At the same location, the contour plot of the predicted maximum shear stress magnitude indicates that shear stresses are at their highest value.

Figure 4-7 illustrates the magnitude and direction of the maximum shear stress distribution under the modeled bias-ply tire load. Unlike the radial tire load responses, the maximum shear stress direction for the bias-ply load appears to be 'pulling the pavement inwards.' The orientation of the directional arrows under the bias-ply tire load is pointed inwards, towards the tire. When compared with the radial tire load results, the magnitude of the predicted maximum shear stress for the bias-ply tire load was significantly lower.

In an effort to isolate the effect of tire-induced lateral stresses, the horizontal stress component in the BISAR input files was set to zero so that only vertical stress was applied. The results of the analyses performed without the lateral tire contact stresses revealed that, for the radial tire load, the direction of the maximum shear stress was reversed. In contrast to that, results for the bias-ply tire load did not give any indication of stress reversal.

Analyses performed with the elastic layer analysis program BISAR provided information on the pavement's response under modeled tires from measured contact stresses. Even though the magnitude of the estimated stresses is sometimes exaggerated due to a discontinuity problem at the edge of the circular load [Jacobs 1995], the overall effect of the non-uniform loading showed that the near-surface stress distribution was highly dependent on tire structure. Lateral stresses induced by radial tires seem to cause a reduction in confinement near the pavement's surface, which reduces the mixture's resistance to shear stress. The combination of high magnitude and outward direction of the maximum shear stresses is believed to create the critical stress conditions contributing to the permanent deformation of the pavement.

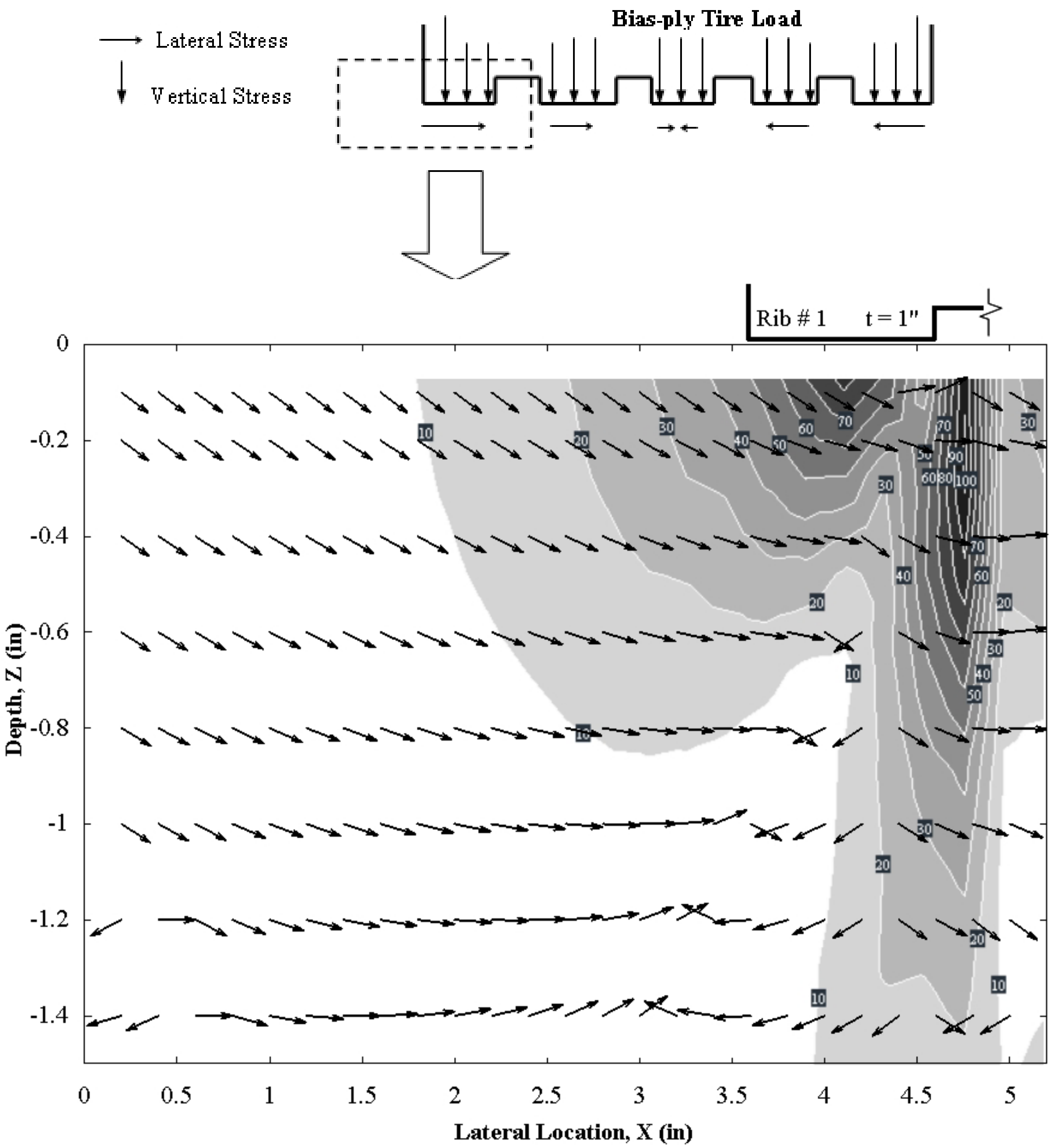

Figure 4-7. Magnitude and direction of maximum shear stresses under bias-ply tire load.

4.2.3 Finite Element Stress Analyses

The three-dimensional finite element model was constructed and analyzed using the commercial finite element code ADINA [Bathe 2001]. The finite element model consisted of 30,204 nine-node elements of varying dimensions. Elements under the loaded area were refined to 0.3 by 0.4 inches in the horizontal plane and 0.2 inches in the vertical plane. To overcome the limitations associated with building a traditional mesh, contact surfaces were introduced to 'bond' fine-graded mesh onto a coarse-graded mesh. This allowed for the introduction of coarse meshes at distances farther away from the loaded area where the change in stress was more gradual. The use of contact surfaces was further justified based on the primary area of interest, the near-surface area under the loaded tire, thus negating any possible negative numerical effects of 'far-away' contact surfaces.

Figures 4-8 and 4-9 show the finite element model with the dimensions used in the analysis. The mesh extended 60 inches in each horizontal direction and 72 inches in the vertical direction. Although these dimensions may seem inadequate for a finite element model, an initial assessment showed that stresses near the tire footprint (area of interest) were not affected by the extent of the boundaries.

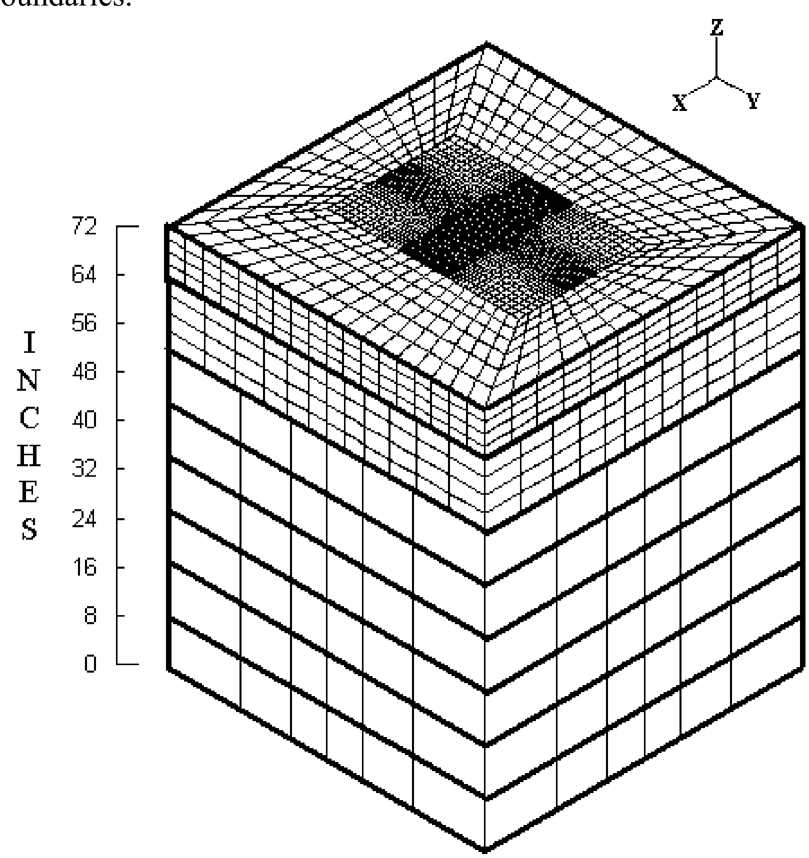

Figure 4-8. Three-dimensional finite element mesh used in the pavement response analysis.

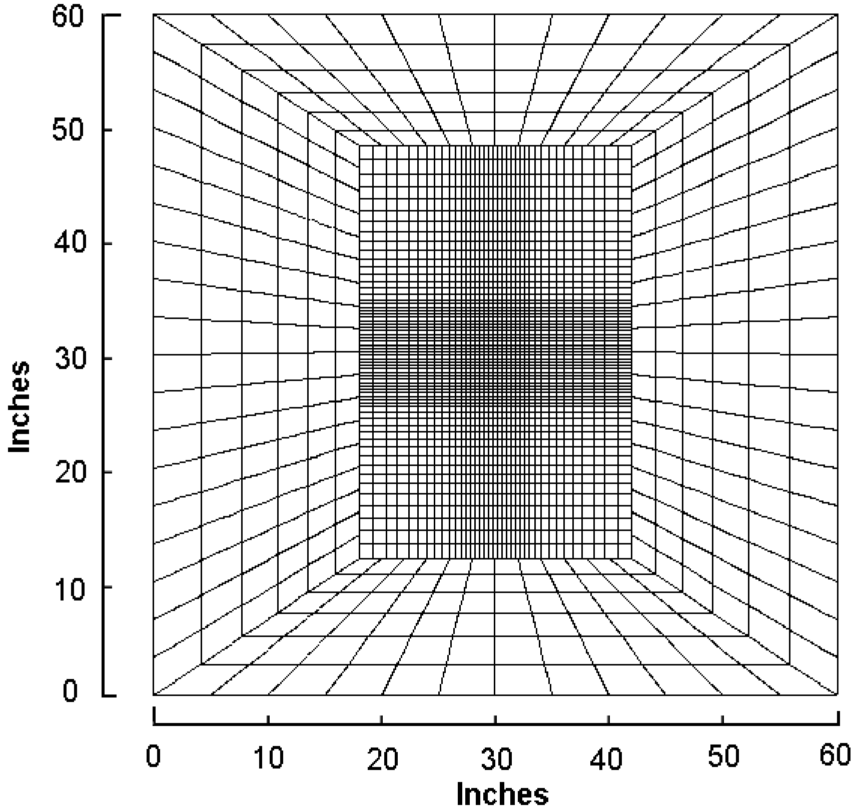

Figure 4-9. Plan view of the contact area of the three-dimensional mesh used in the pavement response analysis.

The boundary conditions for the four sides (faces) of the FEM were fixed in the horizontal (X and Y) direction and free in the vertical (Z) direction, whereas the bottom of the FEM was fixed in all directions. The model consisted of 260,455 nodes, giving it over one million degrees of freedom. The memory required for analysis exceeded 1700 megabytes and took over four hours to complete on a single processor.

The structure used in the analysis was a typical three-layer pavement – asphalt concrete, base, and subgrade – with thicknesses 8, 12, and 52 inches respectively. Each layer was assumed to be isotropic, homogenous, and linear elastic. Table 4-1 shows a summary of the material properties used in the structure. The low asphalt concrete modulus corresponds to a warm

Table 4-1. Material properties and layer thicknesses of FEM pavement structure.

Layer	Modulus (psi)	Poisson's ratio	Thickness (inches)
Asphalt concrete	100,000	0.45	8
Base	40,000	0.45	12
Foundation	15,000	0.45	52

summer day for a new pavement – the most critical time for the onset of instability rutting – while base and subgrade modulus values represent typical materials used in Florida. The Poisson's ratio was selected to ensure minimal volumetric changes, as would be expected from a single moving tire load.

4.2.3-1 Loading the FEM

Dr. Pottinger measured the tire-pavement contact stresses in a fine grid – 0.1 by 0.15 inches – making it almost impossible to load the mesh directly with the recorded stresses. An approximation method was used to convert and redistribute the measured contact stresses to nodal forces. The appropriate force for each element was determined by converting each uniform stress to an equivalent concentrated force. The forces were then converted to nodal forces with the help of shape functions and applied to the respective node [Cook 1995].

Figure 4-10 illustrates the shape-function procedure to redistribute an element force to nodal forces. Parameters ξ and η define the position of the element load relative to the element's center, and their value ranges from zero to one. The shape functions are then calculated for each node based on the ξ and η values. Finally, the nodal forces (F1 to F8) are the product of the element force (P) with the respective nodal shape function (N1 to N8).

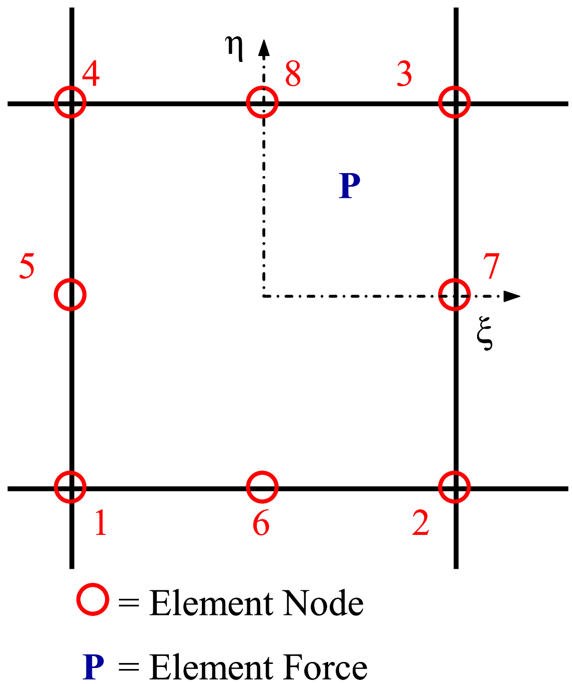

$$\xi = (X_{ele\_center} - X_{load})$$

$$\eta = (Y_{ele\_center} - Y_{load})$$

<u>Shape Functions</u>

$$N1 = \frac{1}{4}(1-\xi)(1-\eta) - \frac{1}{2}(\mathrm{N5}) - \frac{1}{2}(\mathrm{N8})$$

$$N2 = \frac{1}{4}(1+\xi)(1-\eta) - \frac{1}{2}(\mathrm{N5}) - \frac{1}{2}(\mathrm{N6})$$

$$N3 = \frac{1}{4}(1+\xi)(1+\eta) - \frac{1}{2}(\mathrm{N6}) - \frac{1}{2}(\mathrm{N7})$$

$$N4 = \frac{1}{4}(1-\xi)(1+\eta) - \frac{1}{2}(\mathrm{N7}) - \frac{1}{2}(\mathrm{N8})$$

$$N5 = \frac{1}{2}(1-\xi^2)(1-\eta)$$

$$N6 = \frac{1}{2}(1+\xi)(1-\eta^2)$$

$$N7 = \frac{1}{2}(1-\xi^2)(1+\eta)$$

$$N8 = \frac{1}{2}(1-\xi)(1-\eta^2)$$

Figure 4-10. Definition of the shape functions.

Figure 4-11 is a cross section view of the surface elements with the resulting nodal forces for the modeled radial-tire load. The nodal loads are non-uniform and vary in magnitude and direction to simulate the contact stresses found under a radial tire.

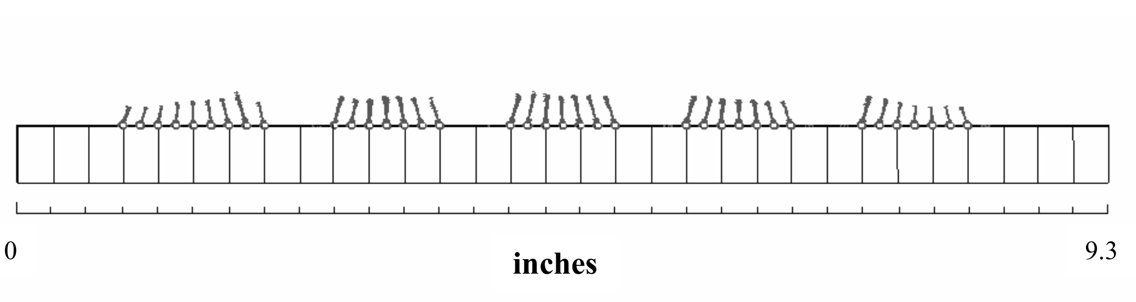

Figure 4-11. Cross-section view of surface elements with nodal forces for the radial-tire load.

4.2.3-2 FEM Results

Figure 4-12 shows the magnitude and direction of the maximum shear stress distribution along a vertical section under the modeled radial-tire load. The distribution of shear stresses is similar to those predicted using BISAR, except the magnitudes of the maximum shear stresses are lower, ranging from 50 to 60 psi compared to values in excess of 100 psi for the BISAR predictions. The difference in magnitude can be attributed to the approximation method used to convert the measured point stresses to circular loads, and to the BISAR overestimation problems mentioned above. However, the key finding is that the overall trend – the formation of the shear planes – remains the same between the two different modeling techniques.

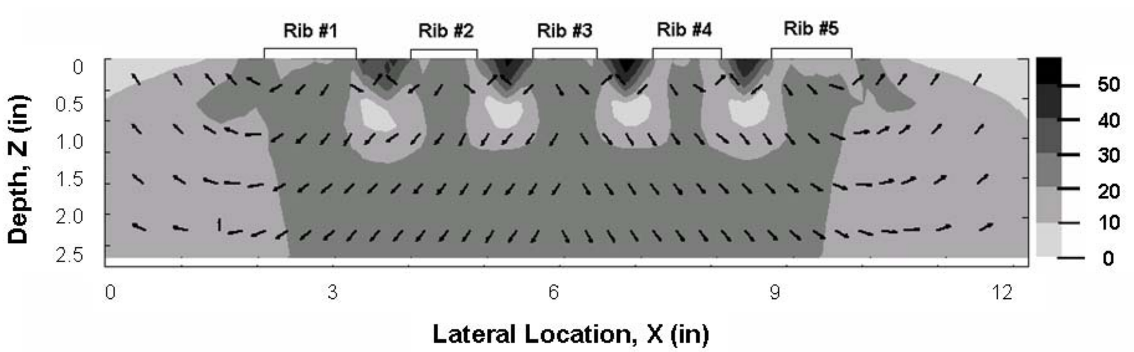

Figure 4-12. Maximum shear stress magnitude (psi) and direction under the modeled radial-tire load.

The plotted vectors indicate the formation of shear planes under the loaded area. Also, it can be seen from the direction of the shear stresses under the first rib of the radial tire that shear planes formed tend to shove the material away from the tire, and the contour plot of the predicted maximum shear stress magnitude indicates that the shear stresses form planes that match the directional arrows.

4.3 APA STRESS ANALYSES

The measured contact stresses between the HMA specimen and the two APA loading mechanisms – pressurized hose and the loading strip – were modeled with finite elements to evaluate the effects of the different loading conditions. The primary objective was to examine whether the loading strip could induce similar stress states in the modeled HMA specimen, as the radial tire induced in the modeled pavement.

The three-dimensional finite element model was constructed using the MSC/PATRAN pre-processor software to build the model geometry and to define the mesh and the HKS/ABAQUS software for the actual analysis [Hibbitt, Karlsson and Sorensen, Inc. 1997]. To build the mesh around the curved surfaces we used an automatic mesh-generating option in PATRAN called paver. The paver is best suited for trimmed surfaces, such as surfaces with holes or cutouts. In this case, the paver meshing algorithm generated quadrilateral elements perpendicular to the curved surfaces and transitional elements to connect to the free edges. At first, the mesh was generated in two-dimensional space and then the 'sweep' action was used to extrude the elements into three-dimensional 'brick' elements.

Figure 4-13 shows the initial two-dimensional model for the APA mold and the HMA specimen. For practical purposes, only one of the two cylindrical-sample slots was used in the model. Furthermore, the model was separated into two main parts – the plastic mold (E = 400000 psi, ν = 0.4) and the asphalt concrete sample (E = 100000 psi, ν = 0.4). Figure 4-14 shows the three-dimensional geometry and mesh definition of the two solids.

As mentioned in Section 3.5, Dr. Pottinger measured the contact stresses under the two loading devices – the original pressurized hose and the new loading strip. The objective in this section was to load the model with the measured contact stresses and analyze the predicted stress states in the specimen. Once again, the measured stresses were converted to nodal forces with the help of shape functions and applied to the respective node (Section 4.2.3-1).

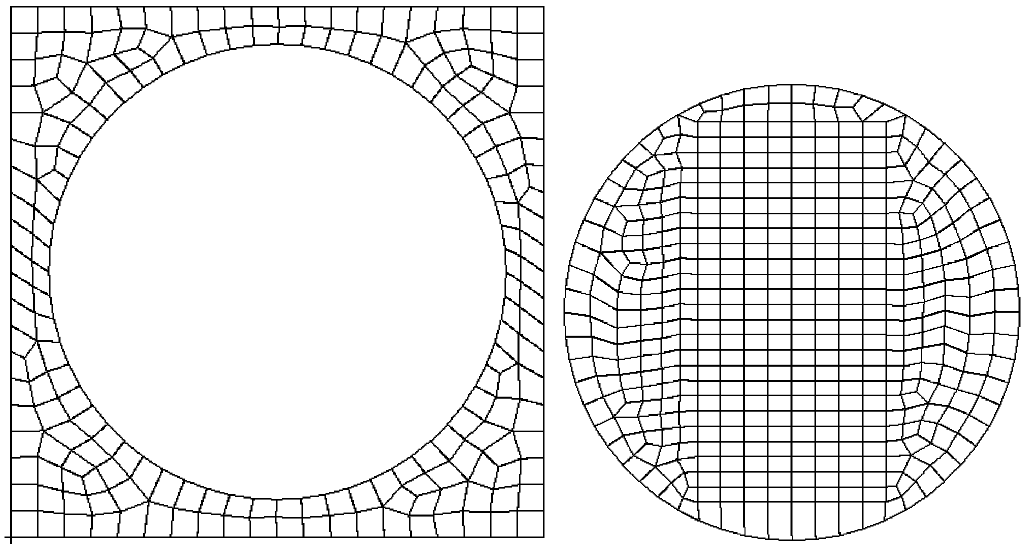

Figure 4-13. Top view of the finite element model for the APA mold and specimen.

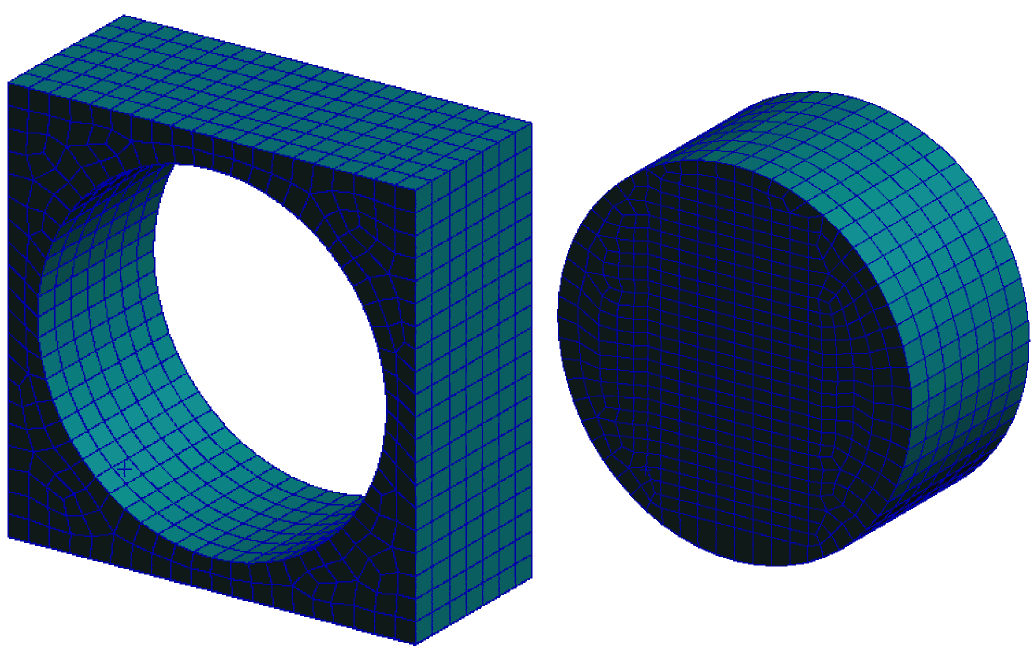

Figure 4-14. Three-dimensional finite element model for the APA mold and specimen.

Figures 4-15 and 4-16 show the predicted magnitude and direction of the maximum shear stress (τ_{max}) distribution, along a vertical section, for the loading strip and pressurized hose loading conditions respectively. The range of the τ_{max} magnitude under the loading strip (3-13 psi) is much lower than that predicted under the pressurized hose (10-80 psi). This magnitude difference can be attributed to the higher vertical stresses measured under the pressurized hose (Section 3.5.2).

The important finding of this analysis was the pattern of the τ_{max} distribution throughout the modeled specimen. Unlike the distribution under the pressurized hose, the modeled loading strip showed that the τ_{max} magnitude peaks near the surface of the specimen, under the loaded area. Furthermore, the magnitude contour plots for the loading strip condition indicate the existence of shear planes under the load, whereas the same is not true for the modeled pressurized hose load. The combination of the τ_{max} magnitude distribution with the τ_{max} direction under the loading strip resembles the pattern found under individual ribs for the modeled radial-tire load (Figure 4-12).

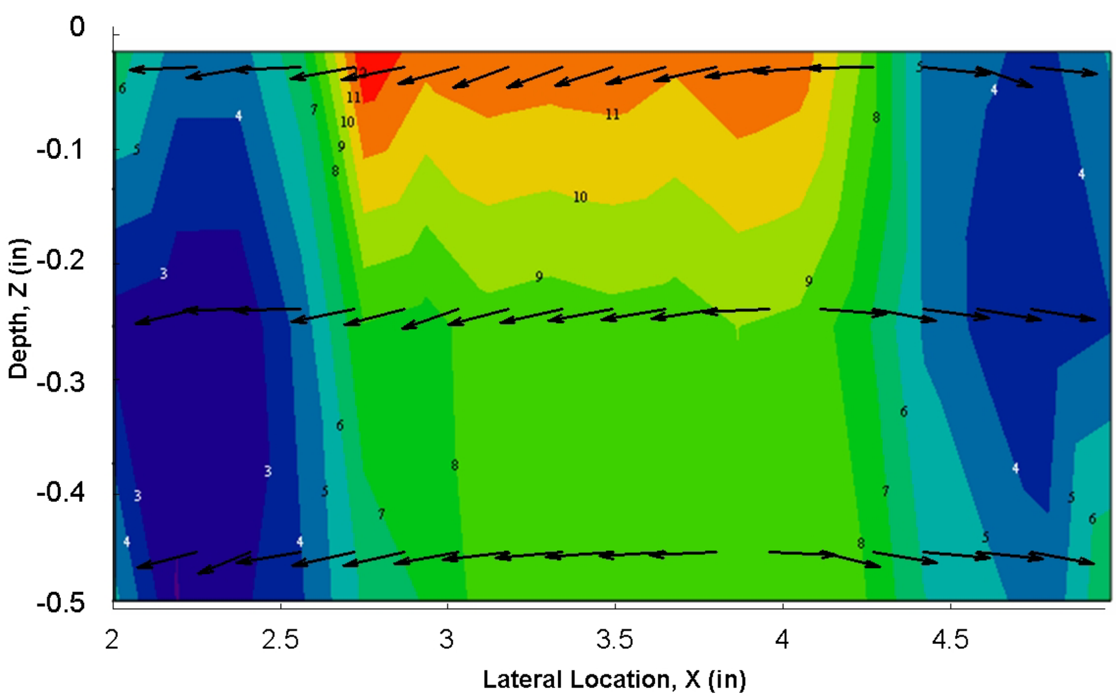

Figure 4-15. Maximum shear stress magnitude (psi) and direction under the modeled loading strip load.

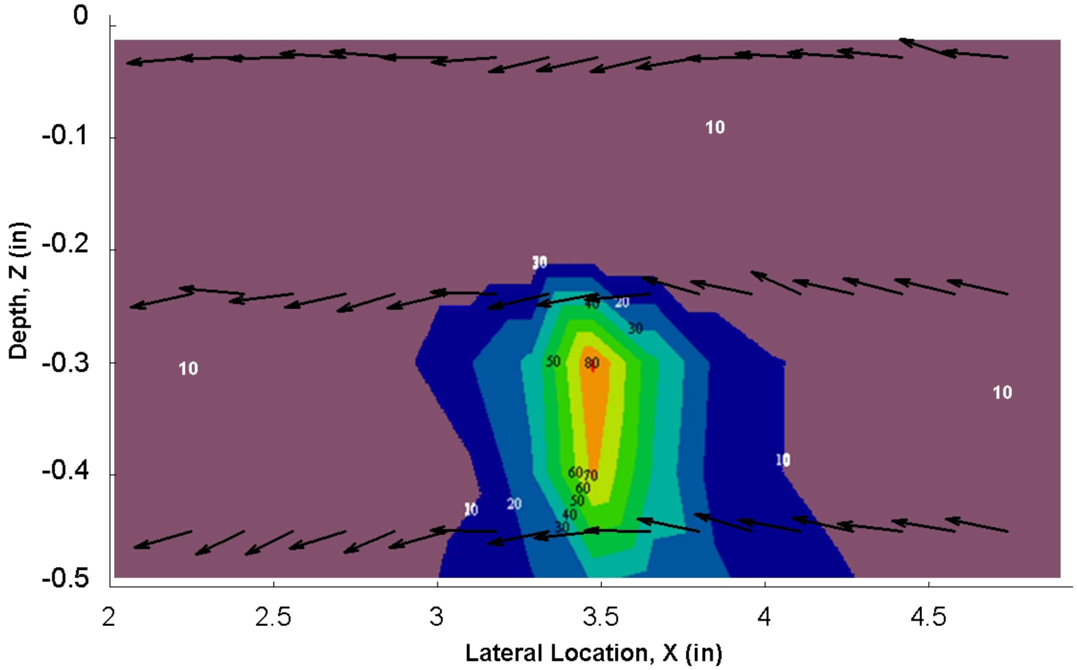

Figure 4-16. Maximum shear stress magnitude (psi) and direction under the modeled pressurized hose load.

4.4 SUMMARY

Analyses performed with the elastic layer analysis program BISAR and the finite element program ADINA provided information on the pavement's response under modeled tires from measured contact stresses. The analyses provided evidence that the radial truck tires induce higher shear stresses near the surface of the pavement than the bias-ply tire. The direction of the maximum shear stresses under the modeled radial tire load appeared to shove the material away from the load, something that was not observed under the modeled bias-ply tire.

The measured contact stresses under the two APA loading devices were used to load the APA finite element model. The analysis showed that the pressurized hose load produced higher magnitude stresses. However, the loading strip replicated (to some extent) the critical stress states identified under the radial-tire load.

CHAPTER 5

MATERIALS AND TESTING METHODS

5.1 OVERVIEW

Two of the three mixtures selected for this study have been placed in Florida in 1998, (see Table 5-1), and the FDOT has been monitoring their field performance ever since. The Job Mix Formula (JMF) of the original FDOT mixtures had a Reclaimed Asphalt Pavement (RAP) component of 15%-20% that formed part of the aggregate constituent. However, the RAP material was no longer available at the time of this research so the percentages of the other aggregates were adjusted to maintain the same gradation for each mix.

Table 5-1. Field location of selected mixtures.

FDOT Project No.	UF Project No.	Placement Date	Route	County
2134391	1	Jan-98	I-10	Madison
2325941	7	Sep-98	Turnpike	Palm Beach

The mixtures were designed and produced according to the Superpave Volumetric Mix Design procedure and the samples compacted with the Pine Gyratory Compactor to 150-mm diameter by 115-mm height gyratory specimens. Finally, the samples were tested with the original and modified Asphalt Pavement Analyzer test procedures to evaluate their rutting performance.

5.2 MATERIALS

Table 5-2 lists the original aggregate types and producers used in the FDOT monitoring projects. Project 1 is a 9.5-mm nominal maximum-size coarse-graded mixture, Project 7 is a 12.5-mm nominal maximum-size fine-graded mixture, and the HVS mixture is a 12.5-mm nominal maximum-size coarse-graded mixture. The last column on the right shows the JMF-blend percentage for each aggregate type. As stated earlier, the Superpave project mixtures – Project 1 & Project 7 – included RAP (milled material) which was not available at the time of this study.

Table 5-2. Aggregate types and sources for the selected FDOT mixtures.

Project No.	Mix No.	Material	FDOT Code	Pit No.	Producer	JMF %
1	97051A	Milled material	-	-	-	20
		#89 Stone	51	GA 185	Martin Marrietta	45
		W-10 Screenings	20	GA 185	Martin Marrietta	25
		M-10 Screenings	21	GA 185	Martin Marrietta	10
7	980139A	Milled material	-	-	-	20
		S1A Stone	41	87-339	White Rock Quarries	20
		S1B Stone	51	87-339	White Rock Quarries	10
		Asphalt Screenings	20	87-339	White Rock Quarries	50
HVS		S1A Stone	41	87-089	Rinker	13.0
		S1B Stone	51	87-089	Rinker	55.0
		Asphalt Screenings	20	29-361	Anderson	32.0

Table 5-3 shows the new aggregate blends that were obtained from the same sources and adjusted without the RAP to reproduce the original JMF. After careful selection, the gradations of the new blends resembled the original JMF for each project – Project 1 & Project 7. Figures 5-1 to 5-3 illustrate the gradation of the laboratory blend in comparison with the original (field) JMF on a 0.45-power chart.

Table 5-3. Aggregate sources and modified blends for the laboratory mixtures.

Project No.	Mix No.	Material	FDOT Code	Pit No.	Producer	JMF %
1	97051A	#89 Stone	51	GA 185	Martin Marrietta	50.0
		W-10 Screenings	20	GA 185	Martin Marrietta	18.5
		M-10 Screenings	21	GA 185	Martin Marrietta	31.5
7	980139A	S1A Stone	41	87-339	White Rock Quarries	24.5
		S1B Stone	51	87-339	White Rock Quarries	12.5
		Asphalt Screenings	20	87-339	White Rock Quarries	63.0
HVS		S1A Stone	41	87-089	Rinker	13.0
		S1B Stone	51	87-089	Rinker	55.0
		Asphalt Screenings	20	29-361	Anderson	32.0

The asphalt binder used for the study is an AC-30 binder with a PG-67-22 grading. It is distributed by Coastal Petroleum Company in Jacksonville (subsidiary of Coastal Caribbean Oils & Minerals, Ltd.) and is a common binder in Florida.

5.3 MIXTURE PREPARATION

All test specimens for the evaluation tests were prepared with the Superpave Volumetric Mix Design procedure. The design procedure uses volumetric properties – air voids (AV), voids in mineral aggregate (VMA), and voids filled with asphalt (VFA) – as the primary criteria to select the optimum asphalt content (% AC) for the specified aggregate blends. The Superpave criteria vary with the specified nominal maximum aggregate size for the JMF and the expected traffic level.

The two Superpave monitoring project mixtures used in this study – Projects 1 & 7 – have been used in various research projects at UF [Asiamah 2002, Darku 2003] and there is ample information about their volumetric properties. For this reason, the values for Rice Specific Gravity, optimum asphalt content, and Ndes were not recalculated. Further information

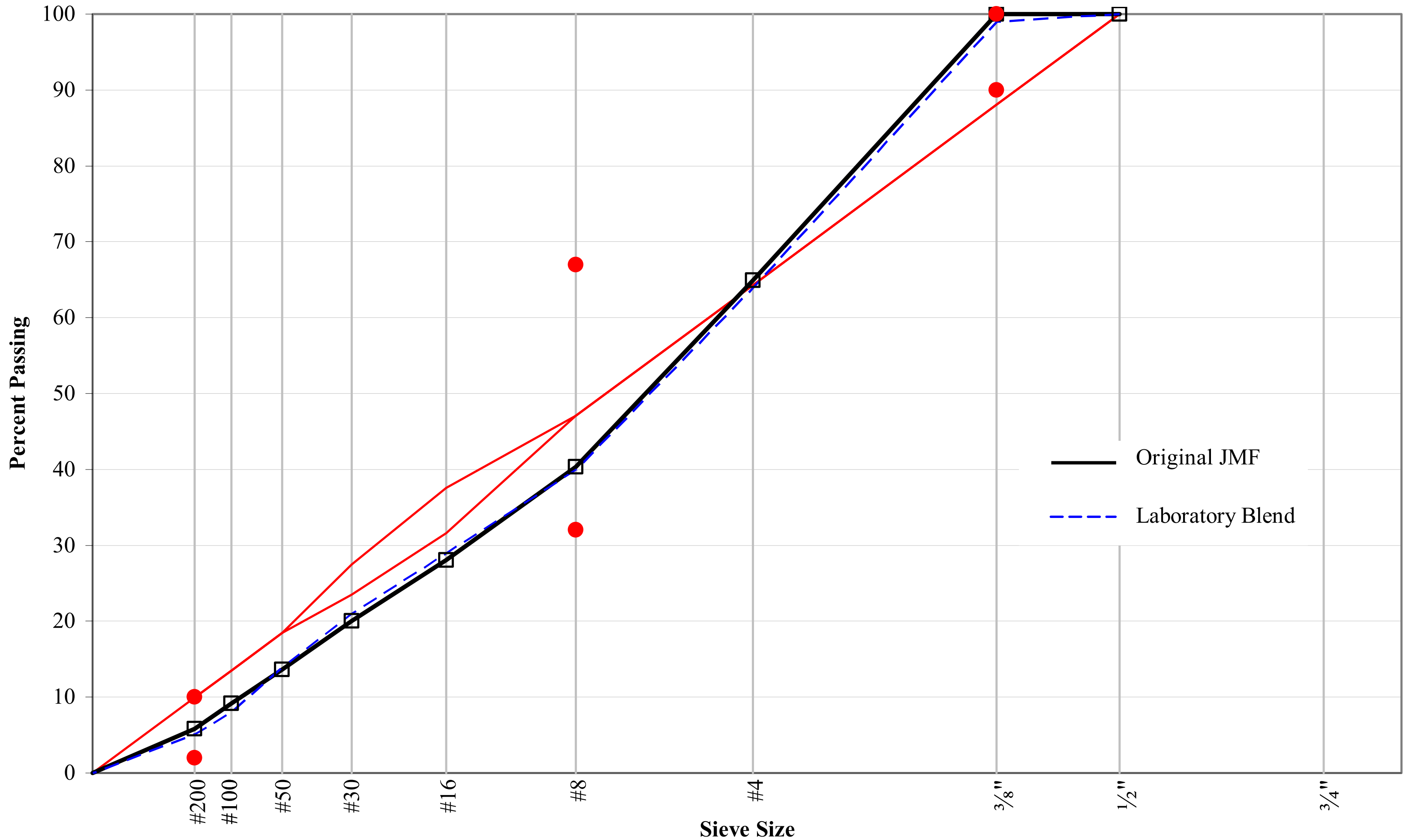

Figure 5-1. Gradation chart for JMF and laboratory blend for Project 1 (9.5 mm maximum nominal size).

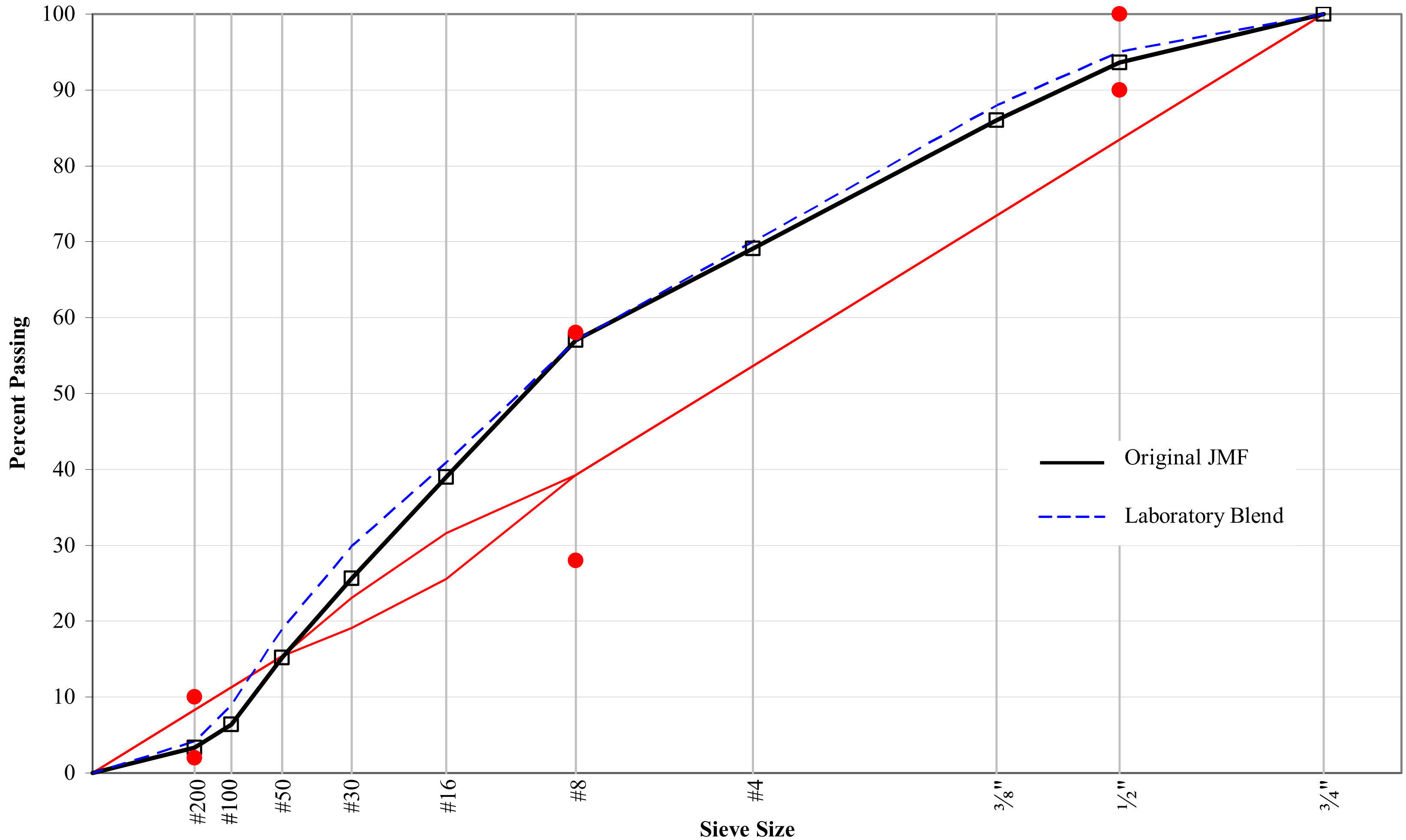

Figure 5-2. Gradation chart for JMF and laboratory blend for Project 7 (12.5 mm maximum nominal size).

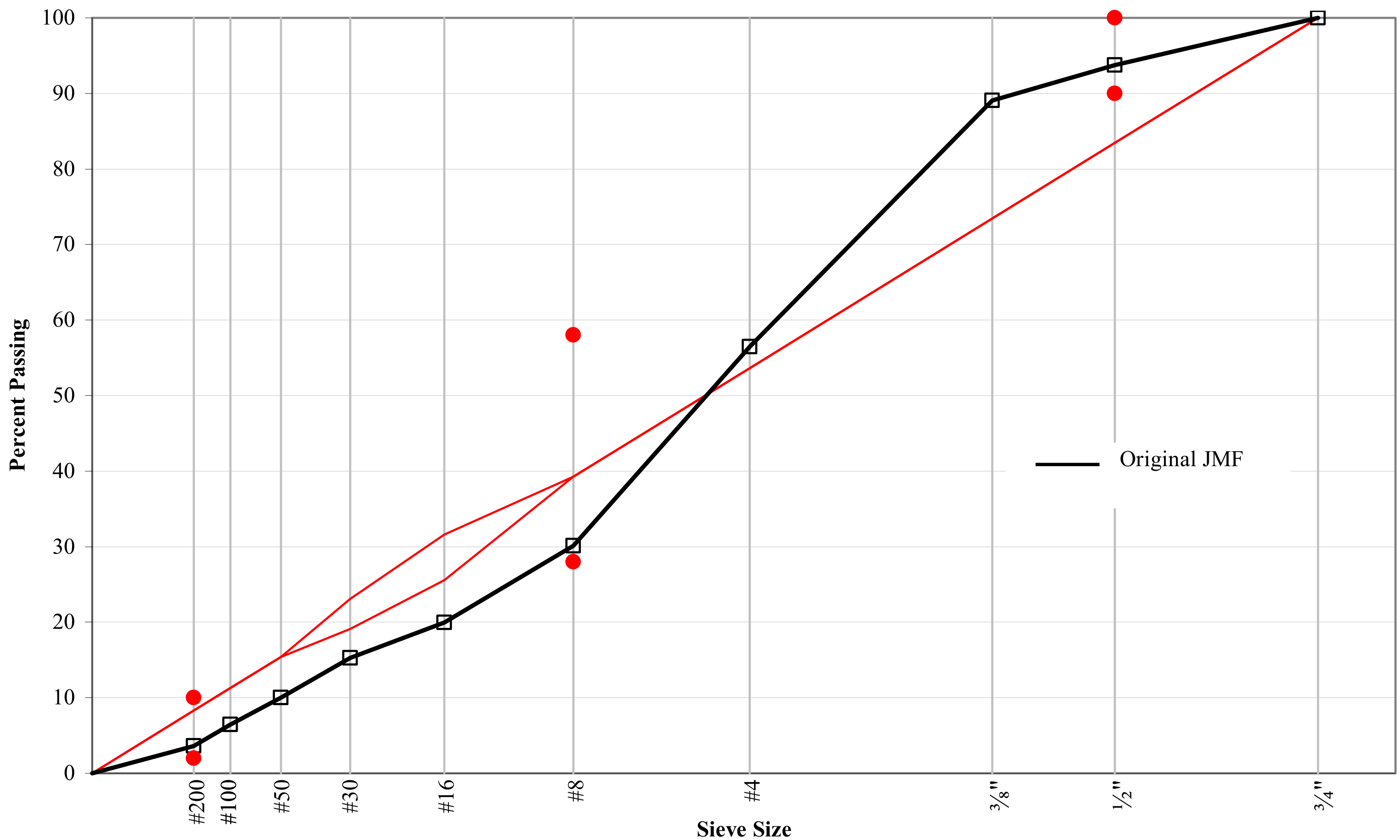

Figure 5-3. Gradation chart for laboratory blend for the HVS coarse-graded mixture (12.5 mm maximum nominal size).

about the volumetric properties of all three mixtures is included in Appendix A. Outlined below is the procedure followed to produce the 75-mm-thick cylindrical specimens used in the APA.

5.3.1 Aggregate Preparation and Batching

- The virgin material was dried in the oven (230 - 300°F) for at least 12 hours and then allowed to cool down to room temperature.
- The material was sieved and separated into its individual particle sizes – ¾”, ½”, ⅜”, #4, #8, #16, #30, #50, #100, #200, & pan.
- The aggregates were batched in 4500g samples (Pine Gyratory Compactor) in accordance with the JMF. Tables showing batch weights for the aggregates are given in Appendix A.

5.3.2 Mixing

- The aggregates, asphalt binder and the mixing equipment – mixing bucket and spatulas – were placed in the oven (300°F) for about two hours.
- Aggregate blend and asphalt binder were mixed in the bucket for about 5 minutes or until the aggregates were thoroughly coated with the asphalt.

5.3.3 Short-Term Oven Aging (STOA) and Compaction

- Before compaction, the samples were spread in a pan and placed in the oven (275°F) for STOA. While in the oven, the mix was stirred after one hour to achieve uniform aging.
- After the STOA, the 4500 g samples were compacted in the Pine Gyratory Compactor (Figure 5-4) to Ndes. Rice specific gravity information is given in Appendix A.
- Compacted specimens were allowed to cool for a minimum of 24 hours at room temperature and then were sawed down to 75 mm thickness.
- The Bulk Specific Gravity (Gmb) was then determined in accordance with ASTM D1189 and D2726 for each specimen.
- The percent air voids for each specimen was computed from the Gmm and the Gmb.

5.4 ASPHALT PAVEMENT ANALYZER PROCEDURE

As we have seen, the APA tests the rutting susceptibility or rutting resistance of HMA. The original configuration of the machine creates the desirable contact pressure with a concave aluminum wheel attached to a reciprocating arm moved along a pressurized hose, whereas a steel wheel loads the loading strip for the modified configuration. The device is able to test either a 75 mm x 125 mm x 300 mm beam specimen, or a 150 mm diameter by 75 mm thick cylindrical specimen. For this study, only cylindrical specimens were evaluated.

Figure 5-4. Pine gyratory compactor.

The APA test procedure was slightly modified to incorporate a new way of recording and analyzing the test results. Instead of using the roller dial gauge to measure a single (the lowest) point on the specimen, the new method uses a contour gauge that captures the entire surface profile of the sample. In case the material fails, the new method (contour gauge) enables the user to monitor the rate and the mode (consolidation/instability) at which the material is failing.

Figure 5-5 shows the original measuring plate with the 3-inch slits where the dial gauge is dragged to locate the lowest (highest dial reading) spot on the specimen. This method is limited to a single measurement that denotes the maximum amount of permanent deformation on the specimen and there is no way to distinguish if that deformation is due to consolidation or plastic flow.

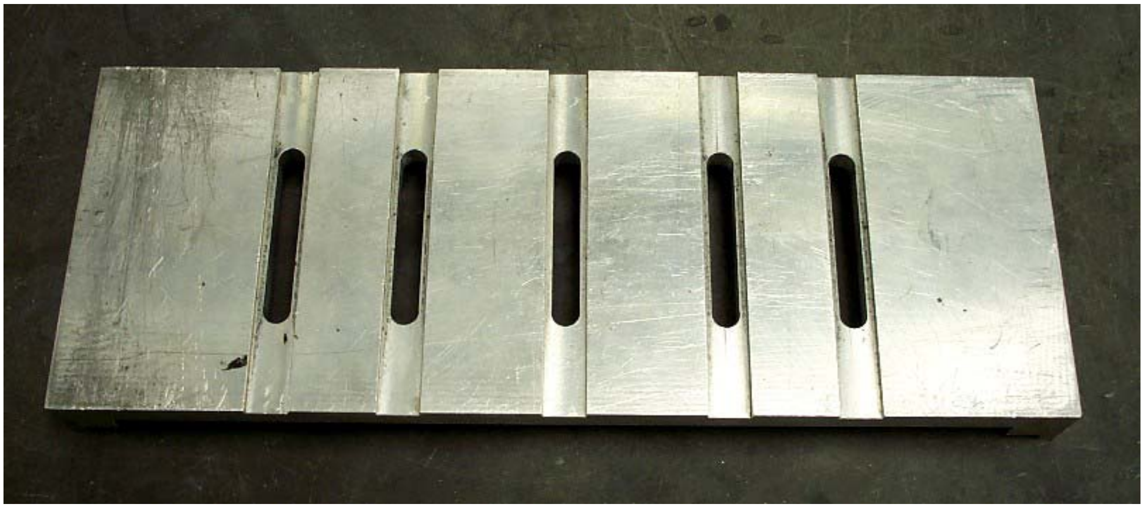

Figure 5-5. Original APA measuring plate.

Figure 5-6 illustrates the aluminum plate used with the new method of measuring the specimen deformation. The slits on the new plate are 5 inches wide at the two extreme locations (marked with an E on Figure 5-6) and 5½ inches at the middle location (marked with an M on Figure 5-6). The contour gauge adjusts to the surface profile of the specimen, which is (the surface profile) recorded and digitized for further analysis.

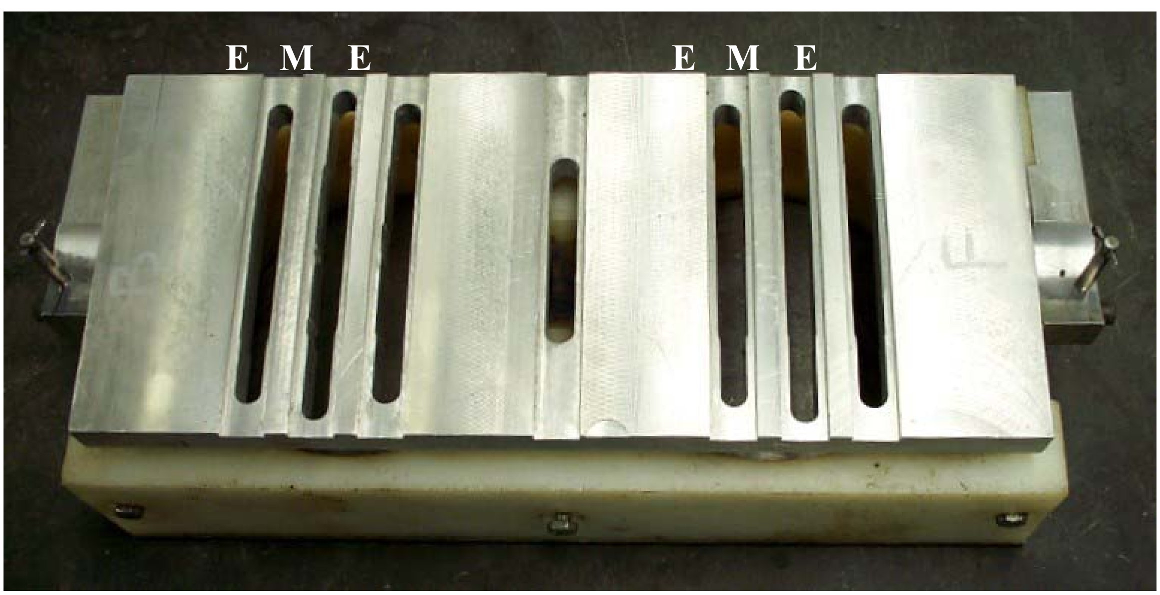

Figure 5-6. New measuring plate with elongated slits.

5.4.1 Surface Profile Measurement

As mentioned above, the new measurement system (contour gauge) was implemented to record the entire surface profile of the specimen. Figure 5-7 shows the contour gauge recording the surface profile at the middle location of the sample. The rods are pushed downwards until they come in contact with the specimen, forcing the contour gauge to assume the shape of the specimen's surface.

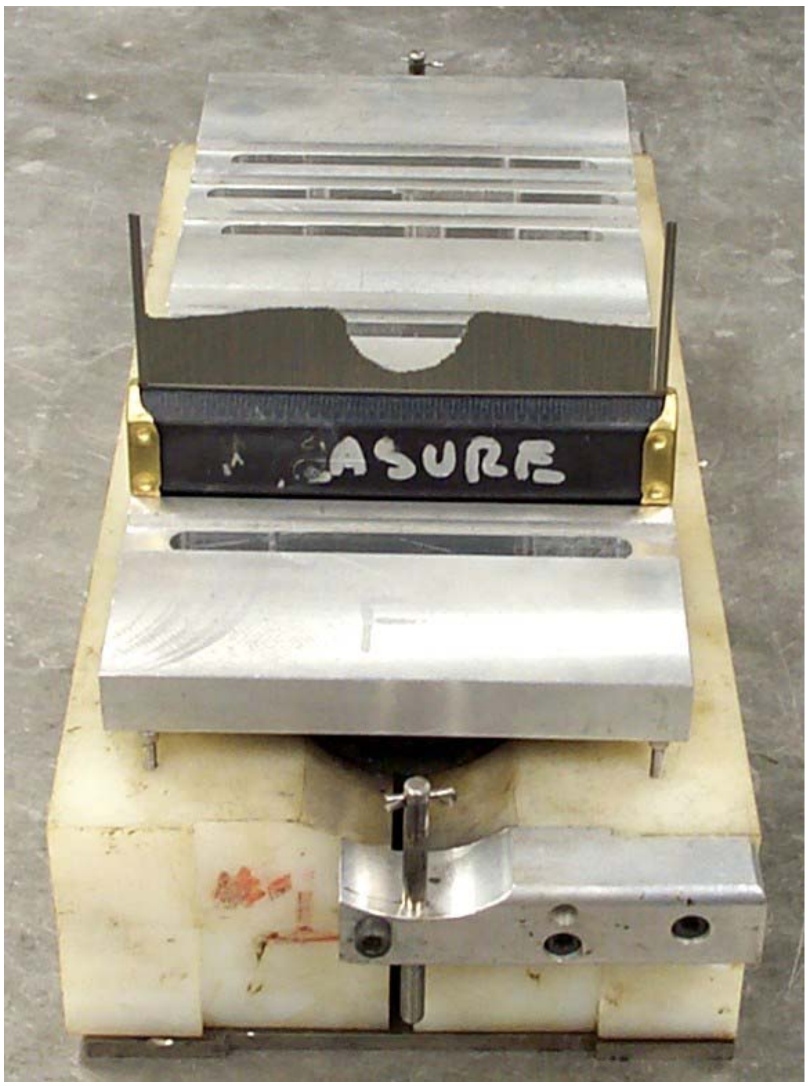

Figure 5-7. Contour gauge measuring the surface profile of the specimen.

Figure 5-8 shows the contour gauge on the custom fabricated holder where the shape of the recorded surface profile, from each location on the measuring plate, is traced on a card. The card slides beneath the contour-gauge rods, whereas two PVC strips restrain the card from any lateral movement.

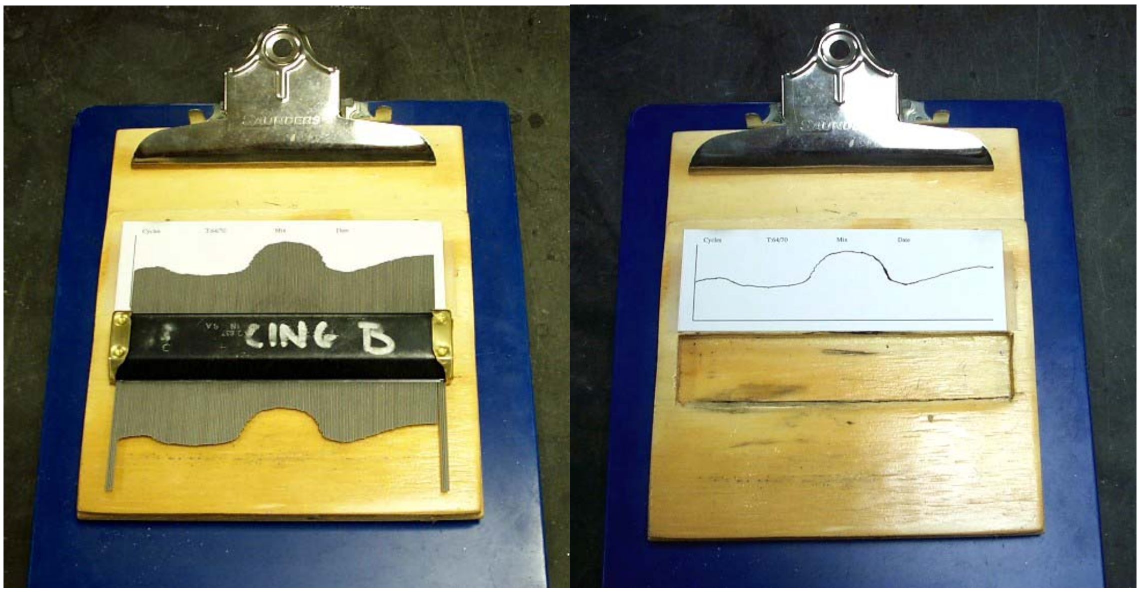

Figure 5-8. Recording the deformed shape of the contour gauge.

5.4.2 APA Hose Testing Procedure

The steps for the APA testing procedure using the pressurized hose are outlined below:

- Preheat the specimen in the APA test chamber to 64ºC (147ºF) for a minimum of 6 hours but not more than 24 hours before the test.
- Set the hose pressure gauge reading to 100±5 psi.
- Calibrate each wheel with the load cell to read a load of 100±5 lb.
- Secure the preheated, molded specimen in the APA, close the chamber doors and allow 10 minutes for the temperature to stabilize.
- Apply 25 load cycles and then take initial (datum) measurements.
- Place the specimen back in the APA, close the chamber doors and allow 10 minutes for the temperature to stabilize.
- Restart the APA and continue rut testing.
- Repeat measurement procedure at 1000, 2000, 4000, and 8000 cycles.

5.4.3 APA Loading Strip Testing Procedure

Outlined below are the steps for the new APA testing procedure:

- Preheat the specimen in the APA test chamber to 64ºC (147ºF) for a minimum of 6 hours but not more than 24 hours before the test.
- Calibrate the steel wheel with the load cell to read a load of 150±5 lb.
- Secure the preheated, molded specimen in the APA, close the chamber doors and allow 10 minutes for the temperature to stabilize.
- Apply 25 load cycles and then take initial (datum) measurements.
- Place the specimen back in the APA, close the chamber doors and allow 10 minutes for the temperature to stabilize.
- Restart the APA and continue rut testing.
- Repeat measurement procedure at 1000, 2000, 4000, and 8000 cycles.

5.5 SUMMARY

The mixtures used in this project contained material that was no longer available (milled material), so the aggregate blend was reconfigured to match the original JMF gradation. Overall, the laboratory engineered mixtures had similar gradations and volumetric properties with the original HMA.

The new testing method for the APA alters the data-recording procedure to gather more information about the sample's performance. Whereas the current FDOT procedure requires four rut-depth measurements per specimen, the new method records approximately 1300 response points per specimen for the analysis. The next chapter describes the data analysis methods as well as the valuable information from the extra measurements.

CHAPTER 6

DATA ANALYSIS METHODOLOGY

6.1 OVERVIEW

The data-recording method in the APA test procedure was modified to incorporate a more detailed way of analyzing the test results. Instead of the dial gauge, used to measure a single (the lowest) point on the specimen, the new method uses a contour gauge to capture the entire surface profile of the sample. The contour gauge's rods are pushed downwards until they come in contact with the specimen, forcing the contour gauge to assume the shape of the specimen's surface. For each of the three locations on the measuring plate, the specimen's surface deformation profile is traced on a card and scanned as a bitmap image for further analysis.

This chapter will focus on the methods used to analyze the data recorded with the contour gauge. The new data-recording method (contour gauge) enables the user to calculate more than just the highest deformation point. With the new method it is possible to monitor the rate and the mode (consolidation/instability) at which the material is failing.

6.2 DIGITIZING THE MEASURED PROFILE

Each specimen requires 15 cards – five measurements at three locations – to capture its rutting profile throughout the 8000-cycle test. To proceed with the data analysis, the cards are scanned as bitmap images (.bmp) and digitized with the help of a program called Grafula3 [Wishnevsky 2003]. Grafula3 allows the user to digitize points from an image of a graph, scanned from originals such as articles, monographs, and diagrams.

Figure 6-1 shows a screen shot of the basic window of the program. Grafula3 reads the bitmap image and, with the help of user-set coordinate axes, it automatically digitizes the selected part of the graph. The data table records the location of each point in Cartesian coordinates that can be transferred into a separate (Excel) spreadsheet for further analysis.

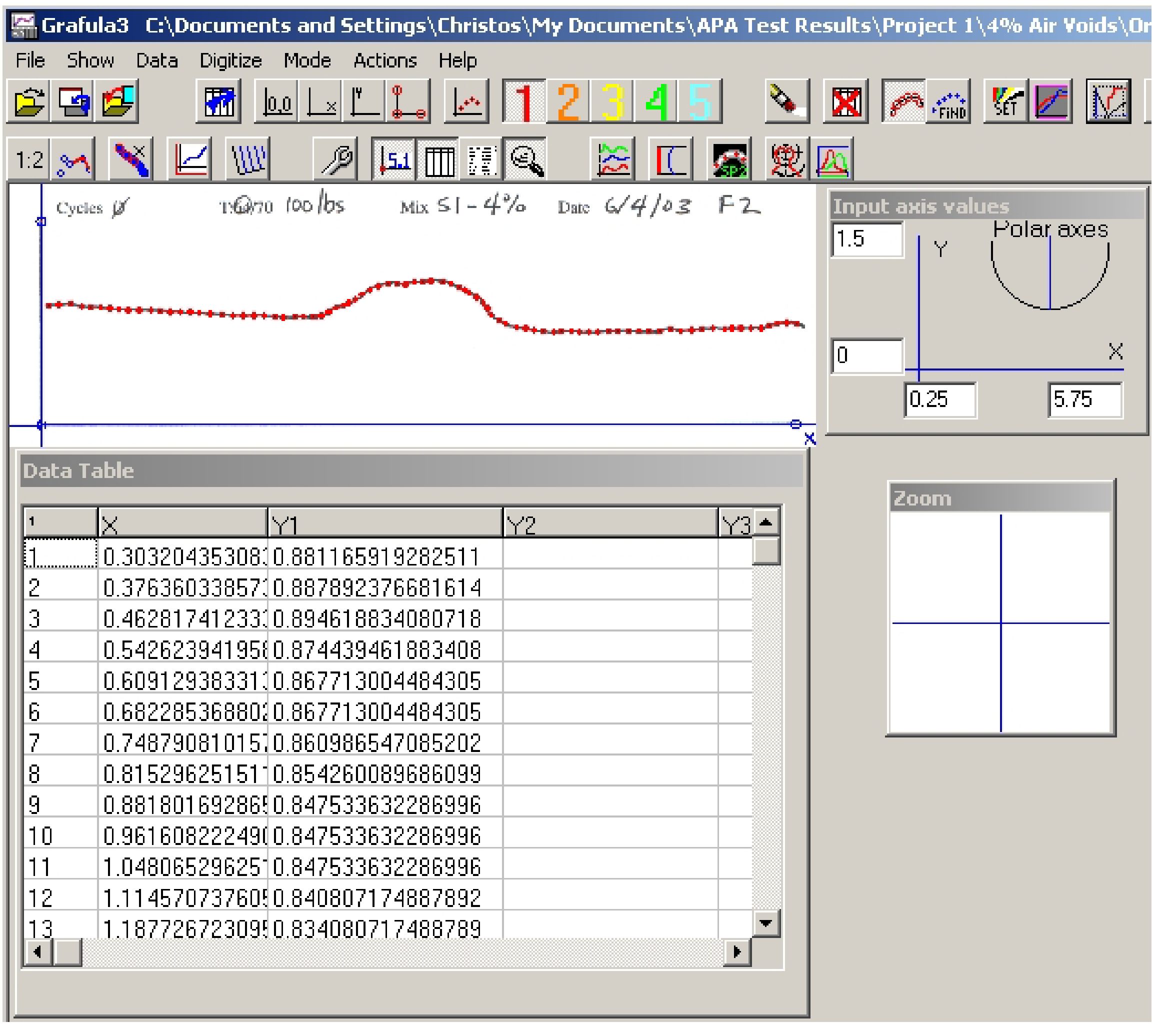

Figure 6-1. Grafula3 screen shot.

6.3 RUT DEPTH CALCULATIONS

The digitized data from the measured surfaced profiles is imported in a spreadsheet and organized per number of remaining cycles. Table 6-1 shows part of a typical table that describes the deformation characteristics of one specimen (at one location) in the course of the test. The cycles are measured in reverse order, so the 8000-cycle measurement is considered to be the initial reference profile (datum).

Table 6-1. Example of a digitized deformation profile from one location.

REMAINING CYCLES									
8000		7000		6000		4000		0	
X	Y	X	Y	X	Y	X	Y	X	Y
0.536	0.816	0.523	0.836	0.543	0.830	0.496	0.803	0.523	0.809
0.609	0.816	0.589	0.823	0.603	0.850	0.569	0.816	0.556	0.823
0.676	0.843	0.656	0.823	0.682	0.863	0.636	0.843	0.609	0.842
0.722	0.863	0.709	0.843	0.762	0.843	0.709	0.836	0.669	0.856
0.775	0.863	0.795	0.843	0.822	0.830	0.789	0.816	0.749	0.842
0.855	0.843	0.835	0.836	0.895	0.830	0.849	0.810	0.802	0.823
0.908	0.830	0.902	0.830	0.955	0.816	0.928	0.803	0.855	0.816
0.995	0.823	0.968	0.823	1.028	0.823	0.982	0.797	0.902	0.809
1.068	0.816	1.048	0.816	1.101	0.823	1.055	0.797	0.982	0.803
1.141	0.823	1.108	0.823	1.188	0.810	1.121	0.797	1.041	0.796
1.208	0.816	1.161	0.823	1.261	0.810	1.194	0.777	1.121	0.803
1.288	0.810	1.234	0.810	1.327	0.823	1.268	0.790	1.188	0.776
1.361	0.823	1.307	0.803	1.401	0.823	1.334	0.783	1.268	0.783
1.434	0.823	1.381	0.823	1.474	0.810	1.407	0.777	1.341	0.783
1.487	0.823	1.460	0.816	1.560	0.810	1.480	0.770	1.421	0.783
1.574	0.810	1.554	0.823	1.633	0.810	1.554	0.777	1.487	0.769

Figure 6-2 illustrates the deformation profile of a specimen tested with the original pressurized hose. An interesting point on this graph is the way the deformation profile changes with the progress of the test. Apparently the material does not only consolidate, but it also heaves to the sides of the loaded area. This is something that the traditional way of measuring the rut-depth results could not show.

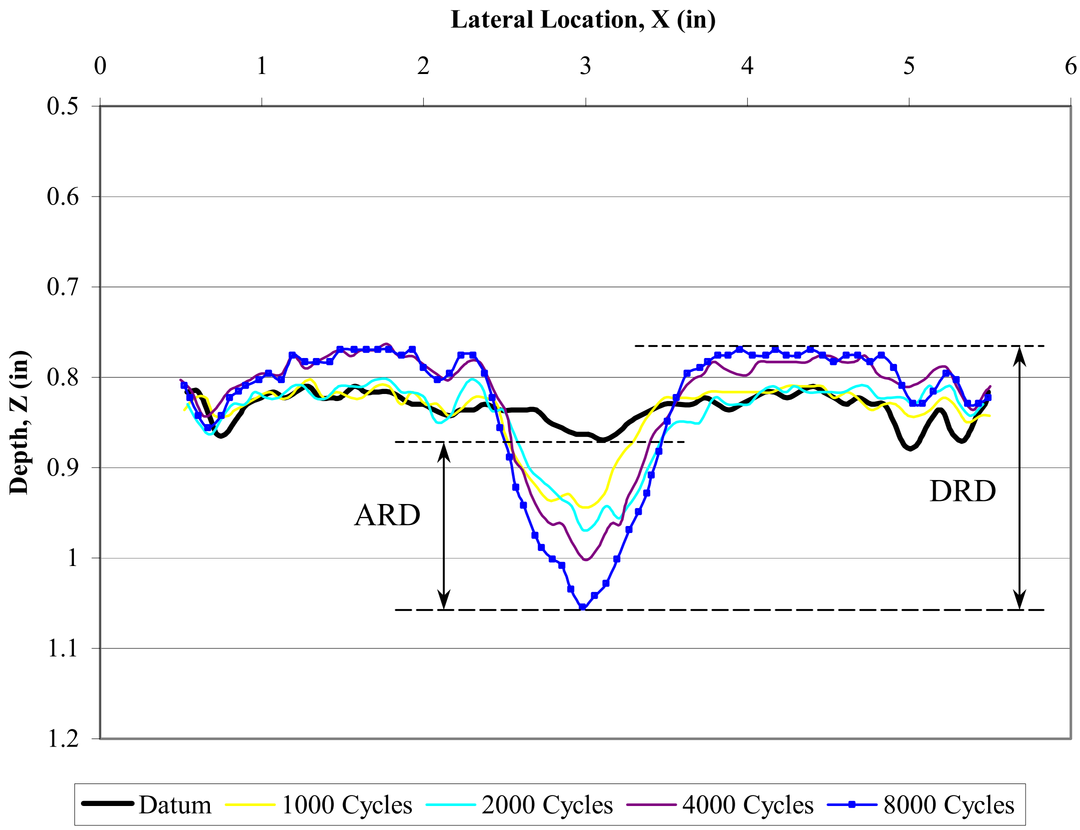

Figure 6-2. Deformation profile for a specimen tested with the pressurized hose.

The traditional way of calculating the rut depth for an APA specimen is to take two measurements – the lowest point at the beginning and the lowest point at the end of the test – and report the difference after 8000 cycles. For the purpose of this study, the traditional way of measuring rut depth will be identified as the Absolute Rut Depth (ARD). The Differential Rut Depth (DRD) is defined as the difference of the lowest point at the beginning of the test and the highest point recorded at the end of the test. Figure 6-2 shows a graphical interpretation of ARD and DRD.

6.4 AREA CALCULATION

In most cases, permanent deformation of asphalt mixtures in the field is a combination of two mechanisms – reduction of air voids and shear deformation. Figure 6-2 proves that the same combination of failure mechanisms applies for HMA specimens tested in the APA. The objective here is to determine which of the two modes of deformation contributes the most in failing the material.

Figure 6-3 illustrates the theory behind the area change calculation. Assume the schematic in Figure 6-3 represents a pavement section that is experiencing excessive rutting. If there was a way to calculate the two shaded areas – A_1 and A_2 – it would be possible to determine if the permanent deformation was primarily due to plastic flow or primarily due to consolidation. In the case that the material fails due to shear deformation, the magnitude of A_1 and A_2 would be equal because the material is shoved to the side. With the same logic, if the material fails primarily due to consolidation the magnitude of A_1 would be lower than A_2.

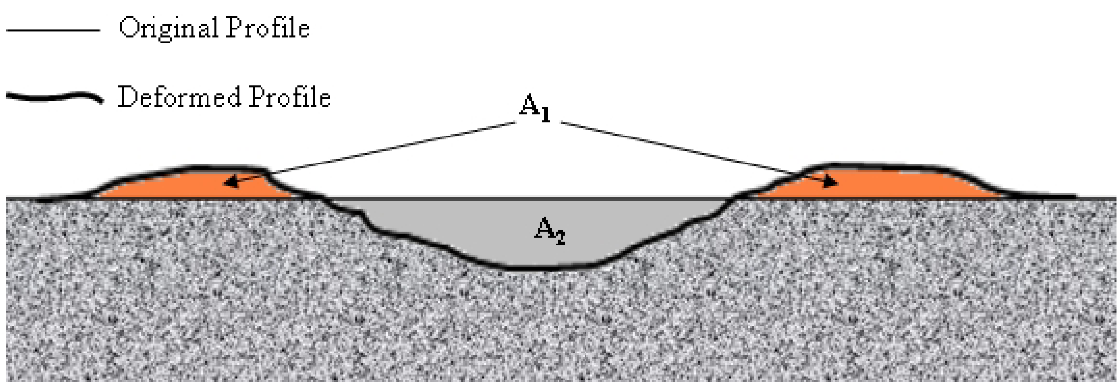

Figure 6-3. Area change interpretation.

To analyze the APA test results, the data was transferred to MathCAD and the LOESS function [Cleveland 1979] was used to fit a polynomial to the original surface-profile data. The LOESS function is best described as a locally-weighted polynomial regression function. The polynomial is fit using weighted least squares, giving more weight to points near the point whose response is being estimated and less weight to points farther away. It is a computational intensive method; however, this is not a problem in our current computing environment unless the data sets are very large.

Once the LOESS function is fitted for the set of surface profile data, the polynomial is integrated over a certain interval to calculate the area under the curve. Figures 6-4 and 6-5 show a graph of the initial and final profile with the smoothed (fitted) polynomial and the calculated areas. Based on the discussion above, the failure mode is primarily consolidation if the initial area (A_i) is less than the final area (A_f). If the A_i is greater or equal to A_f then permanent deformation is primarily due to plastic flow.

A simple way to determine the effect of the area change was to calculate the percent area change (ΔA). A positive ΔA means that the mixture is experiencing instability rutting, whereas a negative ΔA indicates that the mixture is deforming primarily due to consolidation. Therefore:

$$\%\ \text{Area Change} = \frac{A_i - A_f}{A_i} \times 100 \qquad (6\text{-}1)$$

$$\text{If } \%\ \text{Area Change} > 0 \rightarrow \text{Primarily Instability}$$
$$\text{If } \%\ \text{Area Change} \leq 0 \rightarrow \text{Primarily Consolidation}$$

6.5 SUMMARY

The new method of recording data for the APA test provides a plethora of information that can be further analyzed to determine the leading mode of failure. The two new parameters – differential rut depth and percent area change that are calculated from the recorded surface profiles provide insight about the mixture's ability to resist instability rutting. The next chapter discusses the APA tests results and the effects of each factor – loading mechanism, compaction level, and temperature.

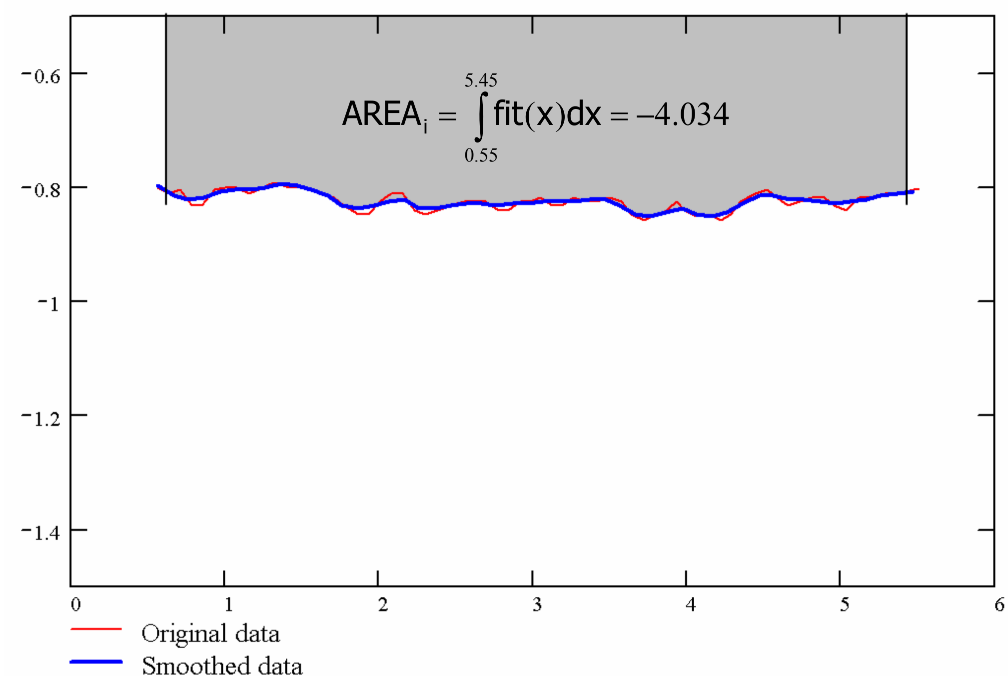

Figure 6-4. Initial surface profile and area calculation.

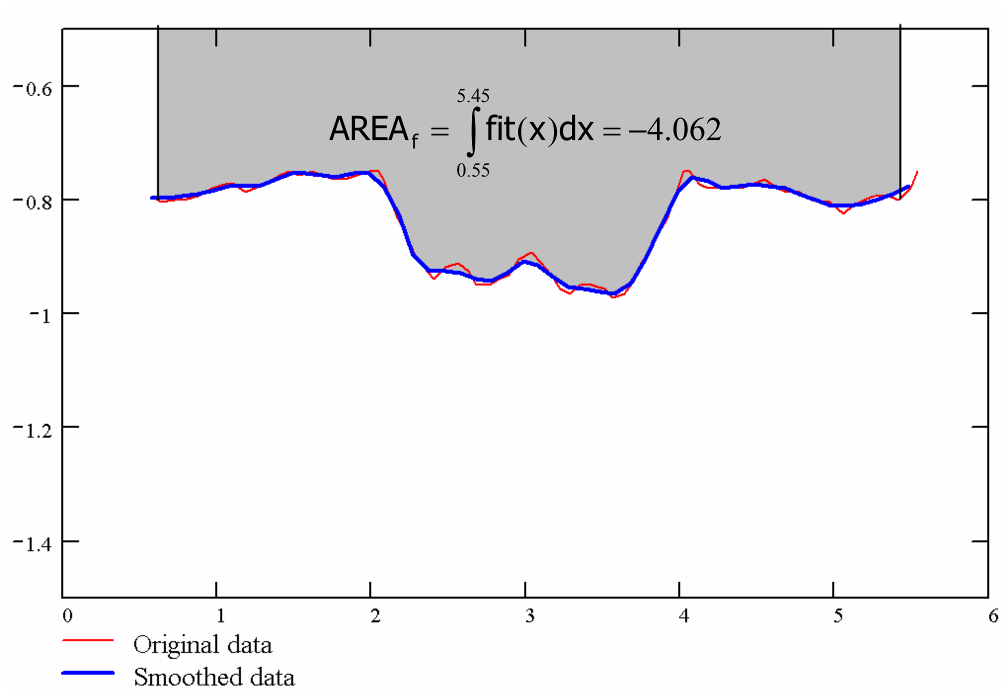

Figure 6-5. Final surface profile and area calculation.

CHAPTER 7
APA TEST RESULTS

7.1 OVERVIEW

Three mixtures – Project 1, Project 7, and the HVS mixture – were tested with the modified and original APA loading devices. The new method for measuring deformations, recording the entire surface profile, was used in both tests. Tests run with the loading strip were performed at two temperatures – 64°C and 70°C – whereas tests with the pressurized hose were run at 64°C. Also, the mixtures were prepared and tested at two air void content levels – 4%AV and 7%AV – to evaluate the effects of compaction on the test's ability to predict permanent deformation.

Field measurements were available for the two Superpave monitoring project mixtures – Project 1 and Project 7. For this reason, the APA results from the various testing procedures were compared to evaluate each test method's reliability in predicting performance. Appendix B contains the results of the one-tailed t-tests performed to examine the statistical significance of the differences. Initially, Project 5 was selected as the third mixture to be included in the test sequence, but the material was no longer available so it was substituted with the HVS coarse-graded mixture.

7.2 FIELD RESULTS

The field rut depths were measured using a transverse profiler at thirty locations of each project. Table 7-1 shows the average accumulated rut depths two years after the end of construction and opening of the pavements to traffic. The measured rut depths show that Project 1 experienced higher rutting while Project 7 shows relatively lower rutting within the same period. Figure 7-1 compares the field rut depth per ESAL between the two Superpave projects. Looking at the normalized rut depth, it is further established that Project 7 performed better in the field, in terms of rutting resistance, than Project 1.

Table 7-1. Field rutting data.

Project No.	Avg. Field Rut Depth After Year 2 (mm)	Estimated ESAL at Year 2 (milion)
1	5.1	1.48
7	2.5	2.99

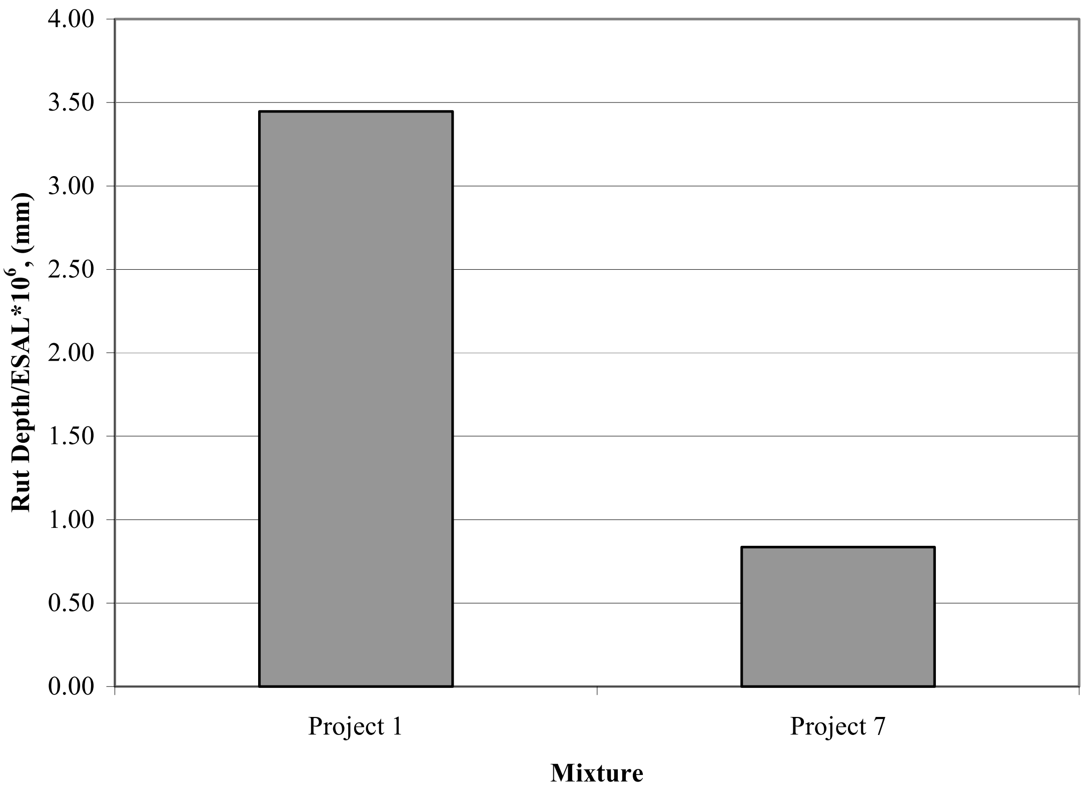

Figure 7-1. Measured field rut depth per million ESAL.

7.3 ABSOLUTE RUT DEPTH

Absolute rut depth is the measured difference between the lowest point of the initial surface profile and the lowest point of the final surface profile. This is the traditional way of measuring the specimen's performance in the APA. Various agencies suggest that the criterion for good field-rutting performance is to keep ARD less than 8 mm [Kandhal and Cooley, Jr. 2002].

Figure 7-2 compares the absolute rut depth results between Project 1 and Project 7 for the three test methods – new APA 64°C, new APA 70°C, and the original APA – at four percent air void content (4%AV). Results from the new and original APA tests at 64°C did not show any significant difference in performance between the two mixtures. However, the new APA tests at 70°C showed that the ARD for Project 1 increased whereas the ARD for Project 7 remained at the same level. Figure 7-3 shows ARD results for the same two projects tested at 7%AV. In the case of 7%AV, results from all three tests showed significant difference between the performances for the two mixtures.

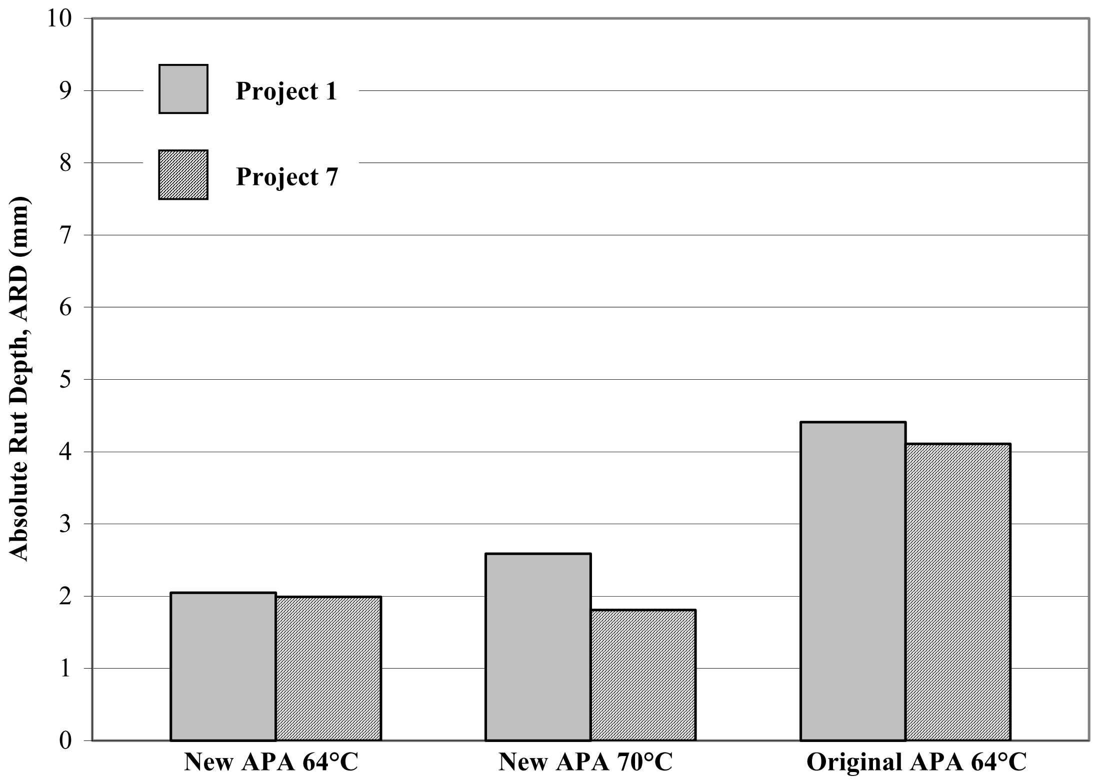

Figure 7-2. Absolute rut depth measurements for Projects 1 and 7 with the two loading devices at 4% AV.

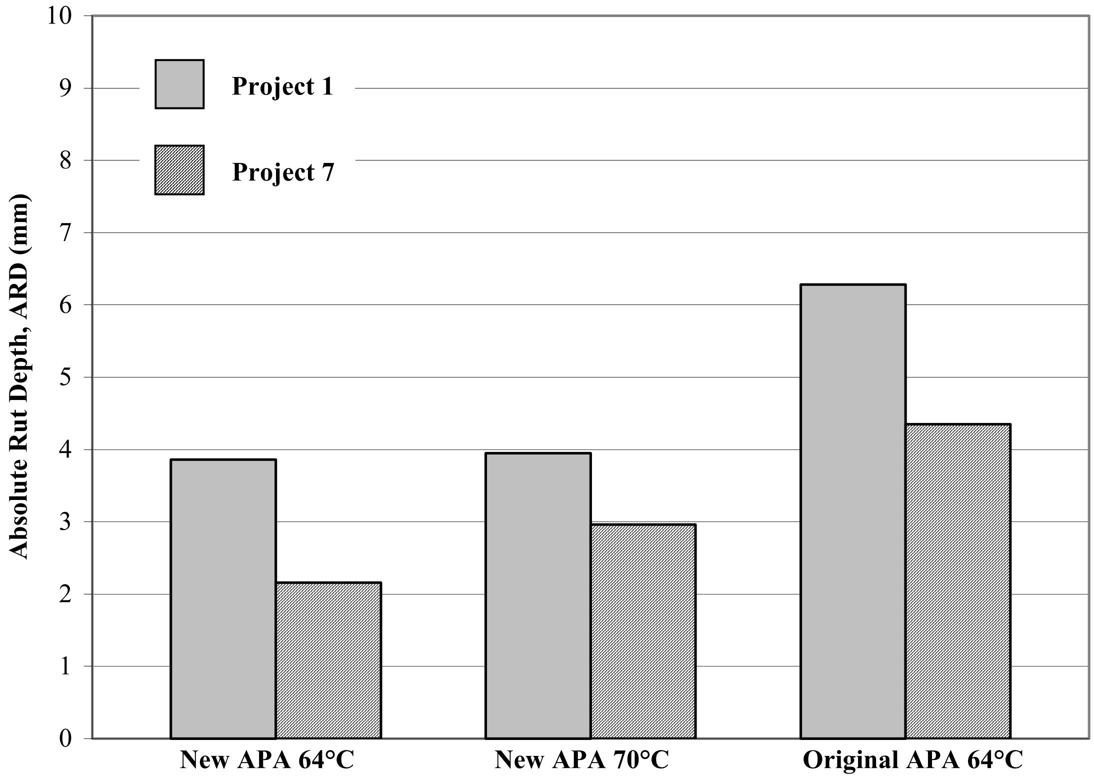

Figure 7-3. Absolute rut depth measurements for Projects 1 and 7 with the two loading devices at 7% AV.

7.4 DIFFERENTIAL RUT DEPTH

The differential rut depth is defined as the difference of the lowest point at the beginning of the test and the highest point recorded at the end of the test. The function of this parameter is to incorporate the instability characteristics of the material into the rutting prediction. Unlike the ARD, the DRD includes the dilated portion of the deformed material into the measurement.

Figure 7-4 compares the differential rut depth results between Project 1 and Project 7 for the three test methods – new APA 64°C, new APA 70°C, and the original APA – at 4% air void content (4%AV). Similar to the ARD results, the new and original APA tests at 64°C did not

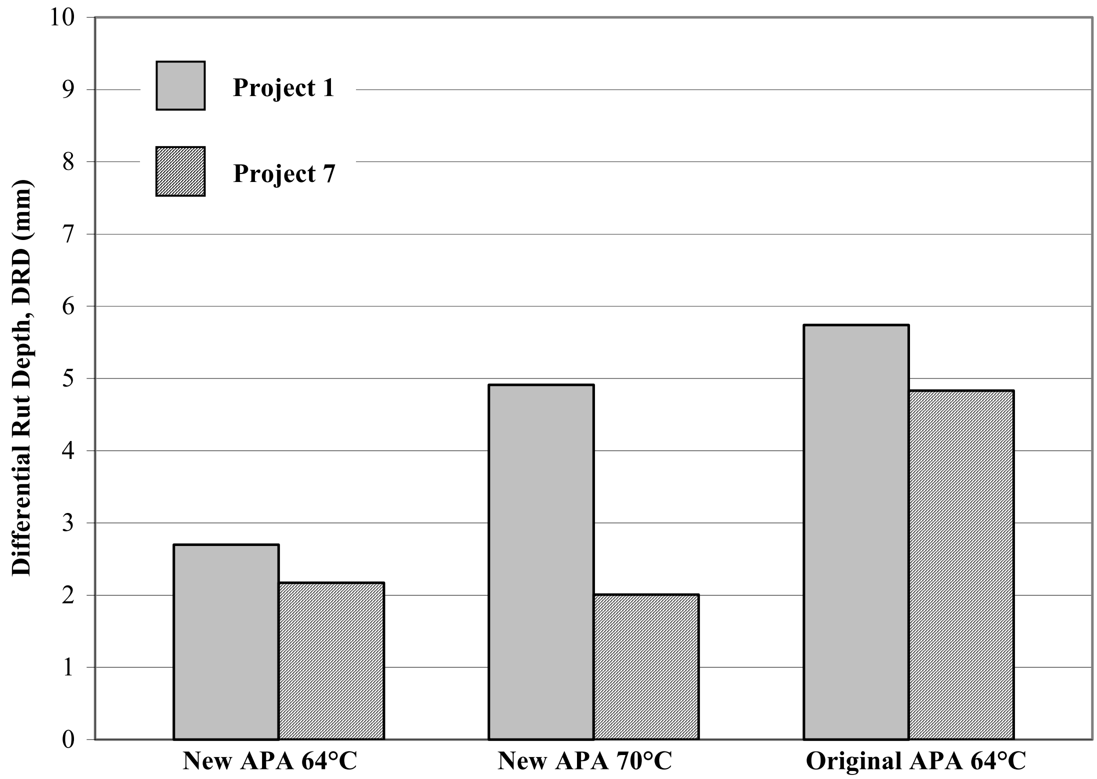

Figure 7-4. Differential rut depth measurements for Projects 1 and 7 with the two loading devices at 4% AV.

show any significant difference in performance between the two mixtures. Once again, the new APA tests at 70°C showed that the DRD for Project 1 increased whereas the DRD for Project 7 remained at the same level. Since the binder is the same for both projects, the difference in DRD suggests that the new APA might be able to account for the effect of aggregate structure in the mixture's ability to resist rutting, something other studies [Kandhal and Cooley, Jr. 2002, Romero and Stuart 1998] showed that the APA was not able to do.

Figure 7-5 shows DRD results for the same two projects tested at 7%AV. Once again, the 7%AV results from all three tests showed significant difference between the performances for the two mixtures.

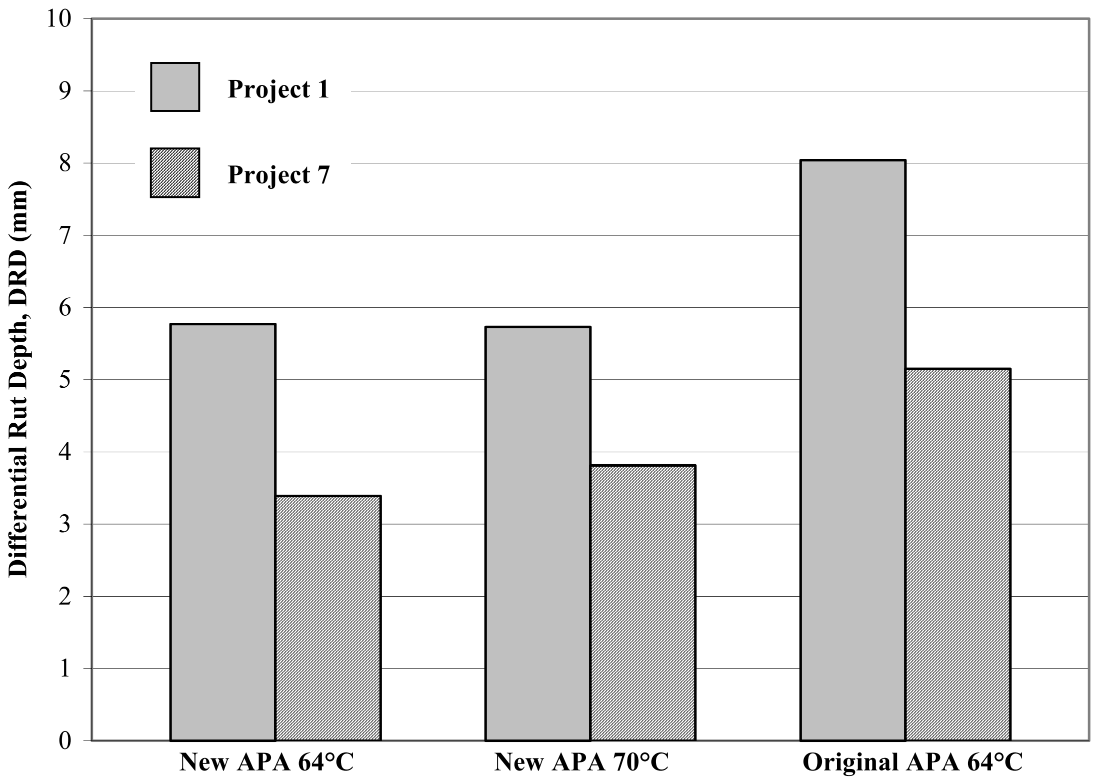

Figure 7-5. Differential rut depth measurements for Projects 1 and 7 with the two loading devices at 7% AV.

7.5 RUT-DEPTH FINDINGS

The two Superpave monitoring project mixtures were tested at two density levels – 4%AV and 7%AV – with the new and original loading devices. Tests with the loading strip were run at two temperatures – 64°C and 70°C. The new measurement system (surface profile) was used to record results for all tests. The key rut-depth findings are the following:

- Based on absolute rut depth measurements at 4%AV, none of the tests were able to distinguish the better performing mixture between Project 1 and Project 7.
- Absolute rut depth results at 7%AV for all test methods – new APA 64°C, new APA 70°C, and the original APA – showed that Project 7 performed better.
- The differential rut depth measurements at 4%AV did not how any difference in the results at 64°C (original and new APA). There was, however, difference in the DRD results for the new APA 70°C.

- All test methods showed a difference for the DRD at 7%AV.

Results from the two Superpave projects tested at 7%AV showed that the new and original APA test methods were able to differentiate the two mixtures according to their field performance. The issue, however, is whether the performance prediction based on rut depth measurement is adequate to describe the mixture's ability to resist permanent deformation. It is known that resistance to consolidation is not necessarily related to resistance to shear instability. Tests performed at 7%AV can not conclusively determine whether the mixture is failing primarily due to instability or because of excessive consolidation. The same mixture that fails at 7%AV might demonstrate adequate performance at a higher density level.

At 4%AV it is easy to assume that most of the measured rutting will be associated with instability. However, rut depth results at 4%AV from the new and original APA at 64°C did not distinguish between the mixtures. Thus, there is a need to identify a measure or a parameter that is uniquely associated with mixture shear instability.

7.6 AREA CHANGE

As discussed earlier (Section 6.4), calculating the area change between the initial and final surface profiles enables us to determine the predominant mode of permanent deformation – consolidation or instability – of HMA mixture. The failure mode is primarily consolidation if A_i is less than A_f (negative percent area change), whereas the failure mode is considered to be primarily consolidation if A_f is less than A_i (positive percent change).

Field observations, reported from the Superpave monitoring project, show that Project 1 is experiencing higher rutting than Project 7 and that the failure mode for the Project 1 rutted sections appears to be instability [Roque and Villiers 2003]. Figure 7-6 shows the percent area change for the two mixtures, at 4%AV, calculated for the new and original APA test methods.

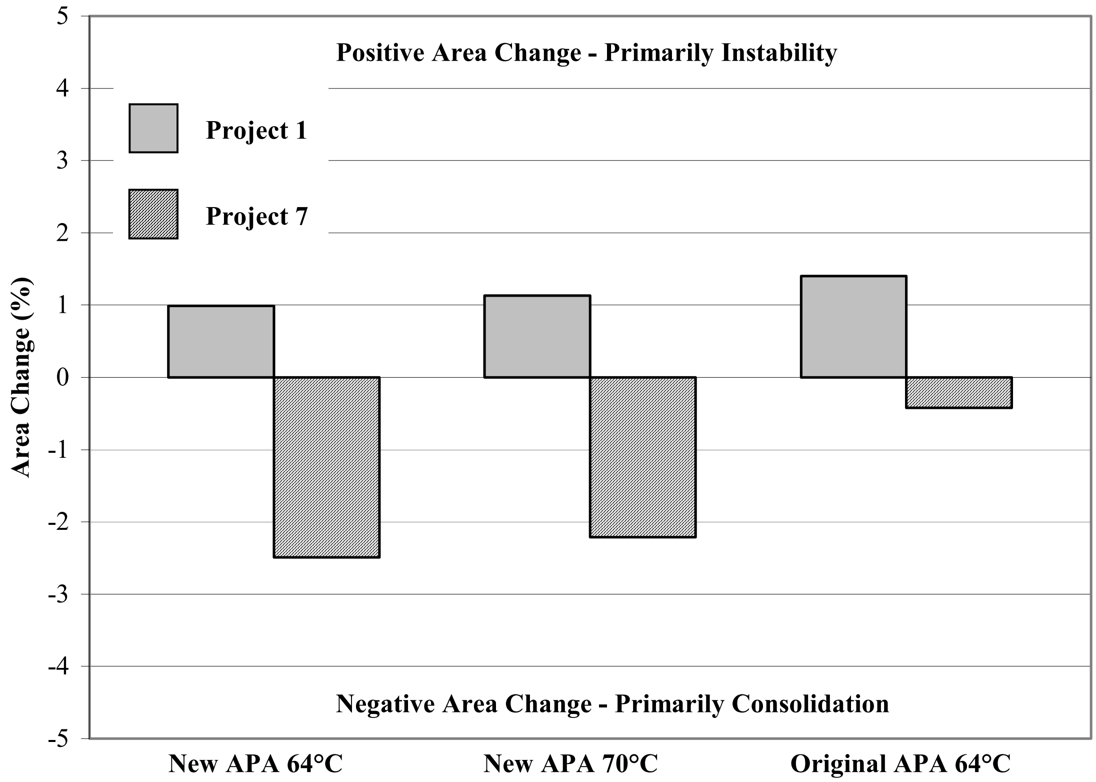

Figure 7-6. Area Change measurements for Projects 1 and 7 with the two loading devices at 4% AV.

All three methods – new APA 64°C, new APA 70°C, and the original APA – predicted positive area change (instability) for Project 1 and negative area change (consolidation) for Project 7.

Figure 7-7 shows the percent area change for the two mixtures, at 7%AV, calculated for the new and original APA test methods. Results for the 7% air void content showed that all three methods predicted positive area change (instability) for Project 1 and negative area change (consolidation) for Project 7. However, statistical analysis for the Original APA results showed no significant difference between the two projects.

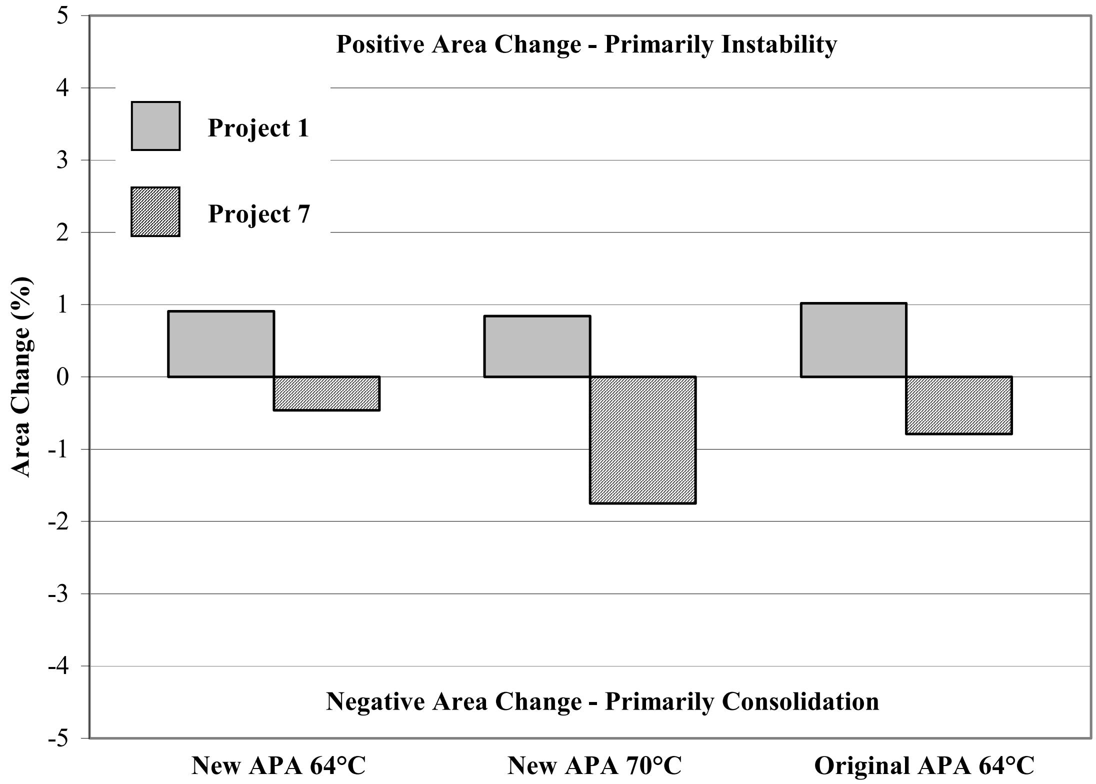

Figure 7-7. Area Change measurements for Projects 1 and 7 with the two loading devices at 7% AV.

7.7 UNIDIRECTIONAL LOADING

One of the objectives of this study was to evaluate the feasibility and the effects of uni-directional (load is applied in one direction only) loading in the APA. The new loading device was used to test the two Superpave projects in unidirectional-load mode at two temperatures – 64°C and 70°C.

The unidirectional loading revealed many issues unknown at the time of the test-planning stage. In unidirectional mode, the APA can test only one sample per mold (the back sample position) because the pneumatic load is applied halfway into the first (front) sample. Figure 7-8 shows the load sequence in unidirectional mode. The pneumatic controller initiates the loading sequence at the beginning of the front sample but the load appears to peak three inches into the load path. Because of the inefficient nature of the test procedure and the limited amount of data, this part of the study is inconclusive.

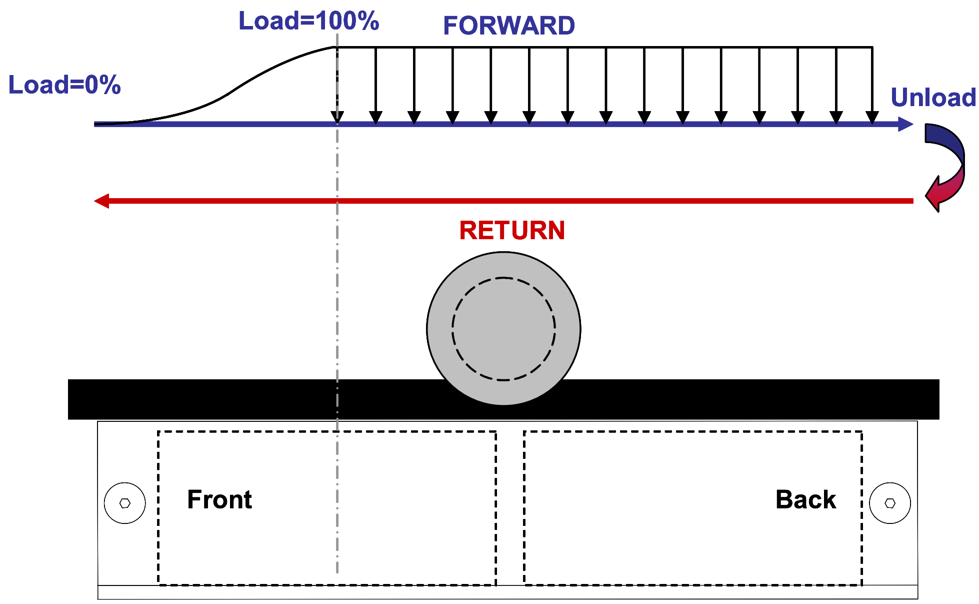

Figure 7-8. Unidirectional loading in the APA.

7.8 HVS MIXTURE

As mentioned earlier, the HVS coarse-graded mixture was substituted because material for Superpave Project 5, a mixture with good field performance, was not available. The HVS coarse-graded mixture was selected because it performed well in tests with the Heavy Vehicle Simulator at the FDOT [Moseley et al. 2003].

Figures 7-9 and 7-10 show the absolute rut depth and differential rut depth results for the HVS mixture respectively. The mixture was tested with the three test methods – new APA 64°C, new APA 70°C, and the original APA at two density levels – 4%AV and 7%AV. All test measurements gave rut-depth predictions – absolute and differential – below 3mm, which corresponds to the Heavy Vehicle Simulator test observations.

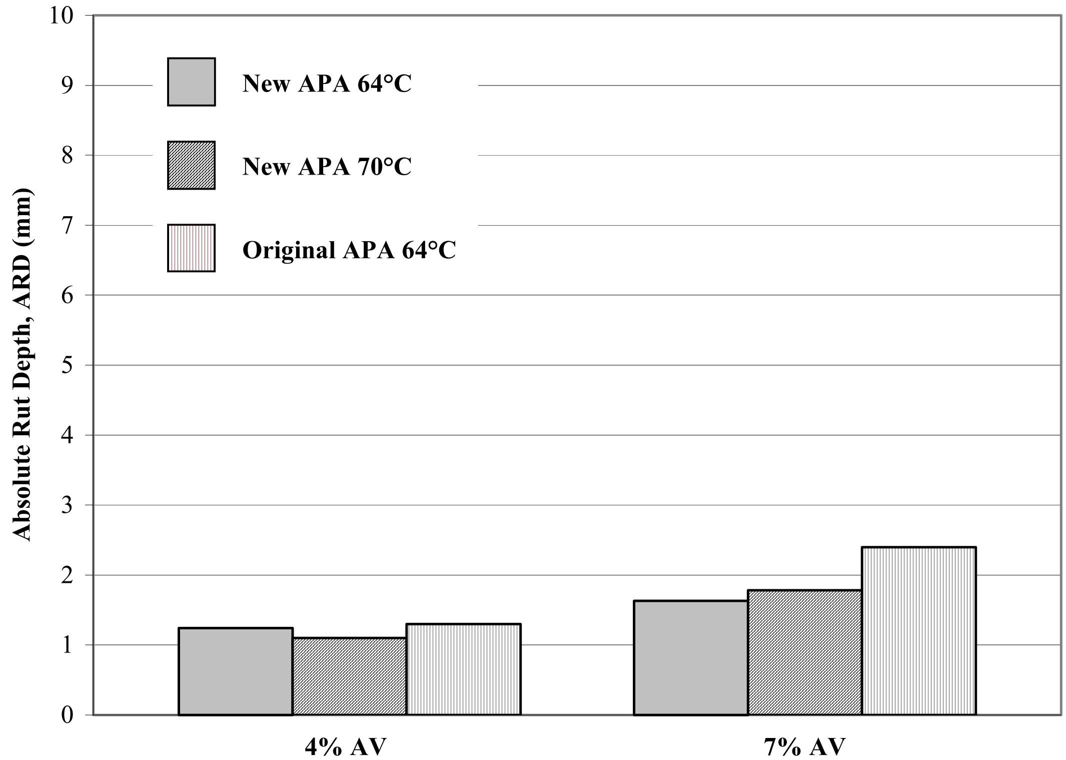

Figure 7-9. Absolute rut depth measurements for the HVS mixture with the two loading devices at two AV levels – 4% and 7%.

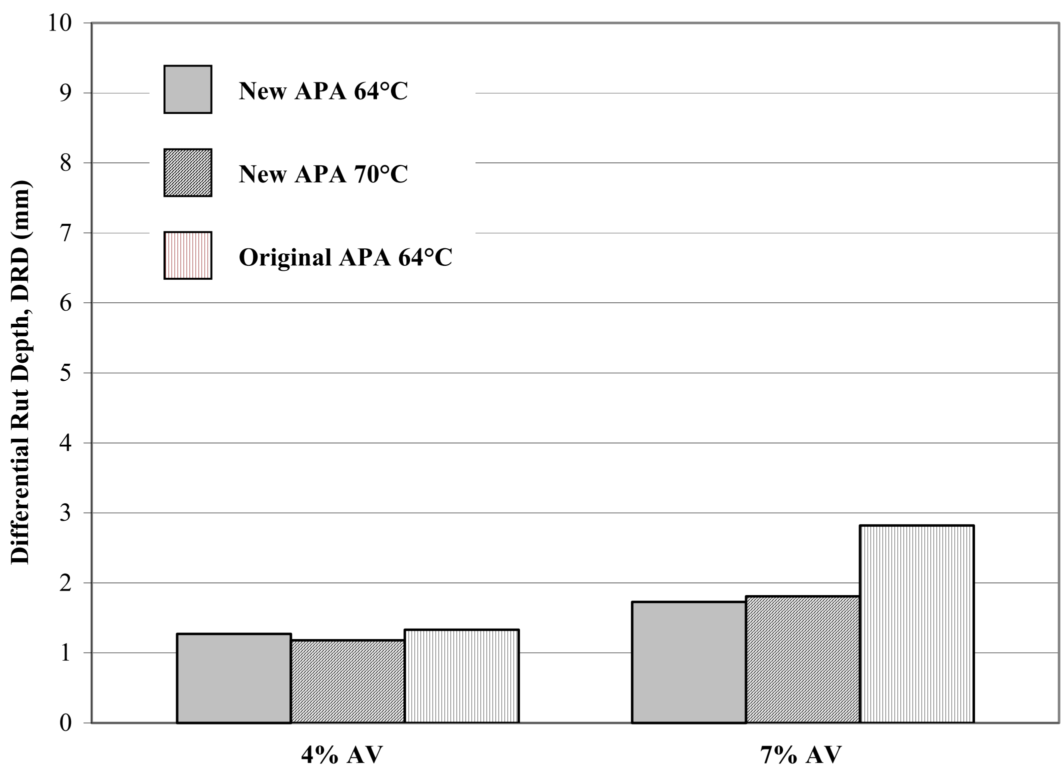

Figure 7-10. Differential rut depth measurements for the HVS mixture with the two loading devices at two AV levels – 4% and 7%.

The measured rut-depth results – ARD and DRD – from the new APA tests at normal (64°C) and high (70°C) temperatures were almost identical. This might be another indication about the ability of the new APA loading device to account for the effect of aggregate structure in rutting prediction.

7.9 DISCUSSION

The rut-depth findings showed that both devices were able to distinguish between the two mixtures according to their field performance. However, rut depth by itself is not adequate to determine whether the measured deformation is primarily due to consolidation or because of shear instability. The introduction of the area-change parameter provided a tool to quantify consolidation and shear instability.

Both loading devices were able to show the difference in the mode of failure (permanent deformation) for the two mixtures. Project 1 had a positive area change – primarily instability – and Project 7 had a negative area change – primarily consolidation. The two loading devices were able to distinguish between the two mixtures for resistance to shear instability even though the stress distributions under the two loading mechanisms were found to be very different. The loading strip was designed and constructed to simulate stresses – in particular the lateral stresses – found under a radial-tire rib. These lateral stresses were found to be a key factor in the mechanism of instability rutting.

Even though the measured stresses under the pressurized hose did not show the presence of lateral stresses, the hose was still able to determine that Project 1 failed primarily due to shear instability. The reason behind this phenomenon is the continuously-changing contact area between the hose and the HMA sample. At the beginning of the test the contact area between the hose and the specimen was measured to be approximately 6-8 mm. Figure 7-11 shows the initial contact area at the hose-specimen interface. At this stage the stresses induced at the hose-specimen interface are primarily vertical stresses (Section 3.5.2).

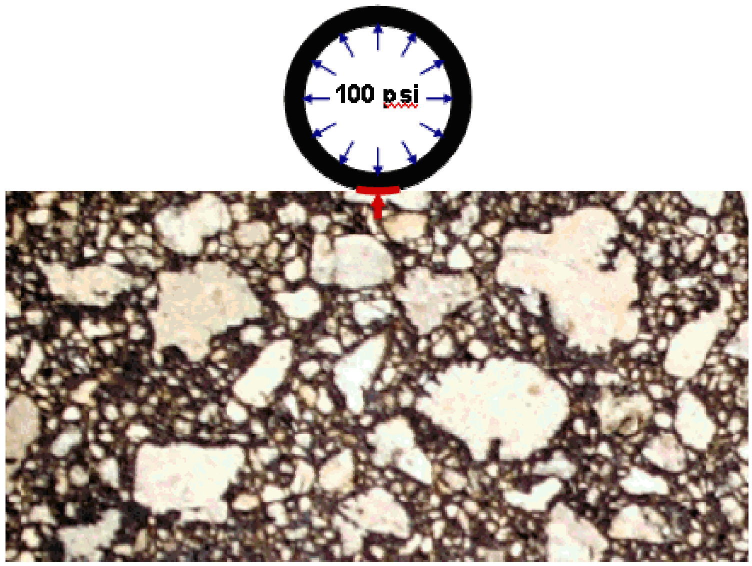

Figure 7-11. Schematic of the initial hose-specimen contact area.

As the test progresses and the specimen consolidates under the vertical stress, the hose 'sinks' into the specimen and the contact area increases. Figure 7-12 shows a hypothetical contact area at some point beyond 4000 cycles. At this point the specimen is experiencing high shear stresses from the walls of the pressurized hose.

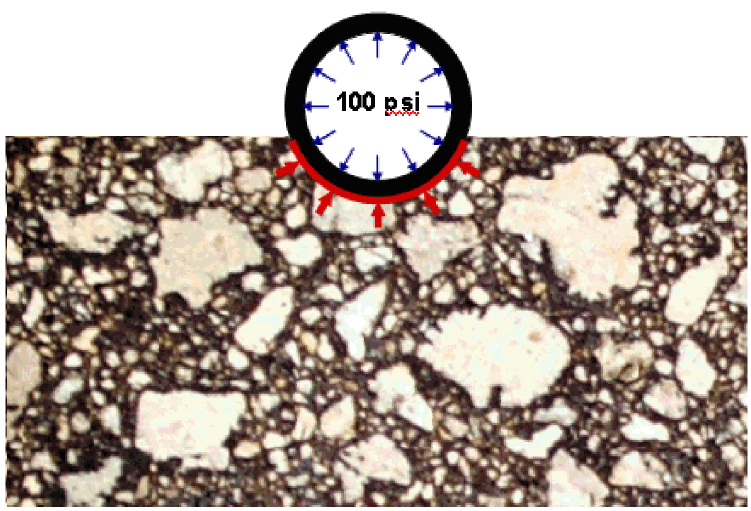

Figure 7-12. Schematic of a hypothetical hose-specimen contact area after 4000 cycles.

Findings from this study showed that both loading devices – loading strip and pressurized hose – were able to distinguish the better performing mixture based on the area-change calculation. However, the mechanism that drives the material to instability failure is different for each loading device. Measurements showed that the loading strip induces lateral stresses on the surface of the specimen at the beginning of the test that remain constant throughout – since the contact area remains the same. Contrary to that, the pressurized hose does not induce these critical stress states (lateral stresses) until after the specimen is consolidated. Thus, for a material that has good resistance to consolidation, the pressurized hose would be less successful in evaluating the mixture's ability to resist shear instability. Likewise, for a material that has poor resistance to consolidation, the pressurized hose could 'sink-in' and induce high shear stresses that could lead to the misinterpretation of the mixture's shear strength.

CHAPTER 8

CONCLUSIONS AND RECOMMENDATIONS

8.1 CONCLUSIONS

The following conclusions were drawn from this study:

- The new system (loading strip and profile measurement method) appears to have greater potential of evaluating a mixture's potential for instability rutting than the original (hose and single rut-depth measurement) configuration.
- It is possible to conduct more reliable interpretation of the original APA (pressurized hose) results by using the new system of measuring the entire surface profile of the specimen.
- The loading strip is a better system in engineering terms, but the APA pressurized hose is more practical and widely available.

8.2 RECOMMENDATIONS

The following recommendations are based on the findings and conclusions from this study:

- The new data-measurement method should be implemented immediately with the existing equipment.
- Whenever possible, specimens should be tested at both 7%AV and 4%AV when evaluating the mixture's ability to resist instability.
- At this point there is not enough evidence to support a move to higher temperature testing for a single-condition test (specimen tested at one temperature).

REFERENCE LIST

Aschenbrener, T., "Evaluation of the Hamburg Wheel-Tracking Device to Predict Moisture Damage in Hot-Mix Asphalt," Transportation Research Record 1492, Transportation Research Board, Washington, DC, 1995, pp. 193-201.

Asiamah, S., "Relationship between Laboratory Mix Properties and Rutting Resistance for Superpave Mixtures," Master's thesis, University of Florida, Gainesville, 2002.

Bathe, K. ADINA System 7.5, User's Manual. ADINA R&D, Inc. Watertown. MA 2001.

Birgisson, B., R. Roque, C. Drakos, M. Novak, and B. Ruth, "Mechanisms of Instability Rutting in Hot Mix Asphalt Pavements," Canadian Technical Asphalt Association, Calgary, Canada, 2002.

Bonaquist, R., J. Sherwood, and K. Stuart, "Accelerated Pavement Testing at the Federal Highway Administration Pavement Testing Facility," Association of Asphalt Paving Technologists, Vol. 67, 1998, pp. 690-716.

Choubane, B., G.C. Page, and J.A. Musselman, "Investigation of the Suitability of the Asphalt Pavement Analyzer for Predicting Pavement Rutting," Research Report FL/DOT/SMO/98-427, Florida Department of Transportation, Gainesville, October 1998.

City of Hamburg, "Tracking Test, Determination of the Track Depth of High-Stability Binding Layers," Construction Bureau, Civil Engineering Office, Department of City Traffic, Hamburg, Germany, 1991.

Cleveland, W.S., "Robust Locally Weighted Regression and Smoothing Scatterplots," Journal of the American Statistical Association, Vol. 74, 1979, pp. 829-836.

Collins, R., D. Watson, and B. Campbell, "Development and Use of the Georgia Loaded Wheel Tester," Transportation Research Record No. 1492, Transportation Research Board, Washington, DC, 1995, pp. 202-207.

Collins, R., H. Shami, and J. S. Lai, "Use of Georgia Loaded Wheel Tester to Evaluate Rutting of Asphalt Samples Prepared by Superpave Gyratory Compactor," Transportation Research Record No. 1545, Transportation Research Board, Washington, DC, 1996, pp. 161-168.

Cook, R. Finite Element Modeling For Stress Analysis. John Wiley and Sons, Inc., New York, 1995.

Cooley, A.L., P.S. Kandhal, and S.M. Buchanan, "Loaded Wheel Testers in the United States: State of Practice," Transportation Research Circular, Number E-C016, July 2000, ISSN00978515.

Corté, J.F., and J.P. Serfass, "The French Approach to Asphalt Mixture Design: A Performance-Related System of Specifications," Association of Asphalt Paving Technologists, Vol. 69, 2000, pp. 794-834.

Darku, D., "Evaluation of the Superpave Gyratory Compactor for Assessing the Rutting Resistance of Asphalt Mixtures," PhD dissertation, University of Florida, Gainesville, 2003.

De Beer, M., C. Fisher, and F. Jooste, "Determination of Pneumatic Tyre/Pavement Interface Contact Stresses Under Moving Loads and Some Effects on Pavements With Thin Asphalt Surfacing Layers," Proceedings of the Eighth International Conference on Asphalt Pavements, Seattle, Washington, 1997, pp. 179-226.

De Jong, D. L., M. G. F. Peatz, and A. R. Korswagen. "Computer Program BISAR, Layered Systems Under Normal and Tangential Loads," Koninklijke/Shell-Laboratorium, External Report AMSR.0006.73, Amsterdam, The Netherlands, 1973.

Drakos, C., "Effect of Measured Tire Contact Stresses on Near Surface Wheel Path Rutting of Asphalt Pavements," Master's thesis, University of Florida, Gainesville, 2000.

Drakos, C., R. Roque, and B. Birgisson, "Effects of Measured Tire Contact Stresses on Near Surface Rutting," Transportation Research Record No. 1764, Transportation Research Board, Washington, DC, 2001, pp. 59-69.

Epps, J., C.L. Monismith, S.B. Seeds, S.C. Ashmore, and T.M. Mitchell, "WesTrack Full-Scale Test Track: Interim Findings," International Symposium on Asphalt Pavements (ISAP), August 1997, http://www.westrack.com/wt_04.htm, last accessed on 2/5/2003.

Federal Highway Administration, SUPERPAVE™ Support and Performance Models Management, "Preliminary Recommendations for the Simple Performance Test," FHWA No. DTFH 61-94-R-00045, Research Report to the U.S. Department of Transportation, University of Maryland, College Park, MD, May 1998.

Harvey, J., and L. Popescu, "Accelerated Pavement Testing of Rutting Performance of Two CalTrans Overlay Strategies," Transportation Research Record No. 1716, Transportation Research Board, Washington, DC, 2000, pp. 116-125.

Hibbitt, Karlsson and Sorensen, Inc., Computer Program ABAQUS. Version 5.7, Pawtucket, RI, 1997.

Huang, Y.H., Pavement Analysis and Design, Prentice-Hall, Englewood Cliffs, NJ, 1993.

Huber, G.A., "Methods To Achieve Rut-Resistance Durable Pavements," Synthesis of Highway Practice 274, Transportation Research Board, National Research Council, Washington, DC, 1999.

Jacobs, Maarten M.J., "Crack Growth in Asphaltic Mixes," PhD dissertation, Delft University of Technology, Delft, The Netherlands, 1995.

Kandhal, P.S., and R.B. Mallick, "Evaluation of Asphalt Pavement Analyzer for HMA Design," Report No. 99-4, National Center for Asphalt Technology, June 1999.

Kandhal, P.S., and L.A. Cooley, Jr., "Evaluation of Permanent Deformation of Asphalt Mixtures Using Loaded Wheel Tester," Report No. 2002-08, National Center for Asphalt Technology, October 2002.

Lai, J.S., "Development of a simplified Method to Predict Rutting Characteristics of Asphalt Mixtures," Research Project 8502, Final Report, Georgia Department of Transportation, Atlanta, 1986.

Lai, J.S., and T.M. Lee, "Use of a Loaded-Wheel Testing Machine to Evaluate Rutting of Asphalt Mixes," Transportation Research Record No. 1269, Transportation Research Board, Washington, DC, 1990, pp. 115-184.

Leahy, R.B., E.T. Harrigan, and H. Von Quintus, "Validation of Relationships Between Specification Properties and Performance," Report No. SHRP-A-409, Transportation Research Board, National Research Council, Washington, DC, 1994.

Marshek, K.M., Chen, H.H., Conell, R.B., and C.L. Saraf, "Effect of Truck Tire Inflation Pressure and Axle Load on Flexible and Rigid Pavement Performance," Transportation Research Record No. 1070, Transportation Research Board, Washington, D.C., 1986, pp. 14-21.

Metcalf, J.B., "Accelerated Pavement Testing, a Brief Review Directed Towards Asphalt Interests," Journal of the Association of Asphalt Paving Technologist, Volume 67, 1998, pp 553-572.

Moseley, H., Page, G., Musselman, J., Sholar, G., and P. Upshaw, "Laboratory Mixture and Binder Rutting Study," Research Report FL/DOT/SMO/03, Florida Department of Transportation, Gainesville, July 2003.

Myers, L., "Mechanism of Whell Path Cracking that Initiates at the Surface of Asphalt Pavements," Master's thesis, University of Florida, Gainesville, 1997.

Myers, L., "Development and Propagation of Surface-Initiated Longitudinal Wheel Path Cracks in Flexible Highway Pavements," PhD dissertation, University of Florida, Gainesville, 2000.

Myers, L., R. Roque, B. Ruth, and C. Drakos, "Measurement of Contact Stresses for Different Truck Tire Types to Evaluate Their Influence on Near-Surface Cracking and Rutting," Transportation Research Record No. 1655, Transportation Research Board, Washington, DC, 1999, pp. 175-184.

Romero, P. and W. Mogawer, "Evaluation of the Superpave Shear Tester Using 19-mm Mixtures from the FHWA ALF," Journal of the Association of Asphalt Paving Technologist, Volume 67, 1998, pp 573-601.

Romero, P., and K. Stuart, “Evaluating Accelerated Rut Testers,” Public Roads, Federal Highway Administration, U.S. Department of Transportation, Vol. 62, No 1, July/August 1998, p.50.

Roque, R., Myers, L., and B.E. Ruth, “Loading Characteristics of Modern Truck Tires and Their Effects on Surface Cracking of Asphalt Pavements,” Proceedings of the Fifth International Conference on the Bearing Capacity of Roads and Airfields, Vol. 1, Trondheim, Norway, 1998, pp. 93-102.

Roque, R., L. A. Myers, and B. Birgisson, “Evaluation of Measured Tire Contact Stresses for the Prediction of Pavement Response and Performance,” Transportation Research Record No. 1716, Transportation Research Board, Washington, DC, 2000, pp. 73-81.

Roque, R., and C. Villiers, “Progress Report No.9: Comprehensive Monitoring of Field Performance of Superpave Project,” UF Project No.: 49104504704-12, Department of Civil and Coastal Engineering, University of Florida, Gainesville, June 2003.

Shenoy, A. and P. Romero, “Superpave Shear Tester as a Simple Standardized Measure to Evaluate Aggregate-Asphalt Mixture Performance,” ASTM – Journal of Testing & Evaluation, Vol. 29, No. 5, Sept. 2001, pp. 50-62.

Sholar, G.A., and G.C. Page, “Follow-up Evaluation of the Asphalt Pavement Analyzer,” Research Report FL/DOT/SMO/99-436, Florida Department of Transportation, Gainesville, September 1999.

Stuart, K.D., and R.P. Izzo, “Correlation of Superpave G*/Sin Delta with Rutting Susceptibility from Laboratory Mixture Tests,” Transportation Research Record No. 1492, Transportation Research Board, Washington, DC, 1995, pp. 176-183.

Stuart, K.D., and W.S. Mogawer, “Validation of Asphalt Binder and Mixture Tests That Predict Rutting Susceptibility Using the FHWA ALF,” Association of Asphalt Paving Technologists, Vol. 66, 1997, pp. 109-152.

Tayebali, A.A., N.P. Khosla, G.A. Malpass, and H.F. Waller, “Evaluation of Superpave Repeated Shear at Constant Height Test To Predict Rutting Potential of Mixes,” Transportation Research Record No. 1681, Transportation Research Board, Washington, DC, 1999, pp. 97-105.

Tekscan, Inc. http://www.tekscan.com/technology.html, last accessed on 3/15/03.

Texas Department of Transportation, Manual of Testing Procedures, available at http://manuals.dot.state.tx.us/dynaweb, last accessed on 2/4/2003.

Tia, M., R. Roque, O. Sirin, and H.J. Kim, “Progress Report No.1: Evaluation of Superpave Mixtures With and Without Polymer Modification by Means of Accelerated Pavement Testing,” UF Project No.: 49104504801-12, Department of Civil and Coastal Engineering, University of Florida, Gainesville, May 2001.

Wang, J.N., C.K. Yang, and T.Y. Luo, "Mechanistic Analysis of Asphalt Pavements, Using Superpave Shear Tester and Hamburg Wheel-Tracking Device," Transportation Research Record No. 1767, Transportation Research Board, Washington, DC, 2001, pp. 102-110.

Wang, L.B., J.D. Frost, and J.S. Lai, "Non-Invasive Measurement of Permanent Strain Field Resulting from Rutting in Asphalt Concrete," Transportation Research Record No. 1687, Transportation Research Board, Washington, DC, 1999, pp. 85-94.

Williams, R.C., and B.D. Prowell, "Comparison of Laboratory Wheel-Tracking Test Results with WesTrack Performance," Transportation Research Record No. 1681, Transportation Research Board, Washington, DC, 1999, pp. 121-128.

Witczak, M.W., K. Kaloush, T. Pellinen, M. El-Basyouny, and H. Von Quintus, "Simple Performance Test for Superpave Mix Design," NCHRP Report 465, Transportation Research Board, Washington, DC, 2002.

Wishnevsky, A. http://home.comset.net/wesik/grafula3/english.htm, last accessed on 6/13/03.

Woodside, A., J. Wilson, and G.X. Liu, "The Distribution of Stresses At the Interface Between Tyre and Road and Their Effect on Surface Chippings," Proceedings of the Seventh International Conference on Asphalt Pavements, Vol. 3, Nottingham, UK, 1992, pp. 428-442.

APPENDIX A

AGGREGATE AND MIXTURE VOLUMETRIC PROPERTIES

Table A-1. Gradations and specific gravity of aggregates for Project 1.

Sieve Size	Sieve	#89 Stone	W-10	M-10	Aggregate Blend			Blend	JMF
(#)	(mm)	(%)	(%)	(%)	(%)			(%)	(%)
					#89 Stone	W-10	M-10		
					50.0	18.7	31.3		
½"	12.5	100	100	100				100.0	100.0
⅜"	9.50	100	100	100				100.0	99.0
#4	4.75	32	96	99				64.9	64.0
#8	2.36	2	73	82				40.3	40.0
#16	1.18	1	47	60				28.1	29.0
#30	0.60	1	29	45				20.0	21.0
#50	0.30	1	15	33				13.6	14.0
#100	0.15	1	6	24				9.1	8.0
#200	0.075	0	3	16				5.8	5.1
Bulk Specific Gravity		**2.689**	**2.682**	**2.700**				**2.691**	**2.667**

Table A-2. Gradations and specific gravity of aggregates for Project 7.

Sieve Size	Sieve	S1-A Stone	S1-B Stone	Asphalt Screens	Aggregate Blend			Blend	JMF
(#)	(mm)	(%)	(%)	(%)	(%)			(%)	(%)
					S1-A Stone	S1-B Stone	Asphalt Screens		
					24.5	12.5	63.0		
¾"	19.0	100	100	100				100.0	100.0
½"	12.5	74	100	100				93.6	95.0
⅜"	9.50	47	92	100				86.0	88.0
#4	4.75	6	37	100				69.1	70.0
#8	2.36	6	6	87				57.0	57.0
#16	1.18	5	5	59				39.0	41.0
#30	0.60	5	4	38				25.7	30.0
#50	0.30	4	3	22				15.2	19.0
#100	0.15	4	3	8				6.4	9.0
#200	0.075	3	3	4				3.3	4.2
Bulk Specific Gravity		**2.407**	**2.407**	**2.508**				**2.471**	**2.490**

Table A-3. Gradations and specific gravity of aggregates for the HVS mixture.

<table>
<tr><th>Sieve Size</th><th>Sieve</th><th>S1-A Stone</th><th>S1-B Stone</th><th>Asphalt Screens</th><th colspan="3">Aggregate Blend</th><th>Blend</th><th>JMF</th></tr>
<tr><th>(#)</th><th>(mm)</th><th>(%)</th><th>(%)</th><th>(%)</th><th colspan="3">(%)</th><th>(%)</th><th>(%)</th></tr>
<tr><td>¾"</td><td>19.0</td><td>100</td><td>100</td><td>100</td><td rowspan="5">S1-A Stone</td><td rowspan="5">S1-B Stone</td><td rowspan="5">Asphalt Screens</td><td>100.0</td><td>100.0</td></tr>
<tr><td>½"</td><td>12.5</td><td>52</td><td>100</td><td>100</td><td>93.8</td><td>93.8</td></tr>
<tr><td>⅜"</td><td>9.50</td><td>20</td><td>99</td><td>100</td><td>89.1</td><td>89.1</td></tr>
<tr><td>#4</td><td>4.75</td><td>5</td><td>48</td><td>92</td><td>56.5</td><td>56.5</td></tr>
<tr><td>#8</td><td>2.36</td><td>3</td><td>11</td><td>74</td><td>30.1</td><td>30.1</td></tr>
<tr><td>#16</td><td>1.18</td><td>3</td><td>3</td><td>56</td><td rowspan="5">13.0</td><td rowspan="5">55.0</td><td rowspan="5">32.0</td><td>20.0</td><td>20.0</td></tr>
<tr><td>#30</td><td>0.60</td><td>3</td><td>2</td><td>43</td><td>15.3</td><td>15.3</td></tr>
<tr><td>#50</td><td>0.30</td><td>2</td><td>2</td><td>27</td><td>10.0</td><td>10.0</td></tr>
<tr><td>#100</td><td>0.15</td><td>2</td><td>2</td><td>16</td><td>6.5</td><td>6.5</td></tr>
<tr><td>#200</td><td>0.075</td><td>2</td><td>2</td><td>8</td><td>3.6</td><td>3.6</td></tr>
<tr><td colspan="2">Bulk Specific Gravity</td><td>2.301</td><td>2.310</td><td>2.316</td><td colspan="3"></td><td>2.311</td><td>2.311</td></tr>
</table>

Table A-4. Batch weight for Project 1.

BATCH WEIGHT, 4500g (Pine)							
4500		Gradation			Batch Weight (g)		
		#89 Stone	W-10 Gra	M-10 Gra	#89 Stone	W-10 Gra	M-10 Gra
Sieve Size	Sieve, mm	50%	18.7%	31.3%			
3/4"	19.0	100	100	100	0	2250	3092
1/2"	12.5	100	100	100	0	2250	3092
3/8"	9.5	100	100	100	0	2250	3092
#4	4.75	32	96	99	1530	2284	3106
#8	2.36	2	73	82	2205	2477	3345
#16	1.18	1	47	60	2228	2696	3655
#30	0.600	1	29	45	2228	2847	3866
#50	0.300	1	15	33	2228	2965	4035
#100	0.150	1	6	24	2228	3041	4162
#200	0.075	0.4	2.7	16.3	2241	3069	4270
Pan	0	0	0	0	2250	3092	4500

Table A-5. Batch weight for Project 7.

BATCH WEIGHT, 4500g (Pine)							
4500		Gradation			Batch Weight (g)		
		S-1-A Stone	S-1-B Stone	Asphalt Scrns	S-1-A Stone	S-1-B Stone	Asp Scrns
Sieve Size	Sieve, mm	24.5%	12.5%	63.0%			
3/4"	19.0	100	100	100	0	1103	1665
1/2"	12.5	74	100	100	287	1103	1665
3/8"	9.5	47	92	100	584	1148	1665
#4	4.75	6	37	100	1036	1457	1665
#8	2.36	6	6	87	1036	1631	2034
#16	1.18	5	5	59	1047	1637	2827
#30	0.600	5	4	38	1047	1643	3423
#50	0.300	4	3	22	1058	1648	3876
#100	0.150	4	3	8	1058	1648	4273
#200	0.075	3	3	3.5	1069	1648	4401
Pan	0	0	0	0	1103	1665	4500

Table A-6. Mixture volumetric properties.

Property		Project 1	Project 7
Design %AC		5.5	6.9
% Air viod	**Nini**	13.74	12.96
	Ndes	4.07	4.50
	Nmax	2.24	2.47
% Gmm	**Nini**	86.26	87.04
	Ndes	95.93	95.50
	Nmax	97.76	97.53
% VMA	**Nini**	24.00	23.43
	Ndes	15.47	15.98
	Nmax	13.86	14.20
Effective VMA (@ 4% AV)		31.5	22.8
% VFA	**Nini**	42.74	44.67
	Ndes	73.73	71.85
	Nmax	83.87	82.58
% AC absorption		0.63	1.68
Effective %AC		4.87	5.22
Gmm		2.509	2.334
Gse		2.736	2.573
Gsb		2.691	2.470
Effective Film thickness (micrometers)		24.4	18.6
Dust/Effective AC ratio		1.2	0.64

APPENDIX B

STATISTICAL ANALYSIS RESULTS

Table B-1. Statistical analyses for Project 1 and Project 7 results at 7% AV with the new APA loading device at 64°C.

P1 vs P7 - 7%AV, 64C, New APA			
Unpaired t test			
Parameter	**ARD**	**DRD**	**Area Change**
P value	0.0017	0.0008	P<0.0001
P value summary	**	***	***
Are means signif. different? (P < 0.05	**Yes**	**Yes**	**Yes**
One- or two-tailed P value?	One-tailed	One-tailed	One-tailed
t, df	t=4.682 df=6	t=5.470 df=6	t=13.43 df=6
How big is the difference?			
Parameter	**ARD**	**DRD**	**Area Change**
Mean ± SEM of column A	3.860 ± 0.2678 N=4	5.765 ± 0.3637 N=4	0.9150 ± 0.09042 N=4
Mean ± SEM of column B	2.155 ± 0.2468 N=4	3.388 ± 0.2380 N=4	-0.4575 ± 0.04768 N=4
Difference between means	1.705 ± 0.3642	2.378 ± 0.4347	1.373 ± 0.1022
95% confidence interval	-2.596 to -0.8139	-3.441 to -1.314	-1.623 to -1.122
R squared	0.7851	0.833	0.9678
F test to compare variances			
Parameter	**ARD**	**DRD**	**Area Change**
F,DFn, Dfd	1.178, 3, 3	2.336, 3, 3	3.597, 3, 3
P value	0.4481	0.2521	0.1605
P value summary	ns	ns	ns
Are variances significantly different?	**No**	**No**	**No**

Table B-2. Statistical analyses for Project 1 and Project 7 results at 7% AV with the new APA loading device at 70°C.

P1 vs P7 - 7%AV, 70C, New APA			
Unpaired t test			
Parameter	**ARD**	**DRD**	**Area Change**
P value	0.048	0.0086	0.0011
P value summary	*	**	**
Are means signif. different? (P < 0.05	**Yes**	**Yes**	**Yes**
One- or two-tailed P value?	One-tailed	One-tailed	One-tailed
t, df	t=1.972 df=6	t=3.261 df=6	t=5.094 df=6
How big is the difference?			
Parameter	**ARD**	**DRD**	**Area Change**
Mean ± SEM of column A	3.950 ± 0.3479 N=4	5.728 ± 0.4383 N=4	0.8350 ± 0.05315 N=4
Mean ± SEM of column B	2.963 ± 0.3600 N=4	3.808 ± 0.3931 N=4	-1.748 ± 0.5042 N=4
Difference between means	0.9875 ± 0.5006	1.920 ± 0.5888	2.583 ± 0.5070
95% confidence interval	-2.213 to 0.2376	-3.361 to -0.4793	-3.823 to -1.342
R squared	0.3934	0.6393	0.8122
F test to compare variances			
Parameter	**ARD**	**DRD**	**Area Change**
F,DFn, Dfd	1.071, 3, 3	1.243, 3, 3	89.98, 3, 3
P value	0.4781	0.4311	0.0019
P value summary	ns	ns	**
Are variances significantly different?	**No**	**No**	**Yes**

Table B-3. Statistical analyses for Project 1 and Project 7 results at 7% AV with the original APA loading device at 64°C.

P1 vs P7 - 7%AV, 64C, Original APA			
Unpaired t test			
Parameter	**ARD**	**DRD**	**Area Change**
P value	P<0.0001	0.0008	0.1825
P value summary	***	***	ns
Are means signif. different? (P < 0.05	**Yes**	**Yes**	**No**
One- or two-tailed P value?	One-tailed	One-tailed	One-tailed
t, df	t=13.68 df=4	t=7.648 df=4	t=1.021 df=4
How big is the difference?			
Parameter	**ARD**	**DRD**	**Area Change**
Mean ± SEM of column A	6.273 ± 0.08253 N=3	8.037 ± 0.2771 N=3	1.017 ± 1.474 N=3
Mean ± SEM of column B	4.347 ± 0.1141 N=3	5.157 ± 0.2550 N=3	-0.7933 ± 0.9855 N=3
Difference between means	1.927 ± 0.1408	2.880 ± 0.3766	1.810 ± 1.773
95% confidence interval	-2.318 to -1.536	-3.925 to -1.835	-6.732 to 3.112
R squared	0.9791	0.936	0.2067
F test to compare variances			
Parameter	**ARD**	**DRD**	**Area Change**
F,DFn, Dfd	1.910, 2, 2	1.182, 2, 2	2.237, 2, 2
P value	0.3436	0.4584	0.3089
P value summary	ns	ns	ns
Are variances significantly different?	**No**	**No**	**No**

Table B-4. Statistical analyses for Project 1 and Project 7 results at 4% AV with the new APA loading device at 64°C.

P1 vs P7 - 4%AV, 64C, New APA			
Unpaired t test			
Parameter	**ARD**	**DRD**	**Area Change**
P value	0.4306	0.4908	0.0001
P value summary	ns	ns	***
Are means signif. different? (P < 0.05	**No**	**No**	**Yes**
One- or two-tailed P value?	One-tailed	One-tailed	One-tailed
t, df	t=0.1826 df=6	t=0.02398 df=6	t=7.750 df=6
How big is the difference?			
Parameter	**ARD**	**DRD**	**Area Change**
Mean ± SEM of column A	2.048 ± 0.1946 N=4	2.195 ± 0.7630 N=4	0.9850 ± 0.2123 N=4
Mean ± SEM of column B	1.990 ± 0.2477 N=4	2.175 ± 0.3365 N=4	-2.493 ± 0.3953 N=4
Difference between means	0.05750 ± 0.3150	0.02000 ± 0.8339	3.478 ± 0.4487
95% confidence interval	-0.8282 to 0.7132	-2.061 to 2.021	-4.576 to -2.379
R squared	0.005524	0.00009585	0.9092
F test to compare variances			
Parameter	**ARD**	**DRD**	**Area Change**
F,DFn, Dfd	1.621, 3, 3	5.142, 3, 3	3.465, 3, 3
P value	0.3507	0.1059	0.1673
P value summary	ns	ns	ns
Are variances significantly different?	**No**	**No**	**No**

Table B-5. Statistical analyses for Project 1 and Project 7 results at 4% AV with the new APA loading device at 70°C.

P1 vs P7 - 4%AV, 70C, New APA			
Unpaired t test			
Parameter	**ARD**	**DRD**	**Area Change**
P value	0.0266	0.0006	0.0006
P value summary	*	***	***
Are means signif. different? (P < 0.05	**Yes**	**Yes**	**Yes**
One- or two-tailed P value?	One-tailed	One-tailed	One-tailed
t, df	t=2.402 df=6	t=5.701 df=6	t=5.836 df=6
How big is the difference?			
Parameter	**ARD**	**DRD**	**Area Change**
Mean ± SEM of column A	2.590 ± 0.2935 N=4	4.910 ± 0.3499 N=4	1.130 ± 0.4950 N=4
Mean ± SEM of column B	1.810 ± 0.1388 N=4	2.010 ± 0.3693 N=4	-2.210 ± 0.2873 N=4
Difference between means	0.7800 ± 0.3247	2.900 ± 0.5087	3.340 ± 0.5723
95% confidence interval	-1.575 to 0.01455	-4.145 to -1.655	-4.741 to -1.939
R squared	0.4902	0.8441	0.8502
F test to compare variances			
Parameter	**ARD**	**DRD**	**Area Change**
F,DFn, Dfd	4.472, 3, 3	1.114, 3, 3	2.968, 3, 3
P value	0.1251	0.4657	0.1978
P value summary	ns	ns	ns
Are variances significantly different?	**No**	**No**	**No**

Table B-6. Statistical analyses for Project 1 and Project 7 results at 4% AV with the original APA loading device at 64°C.

P1 vs P7 - 4%AV, 64C, Original APA			
Unpaired t test			
Parameter	**ARD**	**DRD**	**Area Change**
P value	0.3775	0.2595	0.0237
P value summary	ns	ns	*
Are means signif. different? (P < 0.05	**No**	**No**	**Yes**
One- or two-tailed P value?	One-tailed	One-tailed	One-tailed
t, df	t=0.3341 df=4	t=0.7064 df=4	t=2.827 df=4
How big is the difference?			
Parameter	**ARD**	**DRD**	**Area Change**
Mean ± SEM of column A	4.403 ± 0.1915 N=3	5.743 ± 0.1189 N=3	1.400 ± 0.6352 N=3
Mean ± SEM of column B	4.107 ± 0.8670 N=3	4.827 ± 1.292 N=3	-0.4233 ± 0.1122 N=3
Difference between means	0.2967 ± 0.8879	0.9167 ± 1.298	1.823 ± 0.6450
95% confidence interval	-2.761 to 2.168	-4.519 to 2.686	-3.614 to -0.03284
R squared	0.02715	0.1109	0.6664
F test to compare variances			
Parameter	**ARD**	**DRD**	**Area Change**
F,DFn, Dfd	20.49, 2, 2	118.1, 2, 2	32.08, 2, 2
P value	0.0465	0.0084	0.0302
P value summary	*	**	*
Are variances significantly different?	**Yes**	**Yes**	**Yes**

APPENDIX C

APA RESULTS

Table C-1. APA test results for Project 1.

Project 1									
New APA									
Sample Number	Sample ID	Air Voids Design	Air Voids Actual	Applied Load	Test Temperature	Wheel Tracking	Absolute Rutting (mm)	Differential Rutting (mm)	Area Change (%)
1	1-2-3	7%	7.5	150 lbs	64 °C	Bi-directional	4.42	6.63	0.98
2	1-2-4		6.4				4.19	4.85	0.84
3	S1-7-1		7.7				3.27	5.81	1.13
4	S1-7-2		7.7				3.56	5.77	0.71
5	S1-7-3		6.7			Uni-directional	3.81	5.36	-2.45
6	1-2-7		7.0		70 °C	Bi-directional	4.01	5.93	0.81
7	1-2-8		7.2				3.10	4.45	0.79
8	1-2-9		7.2				3.89	6.10	0.75
9	1-2-10		6.8				4.80	6.43	0.99
10	S1-7-4		6.5			Uni-directional	4.97	7.79	-2.95
11	S1-4-1	4%	3.6	150 lbs	64 °C	Bi-directional	1.86	0.20	1.23
12	S1-4-2		3.4				1.64	1.81	1.45
13	S1-4-3		3.9				2.15	3.50	0.71
14	S1-4-4		3.7				2.54	3.27	0.55
15	S1-4-9		4.4			Uni-directional	1.98	3.05	-1.91
16	1-4-3		3.8		70 °C	Bi-directional	2.60	5.02	1.18
17	1-4-4		4.4				1.78	4.06	2.48
18	S1-4-5		3.9				3.16	5.76	0.69
19	S1-4-6		4.4				2.82	4.80	0.17
20	S1-4-8		3.3			Uni-directional	4.40	7.39	-2.67
Original APA									
21	1-2-2	7%	6.2	100 lbs	64 °C	Bi-directional	6.15	7.56	-0.31
22	1-2-1		7.4				6.43	8.52	-0.60
23	1-2-6		6.5				6.24	8.03	3.96
24	1-4-5	4%	3.9	100 lbs	64 °C	Bi-directional	4.04	5.51	2.38
25	1-5-1		4.4				4.48	5.90	1.61
26	1-5-2		4.4				4.69	5.82	0.21

Table C-2. APA test results for Project 7.

Sample Number	Sample ID	Air Voids Design	Air Voids Actual	Applied Load	Test Temperature	Wheel Tracking	Absolute Rutting (mm)	Differential Rutting (mm)	Area Change (%)
Project 7									
New APA									
1	7-3-4	7%	6.5	150 lbs	64 °C	Bi-directional	2.85	3.67	-0.52
2	7-3-3		6.7				2.09	3.84	-0.54
3	7-2-4		6.1				1.69	2.77	-0.33
4	7-2-5		7.0				1.99	3.27	-0.44
5	S7-7-3		6.7			Uni-directional	2.71	2.99	-1.98
6	7-2-1		8.3		70 °C	Bi-directional	3.39	4.91	-1.94
7	7-2-2		8.3				3.75	3.80	-0.40
8	S7-7-1		6.4				2.44	3.12	-1.81
9	S7-7-2		6.7				2.27	3.40	-2.84
10	S7-7-4		6.0			Uni-directional	3.13	4.16	-3.93
11	S7-4-3	4%	3.8	150 lbs	64 °C	Bi-directional	1.64	1.41	-1.79
12	S7-4-4		3.9				2.65	2.71	-3.62
13	S7-4-5		4.1				2.09	2.77	-2.18
14	S7-4-6		4.1				1.58	1.81	-2.38
15	S7-4-12		3.7			Uni-directional	1.92	2.37	-2.01
16	S7-4-7		4.1		70 °C	Bi-directional	1.81	2.26	-1.74
17	S7-4-8		4.1				1.81	1.98	-2.96
18	S7-4-9		3.9				1.47	1.02	-2.36
19	S7-4-10		4.6				2.15	2.78	-1.78
20	S7-4-11		3.9			Uni-directional	2.10	2.72	-2.33
Original APA									
21	7-3-6	7%	6.4	100 lbs	64 °C	Bi-directional	4.17	5.36	0.39
22	7-3-5		6.5				4.56	5.46	-2.75
23	7-3-2		8.0				4.31	4.65	-0.02
24	7-4-1	4%	4.5	100 lbs	64 °C	Bi-directional	4.40	5.36	-0.47
25	S7-4-1		4.1				2.48	2.37	-0.21
26	S7-4-2		3.9				5.44	6.75	-0.59

Table C-3. APA test results for the HVS mixture.

HVS									
New APA									
Sample Number	Sample ID	Air Voids Design	Air Voids Actual	Applied Load	Test Temperature	Wheel Tracking	Absolute Rutting (mm)	Differential Rutting (mm)	Area Change (%)
1	**HVS-7-1**	**7%**	**7.3**	**150 lbs**	**64 °C**	**Bi-directional**	**1.63**	**1.43**	**-2.68**
2	**HVS-7-2**		**7.3**						
3	**HVS-7-3**		**6.9**		**70 °C**		**1.78**	**1.81**	**-2.74**
4	**HVS-7-4**		**6.8**						
5	**HVS-4-1**	**4%**	**4.6**	**150 lbs**	**64 °C**	**Bi-directional**	**1.24**	**1.07**	**-2.09**
6	**HVS-4-2**		**4.9**						
7	**HVS-4-3**		**4.4**		**70 °C**		**1.10**	**0.98**	**-1.26**
8	**HVS-4-4**		**4.4**						
Original APA									
9	**HVS-7-5**	**7%**	**7.2**	**100 lbs**	**64 °C**	**Bi-directional**	**2.40**	**2.82**	**-1.32**
10	**HVS-7-6**		**7.1**						
11	**HVS-4-5**	**4%**	**4.2**	**100 lbs**	**64 °C**	**Bi-directional**	**1.30**	**1.33**	**-1.20**
12	**HVS-4-6**		**4.1**						